# Dependence of skin drug permeation on microstructure and time dependent alterations following application of more-phasic dermatological formulations studied by the continuous phase drug concentration concept

**Inauguraldissertation**

**zur**
**Erlangung der Würde eines Doktors der Philosophie**
**vorgelegt der**
**Philosophisch-Naturwissenschaftlichen Fakultät**
**der Universität Basel**

**von**

**Heiko Nalenz**
**aus Badenweiler (Deutschland)**

**Basel, 2006**

Genehmigt von der Philosophisch-Naturwissenschaftlichen Fakultät
auf Antrag von

Herrn Prof. Dr. Hans Leuenberger (Fakultätsverantwortlicher)

Herrn Prof. Dr. Georgios Imanidis (Dissertationsleiter)

Herrn PD Dr. Peter van Hoogevest (Korreferent)

Basel, den 6.Juni 2006

Prof. Dr. Hans-Jakob Wirz
Dekan

**Für meine Eltern**

**Rosemarie Nalenz**

**und**

**Franz Nalenz †**

## Acknowledgements / Danksagung

Herrn Prof. Dr. Hans Leuenberger danke ich für die Möglichkeit, dass ich meine Dissertation am Institut für Pharmazeutische Technologie der Universität Basel durchführen konnte.

Bei Prof. Dr. Georgios Imanidis möchte ich mich für die wissenschaftliche Betreuung vorliegender Arbeit bedanken. Er ließ mir alle erdenklichen Freiräume, die Arbeit nach meinen Vorstellungen zu gestalten, war mir aber auch jederzeit mit interessanten und kritischen Diskussionen eine wertvolle Unterstützung.

Bedanken möchte ich mich bei PD Dr. Peter van Hoogevest für das Interesse an meiner Arbeit und die Übernahme des Korreferates.

Sandra Grauwiler und Stefanie Oggier danke ich recht herzlich für das Engagement während Ihrer Diplomarbeiten und das mir entgegengebrachte Vertrauen als Diplomarbeitsbetreuer.

Stefan Winzap danke ich für jegliche technische Unterstützung und für seinen unverzichtbaren Beitrag zum reibungslosen Ablauf des Institutsalltages.

Dr. Daniel Häussinger vom Institut für organische Chemie danke ich recht herzlich für die Durchführung der manchmal sehr arbeitsintensiven NMR Diffusionsmessungen. Marcel Düggelin und Dr. Markus Dürrenberger vom Zentrum für Mikroskopie der Universität Basel Biozentrum/Pharmazentrum danke ich für die rasterelektronenmikroskopischen Aufnahmen.

Weiterhin möchte ich mich bei meinen Kollegen für die freundliche Atmosphäre und all die Dinge bedanken, die dazu beitrugen, dass mir meine Zeit am “Insti” in positiver Erinnerung bleiben wird. Besonders danke ich Johannes von Orelli, Marcel Schneider, Maxim Puchkov und Etienne Krausbauer für die tolle Teamarbeit bei der Durchführung des flüssig-sterilen Praktikums. Dana Daneshvari danke ich für die Durchsicht des Manuskriptes.

Ganz besonders aber bedanke ich mich bei Tana und meiner Familie für die Geduld und die mentale Unterstützung auf meinem Weg zum promovierten Apotheker.

## Contents

## List of Abbreviations

| | |
|---|---|
| β | Buffer capacity |
| BTA-Cl | Benzyltrimethylammonium chloride |
| $C_{cont}$ | Continuous phase drug concentration of a multi-phase formulation |
| $C_{disp}$ | Dispersed phase drug concentration of a multi-phase formulation |
| $C_{tot}$ | Overall drug concentration of a multi-phase formulation |
| CF10 | Complex formulation with 10 weight-% dispersed phase |
| CF50 | Complex formulation with 50 weight-% dispersed phase |
| D | Diffusion coefficient |
| E | Emulsion |
| $K_{d/c}$ | Drug distribution coefficient between dispersed and continuous phase of a multi-phase formulation |
| $K_{S/C}$ | Drug distribution coefficient between stratum corneum and continuous phase of a multi-phase formulation |
| LD | Liposomal dispersion |
| NMR | Nuclear magnetic resonance |
| P | Permeability coefficient |
| $P_{app}$ | Apparent permeability coefficient |
| PCS | Photon correlation spectroscopy |
| $P_{int}$ | Intrinsic permeability coefficient, identical to P |
| SC | Stratum corneum |
| SD | Standard deviation |
| SEM | Scanning electron microscopy |
| TEWL | Transepidermal water loss |

## A. Abstract

In this work, the dependence of transdermal delivery of hydrophilic drugs on mass fraction and microstructure of dispersed phase of multi-phase dermatological o/w formulations was studied. Permeation of sodium nicotinate, caffeine and benzyltrimethylammonium chloride (BTA-Cl), used as model drugs, was studied under occlusive conditions. Sodium nicotinate permeation was also investigated non-occlusively taking especially into consideration alterations these formulations may undergo due to evaporation of volatile components. The study formulations included a typical emulsion (E) consisting of triglycerides, emulsifier (polysorbate 20) aqueous buffer pH 7.4 and ethanol, a typical liposomal dispersion (LD) consisting of phospholipids, aqueous buffer pH 7.4 and ethanol and two complex formulations, CF10 and CF50, each consisting of all these components. These formulations were designed in order to consider not only diversity in their composition but also widely varying ratios of dispersed to continuous phase. CF50 and E contained a high amount of dispersed phase of 50 weight-% and LD and CF10 a comparatively low amount of dispersed phase of 10 weight-%. Permeation was studied in-vitro using Franz-type diffusion cells across excised full-thickness pig ear skin. A concept is proposed for the interpretation of the permeation data. This concept postulates that continuous phase drug concentration of the formulations is the only parameter governing permeation kinetics. As reference, purely aqueous or aqueous/ethanolic gel formulations were used.

Coexisting dispersed structures of the formulations were fractionated using ultracentrifugation. The received fractions of all formulations were characterised by chemical component analysis, scanning electron microscopy and particle size measurements. Emulsion droplets were creaming and liposomes sedimenting, as attested by formulation E and LD, respectively. CF50 comprised emulsion droplets and a microemulsion that consisted of 13 weight-% phospholipids, 13 weight-% triglycerides, 10 weight-% polysorbate 20 and of 64 weight-% hydrophilic phase. NMR-diffusion measurements demonstrated a droplet-like o/w structure for this system. Particle size measurements following different dilution steps indicated a stable droplet size of 20-24 nm. No liposomal structures were detected within CF50. For CF10, a coexistence of liposomes, emulsion droplets and small quantity of microemulsion aggregates was found. The continuous phase of all formulations consisted of aqueous buffer and the total amount of ethanol, independently of dispersed structures. Distribution of the drugs between distinct phases of the formulations was studied using the shake-flask method and ultrafiltration. Sodium nicotinate and BTA-Cl distributed completely into the hydrophilic phase of the formulations, according to their solubility properties, while caffeine showed moderate distribution into triglycerides. Based on these observations, continuous phase drug concentrations were calculated.

Caffeine permeation from the formulations across a silicon membrane gave equal permeability coefficients, calculated with continuous phase drug concentration, clearly demonstrating the validity of the proposed concept. Permeability coefficients across skin, however, were different, depending on the formulation. The same was true also for BTA-Cl and sodium nicotinate. This was not due to variable molecular mobility of drug within the formulations, as attested with sodium nicotinate NMR diffusion experiments. The possible effect of formulations on the barrier function of the skin was investigated by measuring distribution of drugs between the stratum corneum and continuous phase of the formulations and calculating the diffusion coefficients within the stratum corneum. This demonstrated clearly that CF10 and CF50 were able to increase drug diffusion coefficients within the stratum corneum statistical significantly for all model drugs. Furthermore, a reduction of drug distribution between stratum corneum and formulation with increasing amount of dispersed phase of all formulations was observed which was responsible for retardation of skin permeation. Drug permeation was ultimately the combined result of these two contrasting formulation effects on skin barrier function. The diffusion enhancing effect of CF10 and CF50 was shown to be due to the microemulsions contained in these formulations. The presence of ethanol was found to be essential for this effect, demonstrating a synergism of the microemulsions with the ethanol.

During evaporation of volatile formulation compounds, several phase transitions were detected, such as: vesicle to microemulsion in case of CF10, phase inversion from o/w to w/o in case of CF50 and drug precipitation due to exceeded maximum solubility in case of E. For LD and CF10, sodium nicotinate fluxes were continuously increasing in course of the permeation experiments. The emulsion yielded a constant flux, while the phase inversion observed in case of CF50 very likely caused a decrease in permeation. For quantitative interpretation of the permeation data, the continuous phase drug concentration concept was expanded to the situation of non-occlusive application. The increase of permeability for non-occlusively applied formulations was up to tenfold, compared to an occlusively applied purely aqueous gel. This could be explained by the resulting continuous phase drug concentrations, independently of arising microstructures. Hence, this concentration governed sodium nicotinate permeation in this situation alone, without the need to consider formulation effects on skin barrier function. This is in good agreement with the observed synergism of the ethanol with the microemulsions, because ethanol evaporated very quickly from the formulations following non-occlusive application.

To conclude, taking into account continuous phase drug concentration of multi-phase formulations provides a predictive tool in order to delineate the effect of physicochemical formulation parameters and of formulation effects on skin barrier function on delivery rate. This is true for occlusive and non-occlusive application.

## B. Introduction and Objectives

In clinical practice, drugs are normally incorporated in a vehicle in order to be applied to the skin for topical or systemic therapy (1). Vehicles typically consist of several components that are often not mutually miscible, thus forming separate phases. The phases of such dermatological formulations are intermixed, producing macroscopically homogeneous systems. On the microscopic level, however, these phases form different structures, which may be identified using a combination of methods including microscopy, rheology measurements, ultracentrifugation and NMR spectroscopy (2,3,4,5).

Dermatological formulations are developed and optimised with respect to a host of criteria such as applicability, tolerability, stability and foremostly efficacy, which comprises duration and strength of pharmacological action. This regulation may take place based on physicochemical principles or by an interaction of formulation structures with the absorptive epithelium, i.e., the epidermis, affecting its permeability of the drug. In all likelihood, the available drug concentration in the vehicle is the most crucial physicochemical parameter governing permeation kinetics (6), as already demonstrated by Coldman et al. in 1969, who investigated fluocinolone acetonide penetration from different solutions (7). Microemulsions (8,9,10,11) and liposomal vesicles (12,13,14,15) represent classes of multi-phase vehicles which may further affect skin permeation by reducing the transport barrier function of the stratum corneum. For such formulations, however, drug distribution among distinct phases may have additional impact on delivery rate by adjusting the portion of drug that is available for permeation. Hummel and Imanidis showed that ibuprofen distributed strongly into lipophilic dispersed phase structures of multi-phase o/w formulations and the resulting continuous phase drug concentration explained quantitatively permeation kinetics across pig-ear skin in-vitro (4). Thus, for multi-phase formulations, this concentration seems to be an essential parameter to interpret drug skin permeation and, consequently, to identify possible formulation effects on skin barrier function.

Moreover, dermatological formulations are typically applied to the skin as a thin layer under non-occlusive conditions and are intended to deliver the active ingredient for hours. After application, however, the composition of the formulation may change, commonly because of evaporation of volatile components (1,4). Such a change in the composition of a multi-phase system likely elicits alterations of the phase structure of the system and of the concentration and distribution of the active ingredient in it. These alterations in turn can affect delivery performance. This aspect, however, was studied mostly with volatile solutions (7,16) or was not always related to its effect on drug permeation (17,18).

Consequently, a variety of factors combine to complicate a correct interpretation of how drug transport across the skin depends on the delivery formulation. Despite the efforts made to date to elucidate the influence of the formulation on skin absorption on a mechanistic basis, there is still no unifying theory that allows safe prediction of the process (19). Important aspects, such as drug distribution among distinct phases and alterations of the formulation following application are commonly considered empirically, and intuition as well as trial and error often surrogate for science in dermatological formulation development and in clinical practice (1). Thus, there is big need for a general theory that takes into account physicochemical formulation parameters and may be applied to occlusive and non-occlusive delivery conditions in order to test drug skin permeation in-vitro. For this purpose, methodological aspects should further be considered (20). Such a concept would make a valuable contribution to clinical drug delivery and, importantly, to an effective development of dermatological formulations.

### *Objectives*

The purpose of this PhD thesis was to establish a methodology to understand quantitatively the dependence of transdermal drug permeation on microstructure and mass fraction of dispersed phase of multi-phasic dermatological o/w formulations and on changes these parameters may undergo following non-occlusive application. Drug permeation was studied in vitro across full-thickness pig ear skin to control the experimental environment and so to elucidate individual factors that may modify permeation. Representative o/w formulations, consisting of emulsifier, triglycerides, phospholipids, buffer and ethanol, were designed in order to receive diversity of their composition and variety of their phase ratio of dispersed to continuous phase. Different coexisting microstructures were separated using ultracentrifugation and characterised by physicochemical methods. Drug distribution was determined with respect to the microstructure and to mass fraction of dispersed phases of the formulations to calculate continuous phase drug concentrations. This concentration was postulated to describe quantitatively drug permeation rate. The use of hydrophilic model drugs which distribute strongly into the hydrophilic phase of formulations was the basis to test this concept and to detect possible interactions of dispersed formulation structures with the skin. To delineate the effect of formulation structures on skin barrier function more detailed, drug distribution experiments between isolated stratum corneum and formulations were performed and drug diffusion coefficients within stratum corneum were calculated. With respect to clinical practice, permeation was further studied non-occlusively considering changes the formulations undergo due to evaporation of volatile components. Emphasis was laid on the investigation of different phase transitions and on changes of the phase ratios from dispersed to continuous phases in order to expand the continuous phase drug concentration concept to the situation of non-occlusive application.

# C Theoretical Section

## C.1 The Skin

The skin has the primary function to provide a barrier against environmental influences (21) and to protect the body against the loss of endogenous substances (22). Furthermore, the skin is also a major contributor to thermoregulation and performs endocrine functions, e.g. Vitamin D synthesis or peripheral conversion of prohormones (23). Macroscopically, two distinct skin layers are apparent, an unvascularized outer layer (epidermis) and an inner vascularized layer. The vascularized layer consists of the dermis and the hypodermis and has the function to provide physiological support to the unvascularized epidermis. This layer comprises the viable epidermis and the outermost layer of the skin, the stratum corneum, which consists of dead keratin-filled cells. Fig.1 gives an overview about the dimensions and the stratified appearance of the skin.

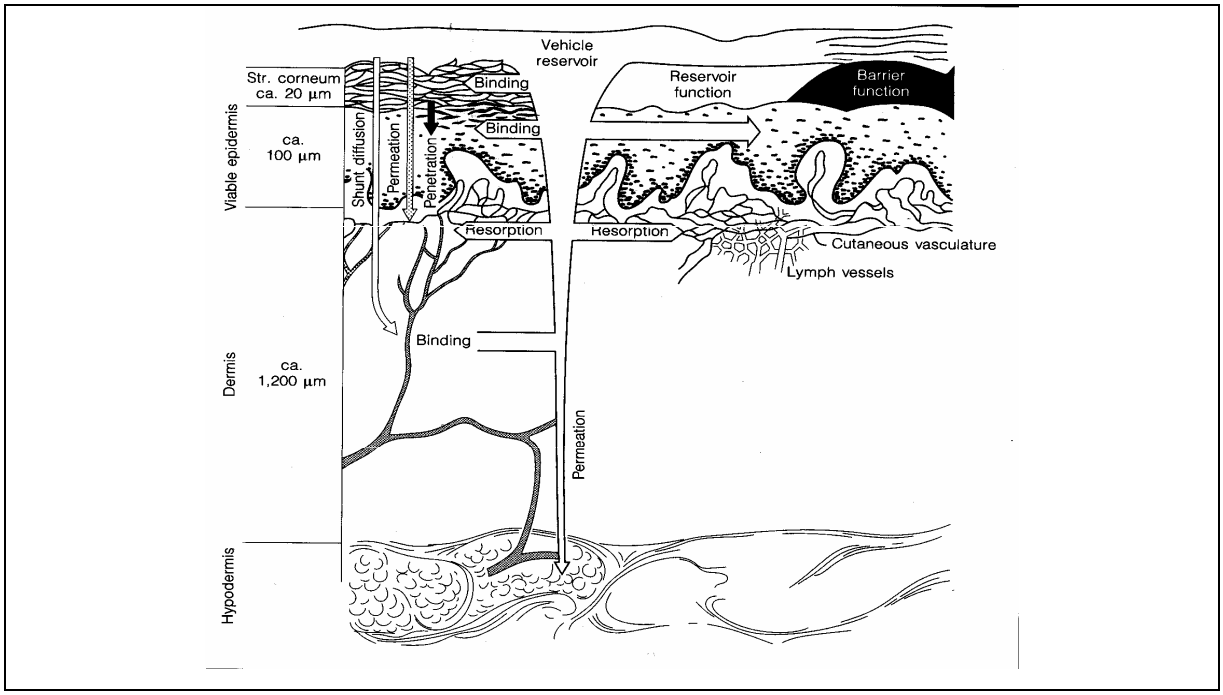


**Figure 1** Skin tissue layers. From Schaefer and Redelmaier, 1993 (21)

### C.1.1 The Viable Epidermis and Epidermal Differentiation

The viable epidermis is divisible into three distinct layers, namely, from inside to outside: Stratum basale, statum spinosum and the stratum granulosum. The cells of these layers undergo continuous differentation to produce the outermost layer of the skin, the stratum corneum, that consists of layers of dead keratin filled cells. Due to this process, histological preparations of the epidermis are of stratified appearance.

The stratum basale is a single layer of epidermal stem cells which are anchored to a basement membrane that separates the epidermal tissue from the underlying dermis. The basal cells are continually dividing, creating cells that undergo several changes while moving towards the skin surface in further course of differentiation. Above, these differentiating cells are forming the stratum spinosum. The cells are now of spiny appearance, due to abundance of desmosomes. In addition to the cell organelles seen in the basal layer, the stratum spinosum also reveals lipid enriched lamellar bodies (also called Odland bodies) and an increase in keratin filaments, indicating the dual character of the differentiation, protein and lipid synthesis (23). On their way to the skin surface, the cells begin to flatten and elongate, forming the stratum granulosum. Distinct keratohyalin granules that become larger in the upper granulocytes reflect an increase in keratin synthesis, accompanied by an increasing number of lamellar bodies. In course of the terminal differentiation of the uppermost granulocytes into a corneocyte, these lamellar bodies are secreted to the extracellular domains, forming the stratum corneum extracellular bilayers. This process is accompanied by the formation of the corneocyte`s cornified envelope, the dissolution of cell organelles and the condensation of the enriched keratin filaments. The nature of the signals that initiate the irreversible process of cornification is still elucidated, but it is evidenced that an extracellular calcium gradient with higher $Ca^{2+}$ concentrations in the upper regions of the viable epidermis triggers the transformation from a granulozyte to a corneozyte. The deceased cells are finally shed from the skin by desquamation. The complete renewing process takes about 3-4 weeks. The viable part of the epidermis also contains melanocytes that are responsible for skin pigmentation, antigen presenting Langerhans cells and Merkel cells (mechanoreceptors) (24).

### C.1.2 The Stratum Corneum

The stratum corneum constitutes the outermost layer of the epidermis and represents the main barrier function, although it is the thinnest and smallest compartment of the skin. It is about 10 to 20 µm thick and consists of several layers of dead, keratin filled corneocytes that represent the final state of epidermal differentiation (see C.1.1). These cells are embedded in a matrix of lipid lamellas that descend from the secreted content of the lamellar bodies, which gives the stratum corneum a brick and mortar organisation (23). A rigid envelope that replaces the plasma membrane surrounds the corneocytes after terminal differentiation. This cornified envelope in turn is coated with long chain ceramides, some of them covalently attached through ester linkages to the outer surface of the envelope. A free interaction of their acid chains with unbound extracellular lipid lamellae assists establishing the lamellar organisation in the extracellular lipids (25). Another speciality of the stratum corneum is the lipid composition, which differs significantly from those of the cells of the lower epidermal layers. The lipid composition of the stratum basale is comparable with that of cells of other tissues and

constitutes mainly of phospholipids. In the stratum granulosum, a drastically decrease in the phospholipids occur for the benefit of sphingolipids and cholesterol. The extracellular lipid matrix of the stratum corneum finally is free of phospholipids and consists of ceramids, cholesterol and free fatty acids in roughly equimolar ratios (23). The ceramides are crucial for the lipid organisation of the stratum corneum barrier, while the cholesterol is promoting the intermixing of different lipid species. Fig.2 points out these differences in lipid composition for the stratum basale, the stratum granulosum and the stratum corneum.

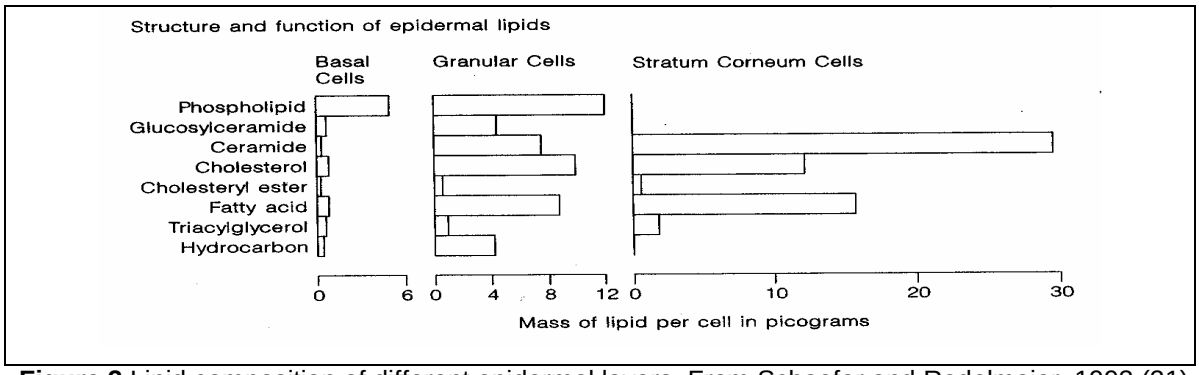


**Figure 2** Lipid composition of different epidermal layers. From Schaefer and Redelmaier, 1993 (21)

Water-holding properties of the stratum corneum are influenced by the rate of proteolysis, which generates a blend of amino acids termed as natural moisturing factors (26). The general degree of hydration of the stratum corneum is between 10 to 30% bound water, depending on the location within the stratum corneum, body site and environmental conditions. Under occlusive conditions (defined as complete impairment of passive transepidermal water loss, see also C.4.2.1), however, the stratum corneum may bind a 2.75 fold amount of water compared to its dry weight (27).

### C.1.3 The Dermis and the Hypodermis

The dermis is connected by the basement membrane to the stratum basale. This junction is of folded appearance, supporting the exchange of nutrients and other physiological substances with the unvascularized epidermis. Main components of the dermis are collagen and elastin fibres that form a vast network of filamentous and amorphous connective tissue that prevents strength and flexibility to the skin (21). Furthermore, the dermis accommodates cellular residents such as fibroblasts, endothelial cells, mast cells and, under conditions of inflammation, macrophages, lymphocytes and leucocytes. The tissue of the dermis has an extensive vascular network that is involved in nutrition, thermal regulation and immune responses. A variety of appendages, such as hair follicles or sweat and sebaceous glands are also derived from this tissue. Underneath the dermis is the hypodermis situated that contains, in contrast to the dermis, loose connective tissue and adipocytes as the main cellular exponent which represent an energy source for the body.

## C.2 Dermatological Vehicles

In clinical situations, a drug is rarely applied to the skin in form of a pure chemical but, instead, is normally incorporated in a carrier system, the vehicle (1). Such preparations vary in their physicochemical nature from powders through semisolids to liquids. However, a uniform and comprehensive classification for dermatological vehicles is currently not yet available. A formulation may be classified by its pharmaceutical nomenclature used in pharmacopoeias (e.g. cream, ointment, gel), by the principle of the structural matrix (e.g. emulsion, liopsomal dispersion) or by macroscopic appearance (e.g. milk, foam, shake). Table 1 gives a simplified possible classification of dermatological vehicles.

**Table 1** Simple classification of dermatological vehicles

| System | Monophasic | Diphasic | Tri-(multi-)phasic |
|---|---|---|---|
| Liquid | nonpolar solution,<br>*often designated as oil*<br><br>polar solution<br>*often designated as paint, lotion, ect.* | emulsion (o/w, w/o)<br>*often designated as milk, lotion, shake, ect.*<br>suspension<br>*often designated as paint, shake, ect*. | emulsion (o/w/o)<br>*often designated as milk, lotion, shake, ect.*<br>suspension<br>*often designated as paint, shake, ect.* |
| Semisolid | water-free polar or nonpolar ointment<br>water containing polar or nonpolar gel | emulsion (o/w, w/o)<br>*often designated as washable (o/w), nonwashable (w/o)or amphiphilic (o/w, w/o) cream*<br>suspension<br>*often designated as paste* | emulsion with powder (o/w, w/o)<br>*often designated as cream pastes* |
| Solid | powder | transdermal patch | transdermal patch |

It is obvious that this classification system is a raw simplification of the diversity of external formulations. It does not account for many of the newer external formulations (e.g. liposomes, microcapsules, microemulsions, ect.)

Adapted from Surber and Smith, 2005 (1)

### C.2.1 Emulsions

Essentially, an emulsion is a heterogeneous system containing two immiscible phases; a hydrophilic liquid phase and a lipophilic or oil phase. If the mixture consists of hydrophilic droplets dispersed in oil, we refer to it as water in oil (w/o) emulsion, even when the hydrophilic liquid is not water. An oil in water (o/w) emulsion has nonpolar liquid droplets dispersed in the aqueous phase; the term oil denotes all lipophilic materials even when they are not true oils in the chemical sense, e.g., hydrocarbons (19). Commonly encountered emulsions will have average droplet sizes of at least several microns, with a rather broad distribution. The volume fraction of dispersed material in emulsions is seldom less than 10 % and sometimes as high as 90% (28). Beside o/w and w/o emulsions, more complicated systems may arise, generally referred to as multiple emulsions. Multiple emulsions are composed of droplets of one liquid dispersed in larger droplets of a second liquid, which is then dispersed in a final continuous phase. Such systems may be w/o/w emulsions where the internal and external phases are

hydrophilic; or o/w/o, which have the reverse composition. Fig.3 gives an overview about these emulsion types.

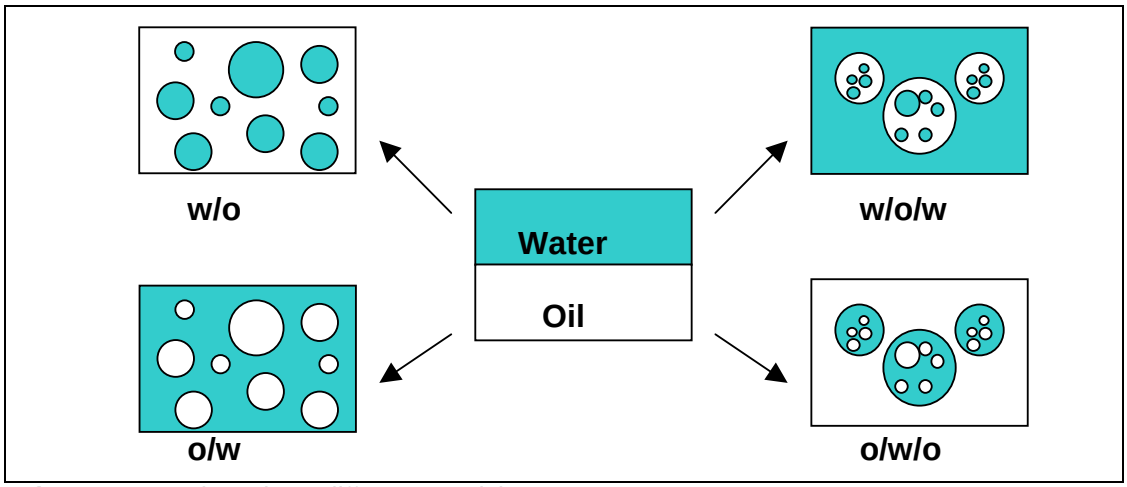


**Figure 3** Overview about different emulsion types

### *C.2.1.1 Physicochemical Properties and Preparation of Emulsions*

The preparation of an emulsion requires the formation of a very large amount of interfacial area between two immiscible liquids. The work *W* required to generate a specific area of new interface is given by

$$W = \sigma i \bullet \Delta A \qquad (1)$$

where $\sigma i$ is the interfacial tension between the two liquid phases and $\Delta A$ is the change in interfacial area. Since the amount of work that is required to increase the interfacial area remains in the system as potential energy, the system is thermodynamically unstable and rapidly undergoes any kind of transformations possible to reduce that energy, in this case, by reducing the interfacial area. To prevent coalescence or at least to reduce its rate to negligible proportions, in almost all practical emulsions, some additive (an emulsifier) is required. The additive, an emulsifier and/or stabilizer, may perform two primary functions: (I) lower the energy requirements of drop formation (i.e., lower the interfacial tension) and (II) retard the process of drop reversion to separate bulk phases. Emulsifying agents may be divided into four groups as follows: Adsorbed nonsurfactant ionic materials, colloidal solids, polymers and surfactants, which represent the most common stabilisation mechanism (28). Furthermore, the type of emulsion that is produced with given hydrophilic and lipophilic compounds, o/w or w/o, depends primarily on the property of the surfactant. This characteristic is referred to as hydrophilic-lipophilic balance (HLB), that is, the polar-nonpolar nature of the emulsifier. Hence, it appears that the type of emulsion is a function of the relative solubility of the surfactant, the

phase in which it is more soluble being the continuous phase. This is sometimes referred to as rule of Bancroft, who observed this phenomenon in 1913 (29).

In principal, two common methods are used to prepare o/w emulsions. The Continental method includes that the emulsifier, the lipophilc phase and parts of the hydrophilic phase form a primary w/o emulsion. The final o/w emulsion is obtained due to phase inversion following addition of more hydrophilic solution. The second method includes dissolving the emulsifier in the hydrophilic phase and the preparation step involves slowly titration with the oil. This method is referred to as English method. Each method, however, requires that energy be put into the system in some form. The energy may be supplied in a variety of ways, such as trituration, heat, agitation or homogenization.

The rotor stator technology, for example, is a well-established method for time-saving and easy emulsion preparation. A typical dispersing aggregate consists of two teeth rings, one of them is fixed and does not move - the stator; the other is driven by a motor through the shaft and turns around inside the stator - the rotor (Fig.4). The shear forces and bounce effects which are created between the running rotor and the stator treat the product mechanically, so for example 2 phases can be homogenized in short time.


**Figure 4** Cross-section of a rotor-stator aggregate

### C.2.2 Liposomes

Liposomes were first describes by Bangham in the early 1960s and shortly thereafter were put to use as models for biological membranes (30). Liposomes are simply vesicles in which an aqueous volume is entirely enclosed by a membrane composed of lipid molecules, usually phospholipids. Liposomal vesicles can be large or small and may be composed from one to several hundred concentric bilayers. Their size ranges from at least 20 nm to several µm, while the thickness of one single bilayer is around 4 nm. With respect to the size and number of bilayers, one may distinguish large multilamellar vesicles (MLV`s), and large and small unilamellar vesicles (LUV`s and SUV`s, respectively). (31).

#### *C.2.2.1 Physicochemical Properties and Preparation of Liposomes*

Phospholipids are diesters of glycerol, the sn-1 and sn-2 positions of the glycerol residue being esterified with fatty acids of varying length and degree of saturation, while the sn-3 position is esterified with phosphoric acid. Normally, a second short chain alcohol is esterified to the

second acidic group of the phosphoric acid. This chemical constitution determines the amphiphilic nature of the phospholipids that, in turn, enables the association in bilayer shields in aqueous media in order to minimize the unfavourable interactions between the aqueous phase and the long hydrocarbon fatty acid chains. Such interactions are completely eliminated when the sheets fold themselves to form closed sealed vesicles (32).

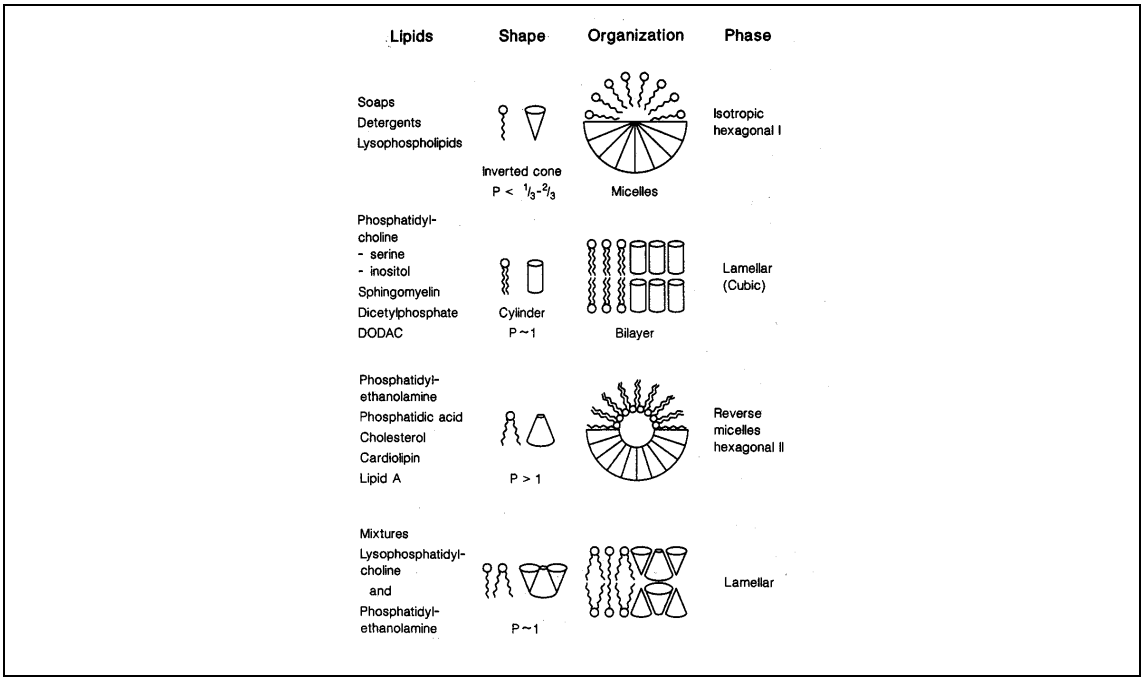


**Figure 5** A model of geometrical packaging of various amphiphiles into colloidal aggregates. P denotes a packing parameter that allows predicting the aggregate shape. From Lasic, 1993 (33)

Fig.5 illustrates how the molecular shape of phospholipids allows the formation of bilayer aggregates in a hydrophilic environment, while the molecular geometry of other amphipilic molecules leads to formation of micelles or reverse micells.

In order to produce liposomes, phospholipid molecules must be introduced into an aqueous environment. Different methods are reported to obtain liposomes, each of which produces vesicles with specific characteristics. Solvent injection methods comprise a simple and valuable method. This class of methods consists of several different variations including a variety of hydrophilic and hydrophobic organic solvents or their mixtures, being injected into different aqueous phases at different experimental conditions (34). The ethanol injection method, for example, enables the preparation of unilamellar liposomes when the phospholipids, dissolved in ethanol, are injected rapidly into an excess of aqueous medium (35).

### C.2.3 Microemulsions

A microemulsion is defined as a system of water, oil and amphiphile, typically a mixture of conventional surfactant and alcohol, which is a transparent, optically isotropic liquid system that is thermodynamically stable (5). Schulman et. al were the first who introduced the concept

of such systems (36,37). Till nowadays, however, there is still uncertainty about the exact microstructure of microemulsions.

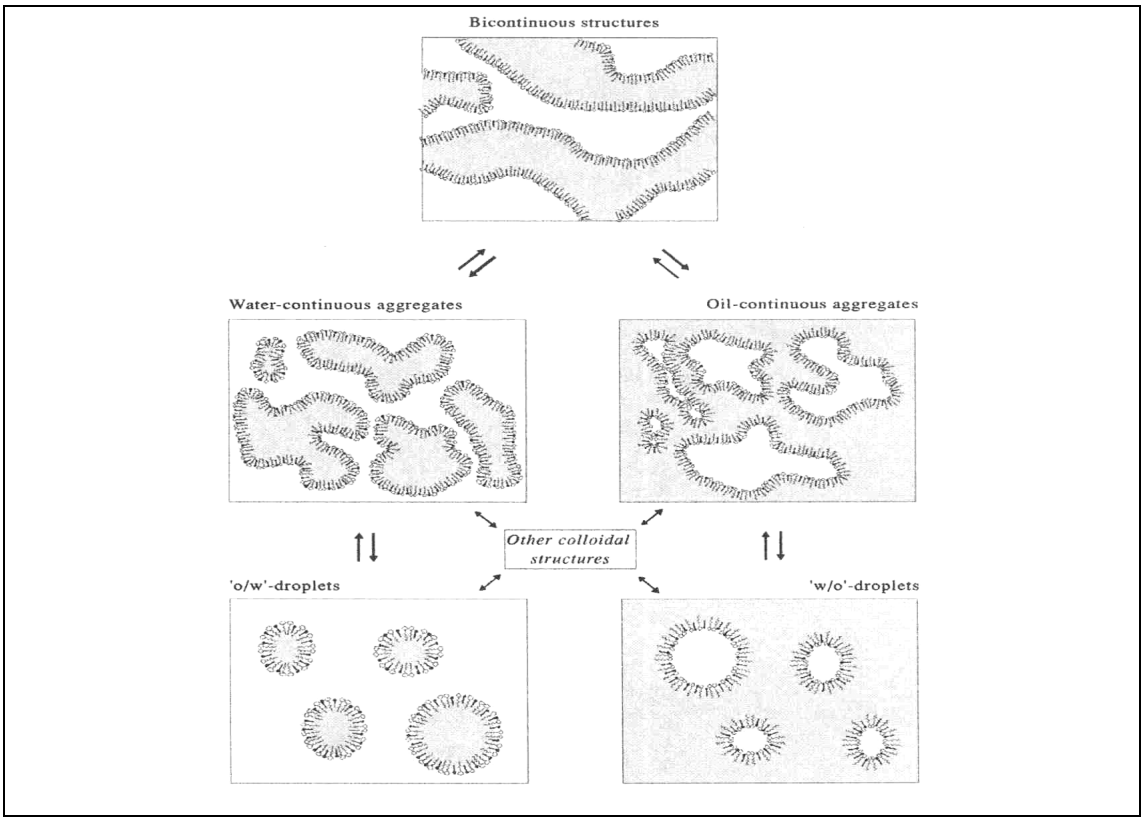


**Figure 6** Basic dynamic microemulsion structures formed by oil phase (grey), aqueous phase (white) and surfactant/cosurfactant film (interfacial). From Kreilgaard, 2002 (5)

Fig.6 gives an overview about assumed arrangements of microemulsion systems. While emulsions consist of roughly spherical droplets of one phase dispersed in another (see C.2.1), microemulsions may constantly evolve between various structures ranging from droplet like micelles to bicontinuous structures. Furthermore, microemulsions may be differentiated from emulsions on the basis of the particle size of the dispersed structures that are typically smaller than 150 nm, also generating the optically isotropy, even if we consider systems of particular microstructure (3).

The majority of examined microemulsion systems, however, contain irritant ionic surfactans or oils such as benzene or hexane, all of which are unacceptable from a pharmaceutical point of view. Hence, several authors have focused on formulation of microemulsions with non-irritant surfactants, such as phospholipids (11,38).

***C.2.3.1 Physicochemical Properties and Preparation of Microemulsions***

In contrast to conventional emulsions, microemulsions are formed spontaneously when admixing the appropriate quantities of the components, without requiring additional mechanical energy, and they are physically stable due to their thermodynamic nature (5). As mentioned above, the structure can be discontinuous or bicontinuous, depending on the phase ratio from hydrophilic to lipophilic phases and surfactant concentrations, respectively. To obtain such

microstructures, however, a few essential conditions are required: (I) Lowering the interfacial tension at the water-oil interface, (II) the formation of a highly fluid interfacial surfactant film and (III) penetration and association of the molecules of the oil phase with the interfacial surfactant film (37). Lowering the interfacial tension and fluidisation is usually done by incorporation of a co-surfactant to the surfactant film, typically a short-chain alcohol. To enable further integration of the oil within the interfacial film, the size of the oil molecules should not be too large (5).

## C.3 Characterisation of Dermatological Vehicles

A number of analytical methods are used for structural elucidation of dermatological formulations, such as optical methods (2), rheological inspections (3) ultracentrifugation (4) or NMR self-diffusion experiments of formulation compounds (5). However, the use of a single method gives usually unsatisfactory results, especially for multi-component systems due to their complexity. Beside the droplet size, the interparticulate interactions induced by the number of ingredients determine the microstructure of such systems. Thus, in the majority of cases a combination of different physicochemical methods for structural investigations of dermatological formulations is required.

### C.3.1 Optical Methods

As mentioned in the above chapters, the structures within dispersed systems may range in their size from about 10 nm (microemulsions) over several hundred nm (liposomes) up to more than several microns (emulsions). Thus, the overall appearance of such systems inherently involves some obvious information about comprising structures by simple visual inspection. Table 2 shows the optical characteristics for the range of particle sizes typically encountered in dispersed systems.

**Table 2** Estimation of particle sizes of dispersed structures by visual inspection

| Appearance | Tyndall scattering | Diameter (µm) |
|---|---|---|
| Two phases | None | Macro globules |
| Pure white | None | Exceeds 0.5 |
| White to gray | Weak blue | 0.3-0.1 |
| White to translucent | Intense blue | 0.14-0.01 |
| Transparent | None | Less than 0.01 |

Modified from Farianto and Rowell, 1983 (2)

However, highly turbid or highly polydisperse samples can wash out a distinguishing appearance, owing to multiple scattering, what requires further methods to characterise the structure of dispersed systems. Structures in the size range larger than 200 nm can be directly visualized with a transmission light microscope (2). Polarized light microscopy provides a tool to identify anisotropic materials within dispersed formulations such as solid drug particles or liquid crystals formed by encountered surfactants (17,39). Briefly, there are two polarizing filters in a polarizing microscope referred to as polarizer and analyzer, situated below and above the specimen stage, respectively. A polarising filter permits only one vibration direction of the light, while the wave model of common light describes light waves vibrating at right angles to the direction of travel of light with all directions being equally probable. When the permitted vibration directions of the polarizer and analyzer are positioned at right angles to each other, no light can pass through the system, except for a specimen of anisotropic material

that will move the vibration direction of the light through the analyzer and finally gives a texture of the anisotropic structures of the specimen in the eyepiece of the microscope.

In order to visualize dispersed structures that are smaller in size than several hundred nanometers and that are optically isotropic, transmission electron microscopy (TEM) (15,39,40) or scanning electron microscopy (SEM) (41,42) is commonly applied to such systems. Most studies described in the literature were performed by TEM using the freeze fracture replica technique. In contrast to conventional thin section methods, the replica technique theoretically avoids artefacts caused by chemical treatment and dehydration. In practice, however, it appeared to be very difficult to clean the replicas and separate them from the original matrix (11). However, in case of freeze fracture scanning electron microscopy, no replica separation and cleaning is necessary, and the fractured original formulation can be observed in the frozen-hydrated state. Specimen preparation for this method involves the following steps: First, a small droplet of the formulation is placed on a specimen table and rapidly frozen in liquid propane (-196℃). Then the samples must be rapidly cryo-transferred into a freeze-fracturing device, where the fracture is performed at low temperature under high vacuum. Due to this treatment, the sample will cleave along a fracture plain with the least cohesion. In case of an emulsion, for example, these are the hydrophobic areas of lipids stabilized by van-der-Waals forces, which are much weaker than the hydrogen bonds of the water domains. By further sublimation of ice to a depth of several nanometers, referred to as etching, structural details otherwise hidden in deeper ice layer can be additional exposed. This fracture plane is finally coated with a metal-carbon film before scanning electron microscopic inspection.

In principle, a scanning electron microscope detects electrons, emitted from an electron source, that are back-scattered from the specimen surface. To achieve this, the specimen surface must be coated with a layer of metal, for example platinum with a thickness of a few nm, to render the surface conductive. If the metal is evaporated unidirectional at a fixed angle, usually 45°, onto the specimen, a shadow effect is generated that gives the image a three dimensional appearance. A carbon film finally reinforces this metal layer. Fig.7 shows the SEM-micrograph of a representative o/w emulsion.

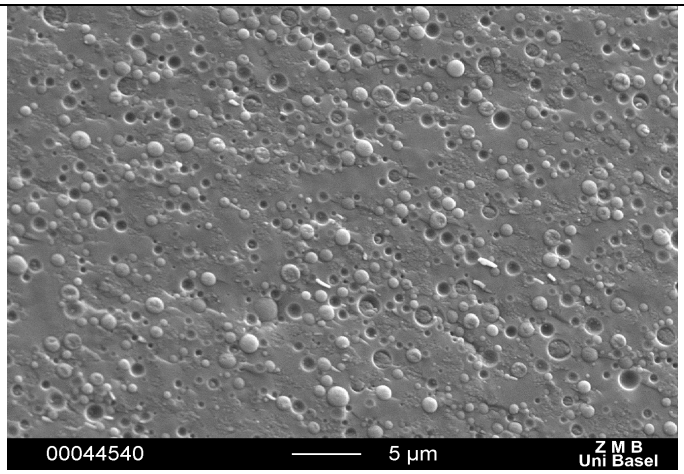


**Figure 7** SEM-image of a conventional oil in water emulsion

### C.3.2 Determination of the Formulation Type

There are several physical methods for distinguishing between the types o/w and w/o of dermatological vehicles, such as optical observation after blending the sample with a hydrophilic/lipohilic dye or simple dilution experiments with the oil or water bulk phase (2,29). The practical application of these methods, however, is commonly restricted to simple emulsions, since other dispersed systems are more complex in their composition and may contain coloured components, which may further complicate an explicit interpretation. A more precise method to test the type of a more phasic system is based upon electric conductivity measurements (9,29). Electric conductivity is a measure for movable particles with electric charge that can carry electricity when a difference of electric potential is placed across a conductor. The conductance *C* in Siemens (S) is the reciprocal of the resistance *R* in ohms (Ω) of the conductor

$$C = \frac{1}{R} \qquad (2)$$

The resistance *R* is given by

$$R = \rho \cdot \frac{l}{A} \qquad (3)$$

with $\rho$ as the specific resistance of the conductor, *l* denotes its length and *A* its cross-section area in $cm^2$. The specific conductance or electric conductivity $\kappa$ in S/cm is the reciprocal of the specific resistance and described by the term:

$$\kappa = C \cdot \frac{l}{A} \qquad (4)$$

To measure the electric conductivity of a dermatological formulation, a pair of electrodes, connected to an external electric source, with the distance *l* and a specific area *A* each, is immersed in the formulation. The ratio *l/A* is referred to as cell-constant of a specific measuring cell. If the water phase is continuous, a current will pass through the emulsion, while a continuous oil phase will fail the emulsion to carry the current. The electric conductivity of o/w formulations was found to be in the same order of magnitude to the bulk continuous phase (43).

### C.3.3 Particle Size Measurements

#### *C.3.3.1 Photon Correlation Spectroscopy*

Photon correlation spectroscopy (PCS) is a method that correlates time depended fluctuations of scattered laser light of particles in solution due to Brownian motion with their size. According to the Stokes-Einstein equation (Eq.5), the diffusion coefficient *D* ($m^2/s$) is inversely proportional to the mean hydrodynamic radius r of a particle in solution.

$$D = \frac{k \cdot T}{6 \cdot \pi \cdot r \cdot \eta} \qquad (5)$$

*T* denotes the absolute temperature, *k* is Boltzmann`s constant and *η* is solvent viscosity. In principle, the sample (dispersion) is irradiated by a laser beam and a photomultiplier assembly, commonly situated at an angle of 90° to the laser b eam, detects the scattered light. For small particles, the fluctuation of the scattered light will be faster due to their more rapid diffusional motion, compared to larger particles. In practice, a mathematical process is carried out in which the intensity of scattered light of an original signal is compared to subsequent time delayed signals, referred to as correlation. This process is described by a correlation function (Eq.5) that is computed during a PCS measurement:

$$g(\Gamma) = e^{-2DK^2\Gamma} \qquad (6)$$

with

$$K = \frac{4 \cdot \pi \cdot n}{\lambda} \cdot \sin\left(\frac{\theta}{2}\right) \qquad (7)$$

where, Γ denotes the delay time and *K* is the scattering vector that depends on refractive index of solvent *n*, wavelength of the laser beam *λ* and the detection angle *θ*. Finally, the hydrodynamic radius of the particles can be determined by inserting *D* (derived from Eq. 6) in the Stokes-Einstein equation (Eq.5). The dependence of the method on D, however, implements the upper limit of detectable particle sizes: fluctuation and sedimentation of the particles might not take place in the sample.

Another quality criterion that is obtained from PCS measurements is the polydispersity index (PI). This index describes the deviation between the theorectical auto correlation function of the calculated mean particle size and the correlation fuction adapted from the light scattering measurements. Hence, the PI is a measure for the size distribution of the sample. For a truly monodisperse particle suspension, the PI is 0. In practice, values between 0.03 and 0.06 are supposed to be monodisperse, while PCS measurements that give values above 0.5 are not analyzable (44).

### *C.3.3.2 Laser Diffraction Measurements*

PCS measurements give unsatisfactory results for larger particles because of the above mentioned limitation (see C.3.3.1). In such cases, laser diffraction (LD) measurements may be applied. Fig.8 shows a typical LD instrumentation that is commonly used for particle size measurements.

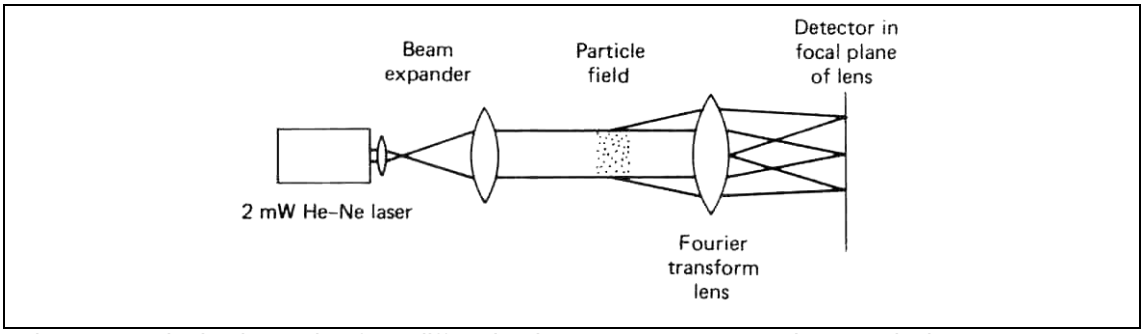


Figure 8 Optical schematic of LD diffraction instrument. From Barth, 1984 (45)

An unpolarized laser beam is spatially filtered, expanded and collimated. Particles are allowed to move across this beam. Diffracted and transmitted light are focused by a lense onto a detector that is in the focal plane of the lense. That detector consists of concentric light sensitive rings separated by equal thickness insulated gaps. In the middle of the detector plane – the optical axis of the laser beam - is a hole located in front of a photodiode. Smaller particles scatter a small, definite amount of light through a fixed, but larger, angle, while larger particles will scatter a greater amount of light through a smaller angle. This imposes typical spherical diffraction patterns that depend on the particle size which is calculated considering the distances of the diffracted light circles from the optical axis. According to a theory referred

to as Frauenhofer diffraction, the result for the intensity *I* of the diffraction pattern for a sphere of radius *r* is

$$I = I_0 \cdot \left[ \frac{2 \cdot J_1 \cdot (x)}{x} \right]^2 \qquad (8)$$

where $I_0$ is the intensity at the center of the pattern, $J_1$ is the first-order spherical bessel function, and *x* is given by

$$x = \frac{2 \cdot \pi \cdot r \cdot s}{\lambda \cdot F} \qquad (9)$$

where *s* is the radial distance in the detection plane as measured from the optical axis and *F* is the focal distance of the lense (45). In praxis, one should consider some fundamental facts understanding the meaning of the results of LD particle size measurements: (I) The result is volume based, (II) the result is expressed in terms of equivalent spheres and (III) the analyzed distribution is expressed in a set of size classes.

**C.3.4 NMR Diffusion Experiments**

Pulsed field gradient spin echo NMR (PFGSE-NMR) is an attractive technique to determine self-diffusion coefficients of formulation compounds that yields a vast amount of structural information without destroying the sample (5,46). Good correlation has also been demonstrated between transdermal drug delivery from various vehicles and the molecular mobility of the active ingredients in them (5). In principle, PFGSE-NMR uses pulse sequences that incorporate pulsed-field magnetic gradients. A gradient is generated that its strength varies linearly along the z-axis that is defined by the required constant magnetic field $B_0$ to align the nuclei-spins for a NMR experiment. For basic theory of NMR-spectroscopy it is referred to the literature (47). The strength of a gradient is experimentally defined in terms of its duration δ, its amplitude G and the gyromagnetic constant of the nucleus γ. In principle, the application of short gradient pulses (about 3ms) allows tracking the positions of the nuclei before (gradient encoding period) and after (gradient decoding period) a specific experimental diffusion time (about 100 ms to up to one second). In order to determine diffusion coefficients, different gradients are used to impose spatial dependent local (i.e. in the xyz coordinate) magnetic fields in the sample so that the signal intensity found after an encoding-decoding period depends on the strength of the gradient. The efficiency of decoding depends on how far the molecules diffuse in average through the sample; the greater the positional change due to diffusion, the poorer the decoding. Hence, self-diffusion of a molecule is directly related to the

decay of the signal intensities or peak areas in the recorded NMR spectra when the amplitude of the gradient pulses *G* is modulated according to

$$\ln \frac{I_g}{I_0} = -\gamma^2 \cdot \delta^2 \cdot G^2 \cdot (\Delta - \frac{\delta}{3}) \cdot D \qquad (10)$$

where, $I_g$ and $I_0$ are the intensities in the presence and absence of magnetic field gradient pulses, $\Delta$ the experimental diffusion time and *D* the diffusion coefficient. In order to receive undistorted high-resolution NMR spectra, however, optimized pulse sequences are required which may consider the number, direction and duration of the radio frequence (rf) pulse that is basis for NMR spectroscopy in general and/or the field gradients described above.

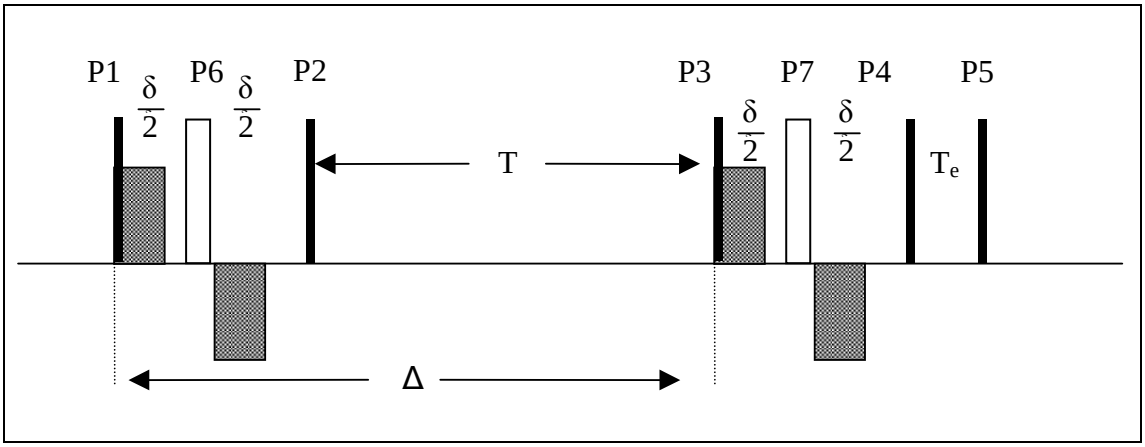


**Figure 9** Pulse sequence for NMR diffusion experiments. T denotes the effective diffusion time. P1,P2,P3,P4 and P5 are 90°pulses, and P6 and P7 are 180°pulses.

Fig.9 shows the pulse sequence that was applied to measure self-diffusion coefficients of sodium nicotinate and benzene in the present work. The rf pulse sandwich P1, P2, P6 is referred to as stimulated echo and allows the majority of the diffusion period to occur in the longitudinal (z) direction. $T_e$ describes an additional delay period after the decoding period of the experiment that allows so called eddy currents, induced by the magnetic fields of the field gradients, to dissipate before NMR signal detection. The rf pulses in combination with the alternating gradients (represented by the grey bars above and below the horizontal line in Fig.9) further improve the quality of the spectra. This special pulse sequence is referred to as bipolar pulse pair longitudinal eddy current delay (48).

### C.3.5 Ultracentrifugation

Ultracentrifugation can yield valuable information about the nature, the composition and, if the density is known, about the size of dispersed structures. This method is commonly applied for stability testing of emulsions (49,50) or for concentration and purification of liposomal formulations (51). Furthermore, ultracentrifugation was also used for structural characterisation of semisolid multi-phase formulations, typically in combination with further physicochemical methods (4,52).

An (ultra)centrifuge is an instrument designed to apply a rotational force to a mass (particle) and if the mass is unrestricted it will move away from the center of rotation. Hence, the acceleration of gravity $g$ is replaced by $\omega^2 x$, where $\omega$ is the angular velocity and $x$ is the distance of the particle from the center of rotation. Stoke`s law is accordingly modified to

$$v = \frac{dx}{dt} = \frac{2 \cdot r^2 \cdot (\rho - \rho_0) \cdot \omega^2 \cdot x}{9 \cdot \eta_0} \qquad (11)$$

where, $v$ is the velocity of sedimentation, $\rho$ and $\rho_0$ the density of the sedimenting spherical particle and the medium, respectively and $\eta_0$ the viscosity of the medium. The instantaneous velocity $v=dx/dt$ of a particle in a unit centrifugal field is expressed in terms of the Svedberg sedimantation coefficient $s$

$$s = \frac{dx/dt}{\omega^2 \cdot r} \qquad (12)$$

The force at which a centrifuge is operated is often expressed in terms of the number of times that the force of gravity is exceeded. For example, the ultracentrifuge Centricon T-1075 with the rotor TFT 7013 (Kontron Instruments, Mailand, Italy) used in the present work to fractionate the formulations produces a force in between 221290 and 448610 g, depending on the distance from the centre of rotation.

## C.4 Drug Delivery Across the Skin

The aim of drug application on the skin may be targeting the drug to three anatomical locations, namely the skin itself (topical delivery), deeper tissue layers (regional delivery) and the systemic circulation (transdermal delivery)(1). The advantage of topical or regional drug delivery is clear, because the treatment of the skin with a systemically applied drug may lead to adverse effects, and only a small fraction of the applied drug will reach the target site. But there are also reasons to favor the transdermal route in systemic drug delivery. Transdermal drug delivery circumvents variables that rest on the anatomical and physiological properties along the gastrointestinal tract, for example pH gradient and nutrition, and the first pass metabolism is bypassed. Furthermore, the use of special drug delivery systems (for example Transdermal Therapeutic Systems, TTS) provides controlled administration and duration of drug action. The quantity of available drugs that may be candidates for the transdermal delivery route, however, is limited by several factors. The amount of permeable drug is limited by the skin barrier properties and the physicochemical properties of the penetrant, which allow only very potent drugs as possible candidates for transdermal administration. Furthermore, the drug of choice must be compatible with the matrix of the delivery system that should not irritate or sensitize the skin itself (53).

Three drug related processes must be taken into consideration when a drug preparation is applied on the skin: (I) The release of the penetrant from the vehicle, followed by (II) its penetration through the different skin barriers and (III) its activation of the desired pharmacological reaction. Fig.10 gives an overview about the drug flux that may arise following application of a suspension vehicle. The drug may undergo any or all of the following events. First, the drug molecules must dissolve to enable its diffusion through the vehicle to the vehicle-stratum corneum interface. For the drug to move trough the skin it must partition into the stratum corneum and diffuse within this almost impermeable layer. Some drug may bind at so-called depot-site; the remainder diffuses to deeper tissues of the epidermis, meets a second interfacial layer and partitions in the viable epidermis (54).

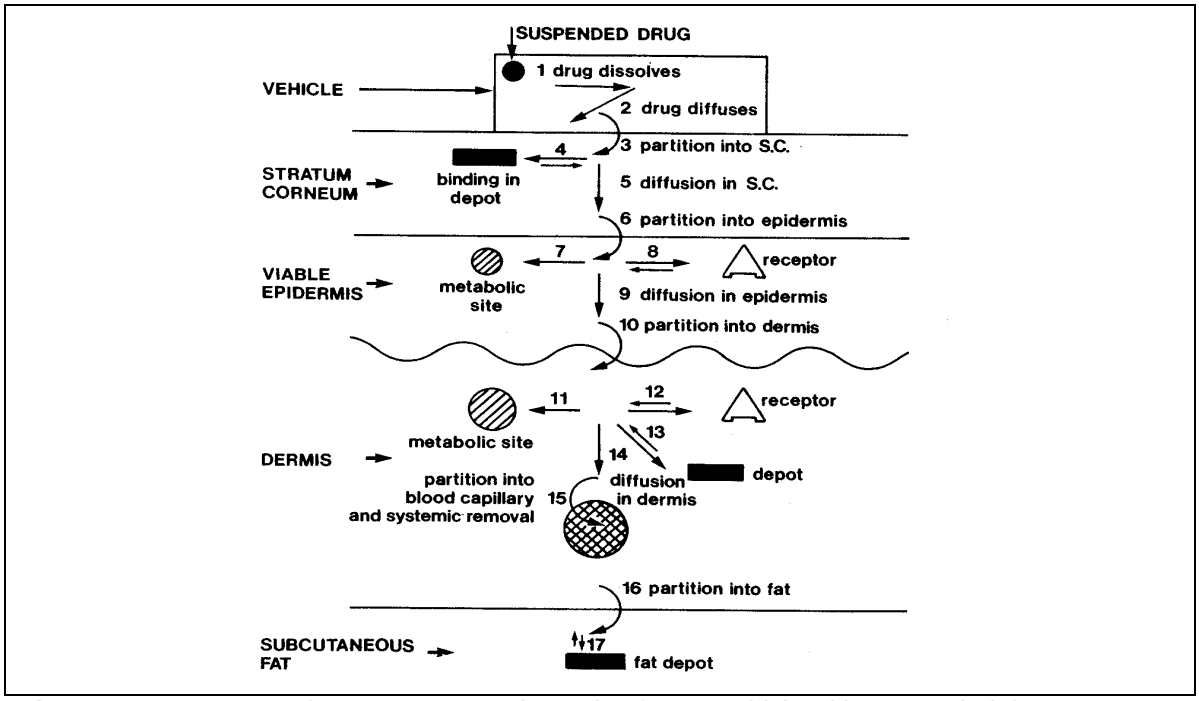


**Figure 10** Some stages in percutaneous absorption from a vehicle with suspended drug. From Barry, 1983 (54)

For most hydrophilic and amphiphilic penetrants, diffusion through the stratum corneum will be the rate-limiting step in percutaneous absorption, whereas lipophilic substances are favored to penetrate this layer. If very lipophilic drugs are used, however, the viable epidermis can act as a rate-limiting factor in permeation across the skin (53). In this case, clearance rate from the barrier will govern percutaneous absorption, while the thermodynamic activity in the vehicle may approach that in the viable epidermis directly below the barrier (55).

The amount of drug permeated through the skin per unit time and unit area is defined as the drug flux J, that is described by Fick`s first diffusion law:

$$J = \frac{dm}{dt \cdot A} = -D \cdot \frac{dc}{dx} \qquad (13)$$

where *m* denotes the drug amount, *t* the time, *A* the effective diffusion area and *D* the diffusion coefficient ($cm^2/s$). *dc/dx* is the concentration gradient over a distance. Assuming the conditions of a perfect sink (receiver concentration negligible, therefore zero) an infinite donor concentration $C_D$, rate limiting membrane (skin) diffusion and partition between donor vehicle and rate limiting membrane, Eq.13 can be expressed as:

$$J = \frac{dm}{dt \cdot A} = -D \cdot \frac{K \cdot C_D}{h} \qquad (14)$$

*K* represents the distribution coefficient of the diffusant between the vehicle and the membrane (skin) and *h* is the thickness of this membrane. Because an exact determination of *h* and *D* is difficult, these parameters may be summarized in term of the permeability coefficient *P* (cm/s):

$$P = D \cdot \frac{K}{h} \qquad (15)$$

The permeability coefficient can be regarded as a characteristic for a specific substance-membrane system and is, beside the drug flux and the totally permeated drug amount after a specific time, a common measure for steady state drug permeation.

### C.4.1 Permeation Routes

The permeation of drugs through the skin includes the diffusion through the intact epidermis and trough skin appendages, for example sweat glands and hair follicles. However, the appendages occupy only 0.1% of the human skin surface so that the contribution of these shunt pathways to transdermal permeation is usually considered to be small (56). Only an increasing molecular weight of the penetrant may lead to a significant role of the appendageal route (57).

As mentioned in chapter C.1.2, the stratum corneum represents the main barrier of the skin. Theoretically, there are two pathways through this layer (Fig.11): A transcellular (across the corneocytes and the lipid matrix) and an intercellular way (via the intercellular lipid domains between the corneocytes). In both cases, however, the permeant has to pass the intercellular lipid matrix.

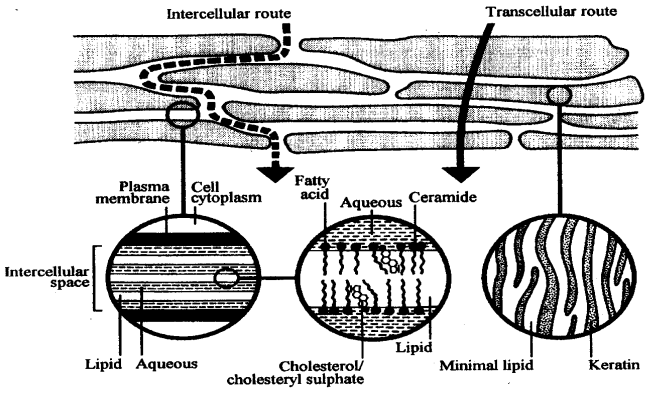


**Figure 11** Permeation routes through the stratum corneum. From Moghimi, 1999 (58)

Intercellular lipids are arranged in multiple layers, containing both, polar and nonpolar components. This suggests that hydrophilic and lipophilic penetrants diffuse through different domains in the lipid matrix. The transcellular pathway is generally the unfavoured route for a drug to permeate through the stratum corneum because of the high diffusional resistance of

the cornified cells (59). Only hydrophilic molecules such as water or short-chain alcohols seem to prefer the transcellular pathway (55).

### C.4.2 Factors Affecting Drug Permeation Through the Skin

Several biological and physicochemical parameters may influence drug permeation across the skin (54). The physicochemical factors that control the passive diffusion of a substance from a vehicle into and across the skin are determined by the molecular properties of the substance, the vehicle and the skin. Hence, the following interactions may have impact on drug delivery: drug-skin, vehicle-skin, drug-vehicle and drug-vehicle-skin. Alterations the vehicle may undergo after application, commonly due to evaporation of volatile components, represent a further crucial parameter that may affect drug permeation.

The biological factors include skin age, body region, metabolism and hydration. At different body sites, the composition and finally barrier properties of the stratum corneum may vary, what includes differences in its thickness, number of cells or, sometimes overemphasized- the density of skin appendages (60). Especially the viable epidermis contains several enzyme systems that may catalyze processes such as oxidation, reduction, hydrolysis or conjugation. Therefore skin metabolism may have additional impact on transdermal delivery of drugs. The effect of age is rather due to the smaller surface-to-volume ratio in case of newborn infants compared with adults than an effect of lower barrier function of younger skin (53). Skin hydration is a crucial and possibly the most frequently investigated factor affecting drug permeation. In practice, there is often a combination of these factors that contribute to (trans-) dermal drug permeation.

#### *C.4.2.1 Skin Hydration and Occlusion*

The normal degree of hydration of the stratum corneum is between 10 to 30% of its own weight (see also C.1.2). Occlusion hydrates the keratin in corneocytes and increases the water content between adjacent intercellular lipid lamellae. For hydrophilic substances, released from an aqueous delivery device, the partition coefficient between stratum corneum and the vehicle increases up to unity (54). Furthermore, skin temperature generally increases form 32℃ to as much as 37℃ under occlusive conditions. Of various approaches employed to enhance the percutaneous absorption of drugs, occlusion is the simplest and perhaps one of the most common methods in use. Beside obvious improved penetration of hydrophilic drugs, however, a trend of occlusion-induced penetration enhancement with increasing penetrant lipophilicity is also apparent. A possible explanation is that hydration magnifies the aqueous regions of the intercellular lipid domains, increasing the hydrophilic character of the stratum corneum. It follows that this, in turn, leads, to a reduction in the stratum corneum- viable epidermis distribution coefficient. This finally favors the kinetics of transfer of penetrants from the stratum

corneum to the viable epidermis. The limit of this mechanism of enhancement would be a complete insolubility of the penetrant in the aqueous phase of the stratum corneum or sterically hindered penetration of the substance, for example due to large molecular size (61). However, a number of studies have shown that hydration-induced skin permeation enhancement appears to be not only a function of lipophilicty and hydrophilicity but also seems to be chemical class dependent (62,63).

### *C.4.2.2 Evaporation of Volatile Vehicle Compounds Following Application*

In clinical and experimental situations, most dermatological vehicles undergo considerable changes following application to the skin, most likely due to evaporation of volatile components, supported by mechanical agitation associated with application of the product (1). It is obvious that such an alteration in vehicle composition, which may increase the activity of a drug in the residual vehicle phase, is possibly necessary for adequate, although generally low, percutaneous absorption and efficiency. Most studies on this aspect report on the changes in solvent concentration after application, often investigated with volatile solvent mixtures. An early work of Coldman et al. showed that volatile solvent systems could be used to generate states with increased thermodynamic activity (supersaturation) that lead to an increased percutaneous absorption when compared to saturated solutions (7). Chiang et al. investigated the permeation of minoxidil form water/ethanol/propylene glycol mixtures as volatile vehicles what confirmed the work of Coldman (16). They further report on drug precipitation that leads to a markedly depression of drug delivery relative to the supersaturated state. An interesting publication reports on a drug delivery device where the evaporation of ethanol from an ethanol-water mixture increased the vehicle-skin partition coefficient of the active substance, compensating for the loss of drug due to skin permeation (64). The consequence is a near zero order flux over the entire application time and an absence of a large excess of drug in the donor reservoir. To summarize, the evaporative concentration effect may even force the drug out of the solution and superimpose a dissolution dependency in the delivery rate.

Other investigations focus more detailed possible changes dermatological formulations may undergo following application, but without correlating the observations with drug delivery (17,18,65). The general, but valuable conclusion of these studies is that respective phase diagrams may reflect the arising structures during evaporation.

The dependence of drug delivery on alterations dermatological formulations comprising coarse and colloidal structures undergo due to evaporation of volatile components, however, does not appear to have been considered to any great extent in the literature. Mueller-Goymann and Alberg related evaporative changes of water containing hydrophilic ointment that was modified by incorporation of ethanol with permeation of hydrocortisone-21-acetate in vitro (66). They reported on a reduced loss of volatile components after the incorporation of ethanol, likely due

to fixation of the alcohol in the microstructure of the ointment. The liberation kinetics across an artificial membrane could be related to the arising drug concentration, but permeation kinetics, however, was equal from both formulations. This was accredited to penetration enhancing effects of the ethanol. The effect of percutaneous absorption of hydrophilic model drugs on the emulsion type after non-occlusive finite dose application is presented by Ferreira et. al (67). Hummel and Imanidis demonstrated that obviously varying in-vitro skin permeation of ibuprofen from several non-occlusively applied multi-phasic dermatological formulations was only governed by the continuous phase drug concentration of the vehicles, independently of existing dispersed structures. The back diffusion of the lipophilic model drug into the dispersed phases compensated for the influence of the rising overall drug concentration due to evaporation of volatile components, so that linear drug flux with time was observed (4).

#### *C.4.2.3 Drug-Skin Interactions*

Potential interactions of the active ingredient with the skin include hydration effects and binding of the drug to tissue components. It is possible that some drugs, which can rapidly penetrate the skin to yield tissue concentrations that are high enough exert an osmotic effect, may increase skin hydration (54). The so-called reservoir effect of topical steroids represents a common example that involves drug-stratum corneum binding. This effect, however, is not restricted to this substance class. Nicotine, caffeine or cationic β-blocking agents are also reportedly retained in the skin after application, followed by a delayed release (68). Another drug-skin interaction is proposed by Al-Saidan, who reports on a self-permeation enhancement of ibuprofen, likely due to disruption of stratum corneum barrier (69).

#### *C.4.2.4 Drug-Vehicle Interactions*

Drug vehicle interactions include the thermodynamic activity of the drug in the vehicle that is related to solute drug concentration in the vehicle and the activity of the drug. The maximum drug transfer into the skin takes place when the vehicle is saturated with the drug at the vehicle-skin interface (1). In this situation, the thermodynamic activity is 1. In some cases, however, thermodynamic activity may be > 1, for example in a supersaturated state due to vehicle evaporation (see C.4.2.2). Hence, when the system deviates from ideality, the concentration must be replaced by activity $\alpha_D$

$$\alpha_D = \gamma_D \cdot C_D \qquad (16)$$

where, $C_D$ denotes the donor concentration and $\gamma_D$ is the activity coefficient. Schwarb et al. reported on a supra-proportionally increased flux of fluocinonide through a silicon membrane with increasing drug concentration, likely due to increasing thermodynamic activity, while in

vivo skin penetration of the drug was only increased by the factor of which the magnitude of concentration in the respective formulation was increased (6).

A further drug-vehicle interaction that may affect drug permeation is the formation of ion pairs of charged drugs with counter ions present in the vehicle. Valenta et. al. found that fluxes of charged lignocaine salts were significantly increased in the presence of organic counter ions, while inorganic salts did not influence the permeation kinetic (70). Several publications that deal with cationic substances and fatty acids as counter ions support this ion pair approach as a possible permeation enhancing effect of the fatty acids (71,72). Furthermore, in some cases drug permeation through the skin is not governed by the impermeability of the stratum corneum, for example when the horny layer is damaged or drug diffusion within the vehicle is exceptionally slow. In such a case, the release rate of the drug from the vehicle provides the rate-limiting step in overall diffusion, and the skin functions as a perfect sink (73).

#### *C.4.2.5 Vehicle-Skin Interactions*

Despite the fact that a drug delivery vehicle should be `inert`, especially vehicles commonly used for topical treatment reportedly have additional effects to the requirement that it should readily release the active moiety for the therapeutic effect (1). The application of pharmaceutical vehicles, such as gels, emulsions, creams or ointments, may superimpose further changes of the integument and finally may affect its permeability. This mechanism of action will probably be a solvent action on the stratum corneum, a hydration effect or a temperature effect (54). The hydration effect is generally due to occlusion effects of the vehicle. Thus, it is obvious that oily materials retard more efficient moisture loss from the skin than for example hydrogels or oil in water emulsions. A detailed description of hydration effects and its influence on skin permeation is given in chapter C.4.2.1. Furthermore, under occlusion or under the influence of a cooling vehicle, the skin temperature may increase or decrease a few degrees, which may affect the diffusion coefficient of a substance due to its temperature dependence. However, any consequent altered permeability is small compared to the more dramatic effect which the resultant increased hydration causes (54). An auspicious tool to improve cutaneous delivery rate is the application of appropriate vehicles, such as microemulsions or liposomes, which may reduce skin barrier function due to direct interaction with the stratum corneum, or to include molecules in the delivery device that may reversibly reduce the barrier resistance of the skin. Such entities are known as penetration enhancers.

### *C.4.2.6 Mode of Action of Penetration Enhancers*

Three permeation enhancement strategies may be postulated based on Ficks first law (see C.4): (i) reducing diffusional resistance, that increases the diffusion coefficient D, (ii) increasing the partition coefficient K between the stratum corneum and the vehicle, and (iii), increasing the concentration in the vehicle $C_D$. Disordering the extracellular stratum corneum lipid matrix can increase the diffusion coefficient. Oleic acid, for example, has been shown to induce phase separation in the stratum corneum lipid domains which results in reduced barrier function (74). Azone, dimethyl sulfoxide (DMSO) and different terpenes are other agents that may provoke lipid disorder in the stratum corneum and hence may increase drug diffusivity (56). Another mode of action is to increase drug solubility in the skin and hence increase the partition coefficient between the stratum corneum and the vehicle. Enhancers that may act in this way are propylene glycol, ethanol, transcutol and N-methyl pyrrolidone (75). Fig.12 represents postulated sites for penetration enhancers to act in the intercellular domain, which is probably their most crucial location of action. An interaction with the polar head groups of the lipids, site A in the diagram, will lead to a disturbing of the hydration spheres and alterations in the head group interactions should upset the packing plane.

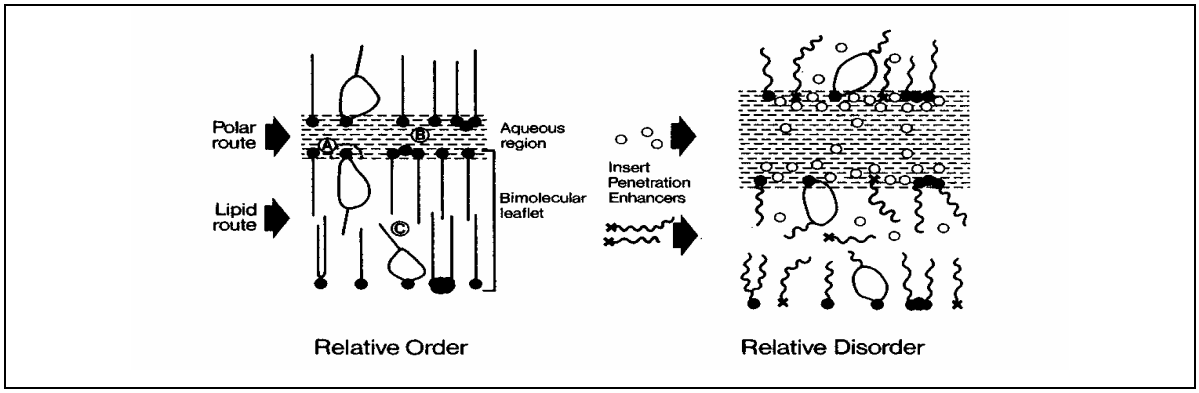


**Figure 12** Postulated sites for penetration enhancers to act in the intercellular domain, from Barry, 1987 (76)

This mechanism should promote the diffusion of polar penetrants due to increased fluidity of the domain that, in turn, allows more aqueous fluid to enter the tissue, increasing the water volume between the lipid bilayers. A second important feature is that a disrupter of the interfacial structure will tend to reflect into an alteration of the packaging of the lipid tails. The hydrophobic route thus becomes more disordered and more readily to be traversed by a lipophilic penetrant (site C in the diagram). Additional effects of an accelerant on the aqueous region may change temporarily the bulk constitution of the domain. For example, high enough concentrations of ethanol may penetrate into the aqueous region of the tissue to alter the solubilizing ability of this site, so that the operational partition coefficient now favors a higher drug concentration in the skin. Many penetration enhancers should, because of their structure,

insert between the hydrophobic tails of the intercellular lipid bilayers (site C in the diagram), so upsetting their packaging, increasing their fluidity and thus permitting easier diffusion of lipid penetrants. The changed lipid packaging can reflect back to cause some disorder in the polar head group region and so improve polar route penetration. (76).

### *C.4.2.7 Mode of Action of Microemulsions*

Even though numerous individual studies of structure, self diffusion coefficients of compounds, formation and transdermal delivery performance of various microemulsion systems have been published, little is known about the correlation between these parameters (5,8,9,10,11). However, two basic trends are observed from the reported studies that may contribute to the favorable drug delivery properties of microemulsions: high drug load capacity and penetration enhancer effects. High drug load capacity increases drug flux due to a larger concentration gradient, which is more drug-vehicle interaction than vehicle-skin interaction. A possible explanation for favored penetration enhancer effects of microemulsions, compared to conventional vehicles such as emulsions, is that microemulsions include ultra low interfacial tension between lipophilic and hydrophilic domains. This ensures an excellent surface contact between the skin and the vehicle constituents over the entire application area. As consequence, amphiphilic and lipophilic ingredients may reach the stratum corneum more easily and, hence, they may interact with stratum corneum lipids as discussed above for penetration enhancers (see chapter C.4.2.6). Furthermore, the high content of lipophilic and aqueous phase, which are assumed to fluctuate continuously, facilitates transition of both lipophilic and hydrophilic drugs from the-typically hydrophilic-vehicle to the lipophilic stratum corneum (5). However, the uncertainty about the exact microstructure of microemulsion systems makes it difficult to link their structure accurately to their drug delivery abilities, which may be further complicated by their possible dynamic, continuously fluctuating nature.

### *C.4.2.8 Mode of Action of Liposomal Vesicles*

Even though liposomes have been proposed to penetrate the skin, the use of liposomal vesicles is one of the most controversial methods to increase drug transport across the skin (22). Mezei and Gulasekharam published the first work on interactions between liposomal vesicles and skin (13). They reported that the application of drugs with liposomes favored the deposition of the active moiety in the epidermis and dermis. Although they strongly suggested that the vesicles penetrated the skin, this implication was received with a lot of skepticism and initiated a number of studies. Two publications from 1984 and 1985, however, could not confirm intact liposome penetration as suggested by Mezei and Gulasekharam (77,78). Verma et al. investigated the penetration of a hydrophilic fluorescence probe, carboxyfluorescein, that enabled a confocal laser scanning microscopy study of the skin after treatment with a liposomal vehicle (12). The results lead them to assume that the vesicles increase the skin

penetration of entrapped and non-entrapped carboxyfluorescein. Other studys showed that only vesicles with proper composition may penetrate the skin, as reported by Cevc, 2004, who introduced Transfersomes® (15). Transfersomes® are sufficiently deformable vesicles due to incorporation of additives in the bilayer. These much more deformable vesicles may squeeze themselves into the smallest pores. Touitou et al., 2000, developed a new system in which liposomes are combined with ethanol, referred to as ethosomes (14). Most probably the ethanol decreases the interfacial tension of the vesicles and, thus, makes them more deformable and elastic, as described for the Transfersomes® above. Additionally, the ethanol itself may disturb the stratum corneum lipids, facilitating a synergistic mechanism with the ethosomes by virtue of their deformable particulate nature. A former study of the same group compared liposomal vesicles with penetration enhancers (79). Interestingly, they observed that liposomes could act as an excellent reservoir in the skin, while penetration enhancers increased the drug transport across the skin. Other authors claim that skin treated with liposomes reveals vesicle fusion. This yields a structural breakdown of the liposomal bilayer. Hence, fusion of the phospholipids with the intercellular lipids of the stratum corneum may induce ultrastructural changes in this region with the consequence of reduced skin barrier function (80). Phospholipids, however, may exist, depending on the temperature and the nature of their fatty acid chains, in a highly ordered state, the gel-state, or a state where the individual lipid molecules possess greater freedom of motion, the liquid crystalline state. Hence, it may also be a crucial factor if gel state or liquid state liposomes are applied on the skin. From several studies, a trend can be observed that the more flexible liquid state liposomes are favoured to penetrate the skin (81,82). To summarize, in spite of the great number of investigations in order to examine the mode of action how liposomes interact with the skin, it is still not well understood whether they penetrate as entire liposomes or not.

### C.4.3 In-Vitro Permeation Experiments

Different in-vitro methods to test percutaneous absorption are offered in the literature, for example the isolated perfused bovine udder (83) or the perfused pig ear (84). However, diffusion experiments across excised human or animal skin are the most common methods in use. The advantage of such in-vitro methods is, in addition to the avoidance of animal experiments or expensive and time consuming experiments in-vivo in human, that the investigator may control the experimental environment and so elucidate individual factors that modify drug penetration. The most commonly used diffusion system is the diffusion cell described by Franz, where the membrane is mounted horizontally in the diffusion cell (85). The chamber beneath the membrane holds the receptor fluid that may be collected frequently through a side arm for analysis (Fig.13). Two advantages of this experimental setup over other in-vitro testing systems in order to simulate clinical situations are obvious; (I) It allows to apply

the delivery vehicle non-occlusively and (II) it allows to apply a small amount of donor vehicle (finite dose).

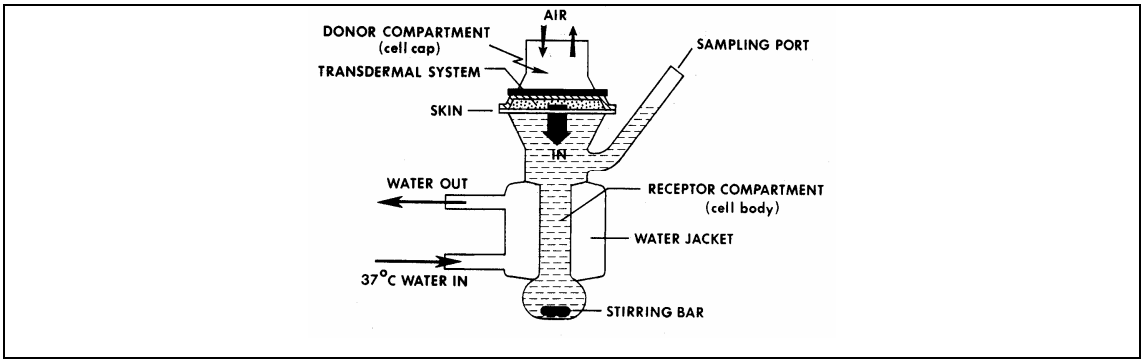


**Figure 13** Diagrammatic illustration of a Franz diffusion cell, from Chien, 1987 (86)

### *C.4.3.1 Membranes for In-Vitro Permeation Experiments*

In-vitro release testing through a membrane with negligible diffusional resistance can, in principle, reveal a lot about the physical attributes (solubility, microscopic viscosity, emulsion state, ect.) of a semisolid dosage form. Hence, such liberation experiments serve primary as a quality control tool to ensure batch to batch reproducibility. The kinetic and thermodynamic processes underlying the release of drugs from dermatological formulations, however, usually differ in fundamental ways from the processes that determine the partition and uptake of the drugs from clinical application of the same dosage form (87). The lipoidal nature of the stratum corneum suggests that lipophilic membranes may provide better in-vitro models for permeation studies. Silicon membranes are of particular interest in this context (88). Undoubtedly, the best membrane for studying transdermal drug diffusion in vitro is excised human or animal skin (73).

### *C.4.3.2 Pig Ear Skin*

Porcine skin is a well-accepted and readily available model for human skin and is often used to assess dermatological formulations in-vitro, for what excised skin from the pig ear has become increasingly used for this purpose (89). Lopez et al. investigated the composition and structure of pig stratum corneum based on the action of different solubilizing agents (90). They report on strongly similar lipid composition and structural organisation of the pig stratum corneum as emphasized in chapter C.1.2 for human stratum corneum. Sekkat et al. evaluated stratum corneum barrier function of pig skin in-vitro during its progressive removal by adhesive tape stripping using the technique of transepidermal water loss and impendance spectroscopy (89). Comparing the results with in-vivo data obtained from human strongly supports the validity of the porcine membrane as good in-vitro model. Table 3 gives the fluxes of four model compounds of widely varying polarity through various skin membranes that are commonly used for in vitro investigations. It is obvious that pigskin appears as the most suitable model for

human skin. Somewhat unexpected, Skinethic™ HRE, a human reconstructed epidermis model that recently has attracted interest as an alternative for excised human epidermis, is much more permeable for all investigated compounds.

**Table 3** Permeation rate (flux) of different test compounds measured with various skin membranes in vitro

| Skin | Terbinafine[a] | Clotrimazole[a] | Hydrocortisone[a] | Salicylic acid[b] |
|---|---|---|---|---|
| Human | 0.01 | 0.02 | 0.023 | 21.9 |
| Domestig Pig | 0.01 | 0.02 | 0.011 | 12.7 |
| Rat | 0.55 | 0.055 | 1.16 | 24.2 |
| Skinethic™ HRE | 0.37 | 18.8 | 5.29 | 152.8 |

Test compounds were applied as a 1% solution in [a]propylene glycol, [b]Propylene glycol/water 9/1. Values denote µg/cm$^2$/h. Modified from Schmock et al., 2001 (91)

### *C.4.3.3 Assessment of Skin Barrier Integrity*

There are three commonly used techniques to establish the barrier integrity of skin. (I) Measurement of the transepidermal water loss, (II) tritiated water permeability measurements and (III) electric resistance measurements (92,93). The application of a Tewameter for the determination of the transepidermal water loss provides a noninvasive and rapid alternative to tritiated water permeation for assessing skin barrier functions. The principle of the measurement is based upon an open chamber system with two humidity and two temperature sensors, placed at 2 and 4 mm distance from the skin surface. This measurement setup allows to estimate the evaporation gradient on the skin surface, which is described by Fick`s first diffusion law:

$$\frac{dm}{dt} = -D \cdot A \cdot \frac{ds}{dl} \qquad (17)$$

where *dm/dt* denotes the diffusion stream across the open chamber, expressed as transported mass of water per time. *A* is the exposed area and *ds/dl* the change of the density over the entire distance. D is the diffusion coefficient of water vapour in the air. Common values for the transepidermal water loss vary widely, depending on the body site and environmental conditions. Disturbance of the integrity of the skin barrier, however, leads to drastically increase in the loss of endogenous water (94).

### *C.4.3.4 Skin-Vehicle Distribution Coefficient*

The dominant role, which the distribution coefficient of a penetrant between a specific vehicle and the stratum corneum may play in controlling the steady state drug flux across the skin is emphasized in chapter C.4.2.6. Common methods to estimate partition coefficients are based

upon equilibrium partitioning experiments. Typically, isolated, accurately weighted stratum corneum pieces are incubated with the specific substance dissolved in the vehicle. Hence, distribution coefficients may be derived from quantification of the remnant in the vehicle or from analyzing the drug amount within stratum corneum after extraction with a suitable solvent (95,96). According to these authors, a common method to isolate stratum corneum is based upon the treatment of excised skin with trypsin solution for several hours. Then, the stratum corneum may be carefully peeled off from the underlying epidermal cells and, after treatment with trypsin inhibitor solution to prevent further degradation, dried and stored in a desiccator over silica gel.

## C.5 References

(1) C. Surber, E.W. Smith, The Mystical Effects of Dermatological Vehicles, Dermatology, 210 (2005) 157-168.

(2) S.R. Farinato, L.R. Rowell, Optical properties of emulsions, in: P. Becher (Ed.), Encyclopedia of emulsion technology, Basic Theory, Vol. 1, Marcel Dekker, New York, 1983, pp. 439-479.

(3) C. Schutz, Microemulsion: Distinctive combination of perfect invisibility and extreme performance, SÖFW-J. 129(8) (2003) 16-19.

(4) D. Hummel, G. Imanidis, in: R. Marks, J.-L. Leveque, R. Voegeli, (Ed.), The Essential Stratum Corneum, Martin Dunitz, London (2002)119-124.

(5) M. Kreilgard, Influence of microemulsions on cutaneous drug delivery, Adv. Drug Del. Rev. 54 Suppl.1 (2002) 77-98.

(6) F.P. Schwarb, G. Imanidis, E.W. Smith, J.M. Haigh, Ch. Surber, Effect of concentration and degree of saturation of topical fluocinolide formulations on in vitro membrane transport and in vivo availability on human skin. Pharm. Res. 16(6) (1999) 909-915.

(7) M.F. Coldman, B.J. Poulsen, T. Higuchi, Enhancement of percutaneous absorption by the use of volatile : nonvolatile systems as vehicles, J. Pharm. Sci., 58 (1969) 1098-1102.

(8) Ph.J. Lee, R. Langer, P.V. Shastri, Novel Microemulsion Enhancer Formulation for Simultaneous Transdermal Delivery of Hydrophilic and Hydrophobic Drugs, Pharm. Res. 20(2) (2003), 264-269.

(9) M.B. Delgado-Charro, G. Iglesias-Vilas, J. Blanco-Méndez, M.A. Lopez-Quintela, J.P. Marty, R.H. Guy, Delivery of a hydrophilic solute through the skin from novel microemulsion systems, Eur. J. Pharm. Biopharm. 43 (1997) 37-42.

(10) U. Schmalfuss, R. Neubert, W. Wohlrab, Modification of drug penetration into human skin using microemulsions. J. Control. Release 46 (1997) 279-285.

(11) F. Dreher, P. Walde, P. Walther, E. Wehrli, Interaction of a lecithin microemulsion gel with human stratum corneum and its effect on transdermal transport, J. Control. Release 45 (1997) 131-140.

(12) D.D. Verma, S. Verma, G. Blume, A. Fahr, Lipososmes increase skin penetration of entrapped and non.entrapped hydrophilic substances into human skin: a skin penetration and confocal laser scanning microscopy study, Eur. J. Pharm. Sci. 55 (2003) 271-277.

(13) M. Mezei, V. Gulasekharam, Liposomes-a selective drug delivery system for the topical route of administration. I. Lotion dosage forms, Life Sci. 26 (1980) 1473-1477

(14) E. Touitou, N. Dayan, L. Bergelson, B. Godin, M. Eliaz, Ethosomes-novel vesicular carriers for enhanced delivery: characterisation and skin penetration properties, J. Control. Release 65 (2000) 403-418.

(15) G. Cevc, Lipid vesicles and other colloids as drug carriers on skin. Adv. Drug Del. Rev. 56 (2004) 675-711.

(16) C.M. Chiang, G.L. Flynn, N.D. Weiner, G.J. Szpunar, Bioavailability assessment of topical delivery systems: Effect of vehicle evaporation upon in vitro delivery of minoxidil from solution formulations, Int. J. Pharm. 55 (1989) 229-236.

(17) S.E. Friberg, H. Tian, P.A. Aikens, Phase changes during evaporation from a vegetable oil emulsion stabilized by a polyoxyethylene (20) sorbitanoleate, Tween 80, Coll. And Surf. A, 121 (1996) 1-7.

(18) A. Al-Bawab, S.E. Friberg, Phase behavior of the α-hydroxyoctanoic acid /Laurth 4/white oil/water system and preliminary evaluation of the phase changes during evaporation of its emulsion. J.Cosmet.Sci. 53 (2002) 151-164.

(19) B.W. Barry, Formulation of dermatological vehicles, In: B.W. Barry (Ed.), Dermatological Formulations Percutaneous absorption, Marcel Decker, New York, 1983, pp. 297-350.

(20) N. Leveque, S. Makki, J. Hadgraft, Ph. Humbert, Comparison of franz cells and microdialysis for assessing salicylic acid penetration through human skin, Int. J. Pharm. 269 (2004) 323-328.

(21) H. Schaefer, T.E. Redelmaier, Strucure and Dynamics of the skin Barrier., In: H. Schaefer, T.E. Redelmaier (Ed.) Skin barrier. Principles of Percutaneous Absorption, Karger, Basel, 1996, pp. 1-42.

(22) J.A. Bouwstra, P.L. Honeywell-Nguyen, Skin structure and mode of action of vesicles, Adv. Drug Del. Rev. 54 Suppl.1 (2002) 41-55.

(23) G.K. Menon, New insights into skin structure: scratching the surface. Adv. Drug Del. Rev. 54 Suppl.1 (2002) 3-17.

(24) K.S. Stenn, The Skin. In: L. Weiss, Histology, Cell and Tissue Biology, Elsevier Science, New York, 1983 pp. 569-606.

(25) E. Candi, R. Schmidt, G. Melino, The cornified envelope: A model of cell death in the skin, Nature Rev., Molecular Cell Biology 6 (2005) 329-340.

(26) A.V. Rawlings, I.R. Scott, C.R. Harding, P.A. Bowser, Stratum corneum moisturization at the molecular level, J. Invest. Dermatol. 103 (1994) 731-740.

(27) J.M. Nitsche, T.-F. Wang, G.B. Kasting, A two phase analysis of solute partitioning into the stratum corneum, J. Pharm. Sci., 95(3) (2006) 649-666.

(28) D. Myers, Emulsions, In: D.Myers (Ed.), Surfaces, Interfaces, and Colloids: Principles and Applications, Second edition, Wiley, VCH, Weinheim, 1999, pp. 253-294.

(29) A. Martin, Coarse dispersions, In: A. Marrtin (Ed.), Physical pharmacy, Fourth edition, Lea&Febiger, Philadelphia, 1993, pp. 477-511.

(30) A.D. Bangham, M.M. Stanish, J.C. Watkins, Diffusion of univalent ions across the lamellae of swollen phospholipids, J. Mol. Biol. 13 (1965) 238-252.

(31) D.D. Lasic, Introduction, In: D.D. Lasic (Ed.), Liposomes from physics to applications, Elsevier Science B.V., Amsterdam, 1993, pp. 3-7.

(32) R.R.C. New, Introduction, In: Liposomes a practical approach, IRL Press, Oxford, 1990, pp. 1-30.

(33) Lasic, D.D., 1993a. Structure of amphiphilic aggregates, In: Liposomes from physics to applications, Elsevier Science B.V., Amsterdam, 1993, pp. 43-62.

(34) D.D. Lasic, Preparation of liposomes, In: Liposomes from physics to applications, Elsevier Science B.V., Amsterdam, 1993, pp. 63-107.

(35) S. Batzri, E.D. Korn, Single bilayer liposomes prepared without sonification, Biochim. Biophys. Acta, 298 (1973) 1015-1019.

(36) T.P. Hoar, J.H. Schulman, Transparent water and oil dispersions: Oleophatic hydromicelle, Nature, 152 (1943) 102-103.

(37) J.H. Schulman, W. Stoeckenius, L.M. Prince, L.M., Mechanism of formation and structure of microemulsions by electron microscopy. J. Phys. Chem. 63 (1959) 1677-1680.

(38) R. Aboofazeli, M.J. Lawrence, Investigations into the formation and characterisation of phospholipid microemulsions: I. Pseudo ternary phase diagrams of systems containing water-lecithin-alcohol-isopropyl myristate, Int. J. Pharm., 93 (1993) 161-175.

(39) I. Stoye, K. Schröder, C.C. Müller-Goymann, Transformation of a liposomal dispersion containing ibuprofen lysinate and phospholipids into mixed micelles-physico-chemical characterisation and influence on drug permeation through excised human stratum corneum, Eur. J. Pharm. Biopharm. 46 (1998) 191-200.

(40) R. Brummer, T. Berg, S. Friedrich, K.-P. Wittern, Definition of the status of development by analysis. Particle sizing, rheology, microscopy and dielectric spectroscopy SÖFW-J. 128(7) (2002) 2-9.

(41) E. Esposito, E. Menegatti, R. Cortesi, Ethosomes and liposomes as topical vehicles for azelaic acid: A preformulation study, J. Cosm. Sci., 55 (3) (2004) 253-264.

(42) A. Manosroi, L. Kongkaneramit, J. Manosroi, Characterisation of amphotericin B liposome formulations, Drug Dev. Indust. Pharm., 30(5) (2004) 535-543.

(43) T. Hanai, 1968. Electrical properties of emulsions, in: Sherman P. (Ed.), Emulsion science, London, New York, Academic press, 1968, pp. 353-478.

(44) R.H. Müller, R. Schuhmann, Teilchengrössenmessung in der Laborpraxis. Photonenkorrelationsspektroskopie, Wissenschaftliche Verlagsgesellschaft mbH Stuttgart, APV paperback, 1997, 23-53.

(45) H.G. Barth, Particle and droplet sizing using frauenhofer diffraction, in: Modern methods of particle size analysis, John Wiley and Sons, New York, Chichester, Brisbane, Toronto, Singapore, 1984, pp. 135-172.

(46) H.P. Kählig, C. Valenta, U. Dampfhart, B.G. Auner, Rheology and NMR self-diffusion experiments as well as skin permeation of diclofenac-sodium and cyproterone acetate of new gel preparations, J. Pharm. Sci., 94 (2) (2004) 288-296.

(47) R.S. Macomber, A complete introduction to modern NMR spectroscopy, Wiley interscience, New York, Chichester, Weinheim, Brisbane, Singapore, Toronto, 1998.

(48) D. Wu, A. Chen, C.S. Johnson Jr., An improved diffusion-ordered spectroscopy experiment incorporating bipolar-gradient pulses, J. of Magnetic Reson. Series A, 115 (1995) 260-264.

(49) K. Strenge, A. Seifert, Determination of coalescence stability of emulsions by analytical ultracentrifugation under separation of dispersed phase, Prog. in Coll. And Polym. Sci., 86 (1991) 76-83.

(50) R.D. Vold, K.L. Mittal, A.U. Hahn, Ultracentrifugal stability of emulsions, Surf. And Coll. Sci., 10 (1978) 45-97.

(51) P. Guichardon, P. Moulin, F. Tosini, L. Cara, F. Charbit, Comparative study of semi-solid liposome purification by different separation methods, Sep. and Purif. Techn., 41(2) (2005) 123-131.

(52) M. Rotenberg, M. Rubin, A. Bor, D. Meyuhas,Y. Talmon, D. Lichtenberg, Physico-chemical characterization of intralipid emulsions, Biochim. Biophys. Acta, 1086(3) (1991) 265-72.

(53) K.A. Walters, Percutaneous absorption and transdermal therapie. Pharm. Technologie 10(3) (1986) 30-46.

(54) B.W. Barry, Properties that Influence percutaneous absorption, In: Dermatological Formulations Percutaneous absorption, Marcel Decker, New York, 1983, pp. 127-233.

(55) B.W. Barry, Skin Transport, In: Dermatological Formulations Percutaneous absorption, Marcel Dekker, New York, 1983, pp. 95-126.

(56) K. Moser, K. Kriwet, A. Naik, Y.N. Kalia, R. Guy, Passive skin penetration enhancement and its quantification in vitro. Eur. J. Pharm. Biopharm. 52 (2001) 103-112.

(57) F. Hueber, W. Schaefer, J. Wepierre, Role of transepidermal and transfollicular routes in percutaneous absorption of steroids: In vitro studies on human skin, Skin Pharmacol. 7 (1994) 237-244.

(58) R.H. Moghimi, B.W. Barry, A.C. Williams, Stratum corneum and barrier performance, In: R.L. Bronaugh, H.I. Maibach (Ed.), Percutaneous absorption, Marcel Dekker, New York, 1999, pp. 515-553.

(59) J. Hadgraft, Percutaneous absorption: Possibilities and problems, Int. J. Pharm. 16 (1983) 255-270.

(60) R.J. Scheuplein, Site variations in diffusion and permeability In: A. Jarret (Ed.), The Physiology and Pathophysiology of the Skin, Academic press, New York, Vol.5, 1978, pp. 1731-1752.

(61) D. Bucks, H.I. Maibach, H.I., Occlusion and Penetration In Vivo, In: R.L. Bronaugh, H.I. Maibach (Ed.), Percutaneous absorption Drugs-Cosmetics-Mechanisms-Methodology, Marcel Dekker, New York, 1999, pp. 81-105.

(62) L.J. Taylor, R.S. Lee, M. Long, A.V. Rawlings, J. Tubek, L. Whitehaed, G.P. Moss, Effect of occlusion on the penetration of linoleic acid and glycerol, Int. J. Pharm. 249(1-2) (2002) 157-164.

(63) S.E. Cross, M.S. Roberts, The effect of occlusion on epidermal penetration of parabens from a commercial allergy test ointment, acetone and ethanol vehicles, J. Invest. Dermat. 115(5) (2000) 914-918.

(64) S.X. Chen, R.T. Lostritto R.T., Maintaining a near zero-order drug delivery from minidose reservoirs: simultaneous drug diffusion and binary vehicle evaporation, J. Pharm. Sci. 86(6) (1997) 739-746

(65) A. Al-Bawab, S.E. Friberg, C. Fusco, Evaporation of a model skin lotion with beta-hydroxy acids, Int. J. Cosmetic Sci. 26 (2004) 273-279.

(66) C.C. Müller-Goymann, U. Alberg, Modified water containing hydrophilic ointment with suspended hydrocortisone-21-acetate – the influence of the microstructure of the cream on the in vitro drug release and in vitro percutaneous penetration, Eur. J. Pharm. Biopharm. 47 (1999) 139-143.

(67) L.A.M. Ferreira, J. Doucet, M. Seiller, J.L. Grossiord, J.P. Marty, J. Wepierre, J., In vitro percutaneous absorption of metronidazole and glucose: comparison of o/w, w/o/w and w/o systems, Int. J. Pharm. 121 (1995) 169-179.

(68) M.S. Roberts, S.E. Cross, Y.G. Anissimov, Factors Affecting the Formation of a Skin Reservoir for Topically Applied Solutes. Skin Pharm. And Phys. 17 (2004) 3-16.

(69) S.M. Al-Saidan, Transdermal self-enhancement of ibuprofen, J. Control. Release 100(2) (2004) 199-209.

(70) C. Valenta, U. Siman, M. Kratzel, J. Hadgraft, The dermal delivery of lignocaine: influence of ion pairing. Int. J. Pharm. 197 (2000) 77-85.

(71) P.G. Green, J. Hadgraft, G. Ridout, Enhanced in vitro skin pemeation of cationic drugs, Pharm. Res., 6(7) (1989) 628-32.

(72) D.A. Dimas, P.P. Dallas, D.M. Rekkas, Ion pair formation as a possible mechanism for the enhancement effect of lauric acid on the transdermal permeation of ondansetron, Pharm. Dev. Techn. 9(3) (2004) 311-320.

(73) B.W. Barry, Methods for studying percutaneous absorption, In: Dermatological Formulations Percutaneous absorption, Marcel Decker, New York, 1983, pp. 234-295.

(74) A. Naik, L.A.R.M. Pechtold, R.O. Potts, R.H. Guy, Mechanism of oleic acid-induced skin penetration enhancement in vivo in humans, J. Control. Release 37 (1995) 299-306.

(75) J. Hadgraft, Passive enhancement strategies in topical and transdermal drug delivery, Int. J. Pharm. 184 (1999) 1-6.

(76) B.W. Barry, Penetration Enhancers. In: B. Schroth and H. Schaefer (Ed.), Skin Pharmacokinetics, Karger, Basel,1987 , pp. 121-37.

(77) N.F.H. Ho, M.G. Ganesan, G.L. Flynn, Mechanism of topical delivery of liposomally entrapped drugs, J.Control. Release 2 (1985) 61-65.

(78) M.G. Ganesan, N.D. Weiner, G.L. Flynn, N.F.H. Ho, Influence of liposomal drug entrapment on percutaneous absorption, Int. J. Pharm. 20 (1984) 139-154.

(79) E. Touitou, N. Levi-Schaefer, N. Dayan, F. Alhaique, F. Riccieri, Modulation of caffeine skin delivery by carrier design: liposomes versus permeation enhancers, Int. J. Pharm. 103 (1993) 131-136.

(80) B.A.I.Van Den Bergh, I.S. de Vries, J.A. Bouwstra, J.A., Interaction between liposomes and human stratum corneum studied by freeze-substitution electron microscopy, Int. J. Pharm., 167 (1998) 57-67.

(81) V.M. Knepp, R.S. Hinz, F.C. Szoka, R.H. Guy, Controlled drug release from a novel liposomal delivery system. I. Investigations of transdermal potential, J. Control. Release 5 (1988) 211-221.

(82) V.M. Knepp, F.C. Szoka, R.H. Guy, R.H., Controlled drug release from a novel liposomal delivery system. II. Transdermal delivery characteristics, J. Control. Release 12 (1990) 25-30.

(83) M. Kietzmann, W. Löscher, D. Arens, P. Maaβ, D. Lubach, The isolated perfused bovine udder as an in vitro model of percutaneous drug absorption – Skin viability and percutaneous absortion of dexamethasone, benzyl peroxide and etofenamate, J. Pharmacol. Tox. Meth. 30 (1993) 75-84.

(84) P. Bruijnzeel, J. De Lange, G. Van der Schans, G. Elliott, The blood –perfused pig ear: a potential in vitro alternative for dermal permeation and toxicity studies, Adv. In Animal Alt. For Safety and Eff. Testing, (1998) 251-260.

(85) T.J. Franz, On the relevance of in vitro data, J. Invest. Dermatol., 64 (1975) 190-195.

(86) Y.W. Chien, Development concepts and practice in transdermal therapeutic systems In: Transdermal controlled systemic medications, Marcel Decker, New York, 1987, pp. 25-81.

(87) G.L. Flynn, V.P. Shah, S.N. Tenjarla, M. Corbo, D. DeMagistris, T.G. Feldman, T.J. Franz, R.M. Deborah, D.M. Pearce, J.A. Sequeira, J. Swarbrick, J.C.T. Wang, A. Yacobi, J.L. Tatz, Assessment of value and application of in vitro testing of topical dermatological drug products, Pharm. Res. 16 (9) (1999) 1325-1330.

(88) S. Geinoz, S. Rey, G. Boss, A.L. Bunge, R.H. Guy, P.-A. Carrupt, M. Reist, B. Testa, Quantitative structure-permeation relationships for solute transport across silicon membranes, Pharm. Res. 19(11) (2002) 1622-1629.

(89) N. Sekkat, Y.N. Kalia, R.H. Guy, Biophysical study of porcine ear skin in vitro and its comparison to human skin in vivo, J. Pharm. Sci. 91(11) (2002) 2376-2381.

(90) O. Lopez, A. de la Maza, L. Coderch, J.L. Parra, Study of the composition and structure of pig stratum corneum based on the action of different solubilizing agents, Coll. And Surf. A: Physicochem. and Eng. Asp. (123-124) (1996) 415-424.

(91) F.P. Schmock, J.G. Meingassner, A. Billich, Comparison of human skin or epidermis models with human and animal skin in in-vitro percutaneous absorption, Int. J. Pharm. 215 (2001) 51-56.

(92) T. Masada, W.I. Higuchi, V. Srinivasan, U. Rohr, J. Fox, C.R. Behrl, S. Pons, Examination of iontophoretic transport of ionic drugs across the skin: baseline studies with the four-electrode system. Int. J. Pharm. 49 (1989) 57-62.

(93) A. Nangia, S. Patil, B. Berner, A. Bomann, H. Maibach, In vitro measurement of transepidermal water loss: a rapid alternative to tritiated water permeation for assessing skin barrier functions. Int. J. Pharm. 170 (1998) 33-40.

(94) D. Schwindt, K.P. Wilhelm, H.I. Maibach, Water diffusion characteristics of human stratum corneum at different anatomical sites in vivo. J. of Invest. Dermatology 111(3) (1998) 385-389.

(95) D. Van der Merwe, J.E. Riviere, Comparative studies on the effects of water, ethanol and water/ethanol mixtures on chemical partitioning into porcine stratum corneum and silastic membrane. Tox. In Vitro 19 (2005) 69-77.

(96) H. Wagner, K.-H. Kostka, C.-M. Lehr, U.F. Schaefer, Correlation between stratum corneum/water-partition coefficient and amounts of flufenamic acid penetrated into the stratum corneum. J. Pharm. Sci. 91 (2002) 1915-1921.D Original Publications

## D.1 Effect of microstructure and continuous phase drug concentration of multi-phase dermatological formulations on hydrophilic drug skin permeation and stratum corneum distribution


### Abstract

The purpose of this study was to investigate the influence of microstructure of occlusively applied multi-phase o/w formulations on transdermal permeation of hydrophilic model drugs (sodium nicotinate, caffeine and benzyltrimethylammonium chloride) across pig ear skin in vitro. A concept for the interpretation of drug permeation is proposed that considers continuous phase drug concentration as the driving force for permeation, drug distribution between stratum corneum and formulations and drug diffusion in the stratum corneum. The studied o/w formulations consisted of phospholipids, triglycerides, emulsifier, ethanol and water in proportions covering a wide range of values and phase ratios of dispersed to continuous phase. Depending on the individual composition, coexisting dispersed phase structures, such as liposomes, emulsion droplets and microemulsions in a hydrophilic continuous environment were formed, as attested by ultracentrifugation experiments. Particle size measurements and NMR diffusion experiments revealed a droplet-like structure for the detected microemulsions. For all tested drugs, these microemulsion structures had the potential to increase significantly the diffusion coefficient of the drug in the stratum corneum, while increasing dispersed phase generally decreased drug distribution coefficients between stratum corneum and the formulations. Hence, the proposed concept offers a tool to delineate the effect of physicochemical formulation parameters and of the interaction of formulation structures with the skin on regulation of drug skin permeation.


### 1 Introduction

In clinical practice, drugs are incorporated in a vehicle in order to be applied to the skin for topical or systemic therapy (1). Vehicles typically consist of several components that are often not mutually miscible, thus forming separate phases. The phases of such a formulation are intermixed, producing macroscopically homogeneous systems. On the microscopic level, however, these phases form different structures which may be identified using a combination of methods including microscopy, NMR spectroscopy, and rheology measurements (2,3,4).

Formulations for cutaneous application are developed and optimized with respect to a host of criteria such as applicability, tolerability, stability and foremostly efficacy, which comprises duration and strength of pharmacological action. It is meanwhile widely acknowledged that the formulation of a drug product, which is conceived as a drug delivery system, regulates

transdermal permeation. This regulation may take place not only based on physicochemical principles such as diffusion and partitioning of the active ingredient but also by an interaction with the absorptive epithelium, i.e., the epidermis, affecting its permeability of the drug. Liposomal vesicles (5,6,7,8,9,10) and microemulsions (11,12,13,14), for example, represent classes of drug vehicles which may affect skin permeation by reducing the transport barrier function of the stratum corneum. However, despite the efforts made to date to elucidate the influence of the formulation on skin absorption on a mechanistic basis, there is still no unifying theory that allows safe prediction of the process (15). This theory should take into account thermodynamic and methodological aspects (16,17).

In a separate manuscript (18), a concept for the interpretation of transdermal drug permeation using multi-phase formulations was proposed by the authors that considers drug distribution among the phases of the formulation and postulates that continuous phase drug concentration alone governs drug permeation kinetics. With the derived quantitative model it was possible to explain in vitro skin permeation of sodium nicotinate, a hydrophilic drug, for representative o/w vehicles that were applied under non-occlusive conditions. This model could also accurately explain changes of the permeation rate occurring because of the alteration of the inner structure of the formulation over time during the application (18). This alteration was because of the evaporation of volatile vehicle components. No interaction of the vehicle with the epidermis was evident in that study. In a previous work, the proposed concept was further shown to be consistent with the permeation behaviour of a lipophilic drug (ibuprofen) through the epidermis for o/w vehicles applied non-occlusively (19).

The goal of the present work was to implement the above concept in the occlusive application of vehicles similar to those used before (18) in order to confirm its validity and, importantly, use it as a tool to detect possible interactions of the vehicle with the stratum corneum under experimental conditions allowing no vehicle alteration. In this context, the developed model is employed to delineate the regulation of skin permeation by the formulation as a result of controlling continuous phase drug concentration and/or as a result of affecting skin permeability of the drug due to a vehicle-stratum corneum interaction. Gaining a deeper understanding of the mode of this interaction and its dependence on the physicochemical structure of the formulation rounds up the goal of the present work.

The studied o/w formulations consisted of phospholipids, triglycerides, emulsifier, ethanol and water in proportions covering a wide range of values and formed depending on the composition coexisting phase structures, i.e., liposomes, macro-emulsion oil droplets and microemulsion aggregates in a hydrophilic continuous environment (18). These formulations were designed specifically for investigating the effect of structure and mass fraction of the formed phases on transdermal delivery. Three hydrophilic model drugs with different structure

and charge, sodium nicotine, benzyltrimethylammonium chloride (BTA-Cl) and caffeine were investigated.

The influence of the used drug on phase formation of the formulations was examined. Methods were developed and optimized for determining the free drug concentration in the continuous phase of the formulations. Permeation experiments were carried out in vitro using pig ear skin as a model for human skin (20). A practically infinite amount of formulation was applied in order to determine steady state flux values that facilitate the data evaluation. This was deemed appropriate for reaching the specific goals of this study. The interaction of the vehicles with the stratum corneum was investigated by separately evaluating the diffusion coefficient of the drug in the stratum corneum and its distribution coefficient between stratum corneum and the continuous phase of the formulation (21,22,23).

## 2 Materials and methods

### *2.1 Materials*

Nicotinic acid was purchased from Sigma (St. Louis, MO, USA). Benzyltrimethylammonium chloride (BTA-Cl) was purchased from Fluka Chemie GmbH (Buchs, Switzerland) and caffeine was a gift from Sandoz AG (Basel, Switzerland). Mygliol 812N®, medium chain triglycerides, was a gift from Hüls AG (Witten, Germany). Phospholipon 80, a soy bean lipid extract with 76 weight-% phosphatidylcholine, and NAT 8539®, a mixture of 75 weight-% Phospholipon 80 and 25 weight-% ethanol, were gifts from Phospholipid GmbH (Cologne, Germany). Polysorbate 20, sodium dihydrogenphosphate dihydrate, sodium azide and 1-octanesulfonic acid sodium salt monohydrate, puriss.p.a., were purchased from Fluka Chemie GmbH (Buchs, Switzerland). Alcohol dehydrogenase 100mg (3.4ml) suspension, aldehyde dehydrogenase, lyophilized powder, 250U and NAD, free acid, grade II, approx.98%, were purchased from Roche Diagnostics AG (Rotkreuz, Swizterland). Tetra-n-butylammonium hydrogensulfate (LiChropur), CombiTitrant5, a one-component reagent for the volumetric Karl Fischer titration, methanol and tetrahydrofurane, (LiChrosolv), were obtained from Merck (Darmstadt, Germany). Acetonitril (HPLC, gradient grade) was obtained from Biosolv (Valheesward, Netherlands). 0.25% Trypsin, 1mM EDTA solution was purchased from LuBioScience (Lucerne, Switzerland). All other chemicals and reagents used in this study were of analytical grade. Bidistilled water was used in all cases.

### *2.2 Methods*

#### 2.2.1 Manufacturing of the formulations

The study formulations (for composition see Table 1) were prepared by mixing NAT 8539® and tocopherol with the ethanol (mixture1), dissolving the respective model drug (nicotinic acid, BTA-Cl or caffeine) in aqueous phosphate buffer (β=0.01) adjusted to pH of 7.4 (mixture 2)

and suspending polysorbate 20 in Mygliol 812N® (mixture 3). For manufacturing CF10 and CF50, mixture 2 was first added to mixture 3 and homogenized for 5 minutes at 20000 rpm using a Polytron Pt 3000 (Kinematica AG Littau, Switzerland). Subsequently, mixture 1 was added and the product was homogenized once again for 5 minutes. E was produced by adding mixture 2, additionally containing the ethanol, to mixture 3, and LD was obtained by adding mixture 1 to mixture 2, followed by homogenization as above. Xanthan gum was added at the end to the formulations followed by further homogenization for 30 seconds, except for the formulations that were used for ultracentrifugation (see 2.2.2). The gel was produced by adding 0.5 weight- % xanthan gum to mixture 2, additionally containing the ethanol, followed by homogenization as above. Different emulsion formulations with varying amounts of dispersed phase of 2, 20 and 70 weight-% (E2, E20, E70, respectively) were prepared as formulation E. For that purpose, the ratio of buffer pH 7.4 to ethanol of mixture 2 was kept constant. Different liposomal dispersions with dispersed phase of 2, 5 and 20 weight-% (LD2, LD5 and LD20, respectively) were prepared according to LD. The appropriate amount of ethanol was added to achieve a constant ratio of ethanol to buffer in the final formulations. For manufacturing ethanol-free formulations, total ethanol of formulations was replaced with buffer and NAT 8539® was replaced with the 0.75 fold amount of Phospholipon 80. Nicotinic acid was dissolved in buffer, adjusted to a pH of 7.4, added to the combined remaining compounds and homogenized as above. All formulations were allowed to equilibrate for at least 24 hours before use. The pH of the formulations was measured using a pH-meter 691 and a sensor type Porotrode (Metrohm AG, Herisau, Switzerland).

### 2.2.2 Ultracentrifugation and chemical analysis of formulations

The study formulations were fractionated by ultracentrifugation using an ultracentrifuge type Centricon T-1075 and a rotor TFT 7013 (Kontron Instruments, Mailand, Italy). Quick-Seal centrifuge tubes, 5/8X3 (Beckman Instruments, Palo Alto, USA) were used. CF10 and LD were centrifuged for 2 hours, and CF50 and E for 1 hour at 222000-450000 g. The different operation times were optimized to fractionate intact structures. Following this treatment, the received fractions were carefully isolated by a syringe and analyzed for water, ethanol and the drug.

Water was assayed by Karl-Fischer titration using a KF 701 Titrino (Metrohm AG, Herisau, Switzerland) and a one-component reagent CombiTitrant 5. The titer was exactly determined with double distilled water prior to every analytical run. EtOH was quantified by an enzymatic method (24), based upon spectroscopic determination of accumulated NADH at 340 nm using a Perkin Elmer Lambda 20 Spectrometer (Perkin Elmer, Ueberlingen, Germany).

All model drugs were assayed by HPLC (Hewlett Packard, series 1050, Hewlett Packard, Waldborn, Germany). For nicotinic acid, a reversed phase RP-18 column (CC 125/2

Lichrospher 100-5 RP-18 ec) was used. The mobile phase consisted of 95% phosphate buffer (pH 7.4, β=0.05), containing 5mM tetrabutylammonium hydrogenphosphate and 5% methanol. The mobile phase for BTA-Cl quantification consisted of 15% acetonitrile and 85% phosphate buffer (pH 3.5, β=0.05) containing 5 mM 1-octanesulfonic acid sodium salt. The same column was used as for nicotinic acid. For caffeine, a reversed phase RP-8 column was used (CC 125/2 Nucleosil 100-5 C8 ec). The mobile phase consisted of 10% acetonitril and 90 % phosphate buffer (pH 3.5, β=0.05). Detection was performed UV-spectrophotometrically at 214, 210 and 255 nm for nicotinic acid, BTA-Cl and caffeine, respectively. The flow rate was 0.25 ml/min in all cases. The samples were prepared by extraction with at least 100 fold amount of buffer pH 7.4, sonification for 5 minutes and filtration through a syringe filter (Titan 2, PTFE, 0.2 µm, Sun Sri, NC, USA) prior to injection.

### 2.2.3 Particle size measurements

The z-average of liposomal vesicles and microemulsion droplets was determined by photon correlation spectroscopy (PCS) at 25°C using a Malvern Zetasizer 1000HSa (Malvern Instruments Ltd., Malvern, UK). Samples were diluted with filtered aqueous buffer pH 7.4 (0.2 µm) until counting rates between 100 and 300 KCts/s were reached. For particle size determination of microemulsion aggregates, dilution steps from 1/5 to 1/100 were prepared with filtered buffer as above. The pinholes for the laser beam were varied to obtain the above counting rates for these samples. The mean diameter of emulsion droplets was determined by laser diffraction using a Mastersizer S (Malvern Instruments Ltd., Malvern, UK) with a small sample unit and a beam lens with 300 mm focal distance. All samples were diluted with demineralized water till an obscuration of approx. 20% was reached.

### 2.2.4 NMR Diffusion experiments

Self-diffusion measurements of sodium nicotinate and benzene were performed with the bipolar gradient pulse sequence of Wu et al. (25) using a Bruker Avance DRX NMR spectrometer operating 600.13 MHz proton frequency. The instrument is equipped with a 5-mm broadband inverse probe with a shielded z-gradient coil and a GAB gradient amplifier (10 Ampere, maximum gradient strength 52.5 G/cm).

All samples contained 5% $D_2O$ as lock substance. The diffusion experiments were performed at 295 K and the temperature was calibrated using a methanol standard showing accuracy within +/- 0.2 K. The gradient strength was calibrated using a Shigemi tube filled with $H_2O$ to a height of 4.0 mm and imaging this water cylinder (26). The resulting gradient calibration was validated by determining the diffusion coefficient of water at 310 K and reproduced the literature value within 5%.

The diffusion experiments were performed by varying the gradient strength between 2% and 95% of the maximum strength in typically 8 or 16 single experiments while keeping the

diffusion times and gradient lengths constant. The entire experiment was then repeated with a different diffusion time (100 ms to 500 ms). The intensity decrease of the signal of interest was determined and fitted with a Bruker t1/t2 software package suitable for dosy experiments, which is included in the XWINNMR software (27). Eq. (1) was used in order to obtain the self-diffusion coefficients:

$$I_g = I_0 \cdot e^{-D\cdot(\delta\cdot H\cdot G\cdot 2\cdot\pi)^2\cdot(\Delta-\frac{\delta}{3})\cdot 10000} \qquad (1)$$

where, $I_g$ and $I_0$ are the signal intensities in the presence and absence of magnetic field gradient pulses with the amplitude G and the duration δ. $\Delta$ Denotes the experimental diffusion time, $D$ the diffusion coefficient and H is given with 4258 Hz/G and depends on the gyromagnetic constant for $^1$H.

### 2.2.5 Distribution coefficient determination

Caffeine, BTA-Cl and sodium nicotinate drug distribution between Mygliol 812N® (triglycerides) and the simulated hydrophilic phase of formulations was determined by the shake-flask method. Briefly, 1 weight-% of drug was dissolved in aqueous buffer pH 7.4, containing 17 weight-% of ethanol. This solution was transferred into a separation funnel together with an equal amount of triglycerides. The mixture was extensively shaken for 10 min. The two phases were allowed to separate for at least one hour before hydrophilic phase was isolated, followed by centrifugation for 10 min at 15800 g. Floating triglyceride droplets were removed and the hydrophilic phase was analyzed for containing model drug by HPLC (for conditions see 2.2.2). Distribution coefficients were calculated as the ratio of the concentration of the triglyceride phase, obtained from mass balance, to the measured concentration of the hydrophilic phase.

### 2.2.6 Determination of continuous phase drug concentration

Continuous phase drug concentration was calculated according to Eq. (2). For a multi-phase formulation with mass fraction of the continuous phase $\phi_{cont}$, this concentration $C_{cont}$ is given by:

$$C_{cont} = \frac{C_{tot}}{(1-\phi_{cont})\cdot(K_{d/c}-1)+1} \qquad (2)$$

where, $C_{tot}$ denotes the overall drug concentration of this formulation and $K_{d/c}$ the distribution coefficient of the drug between the dispersed and the continuous phase. Mass concentrations (mg/g) and mass fractions (weight-%/100) were considered. For detailed derivation of Eq. (2), see (18).

In addition, ultrafiltration was applied to determine directly continuous phase drug concentrations of the formulations. Centrifugal filter devices (Microcon YM3) with a molecular

weight cut-off of 3000 (Millipore, Bedford, MA, USA) were used. The filtrate was analyzed for the drug by HPLC after suitable dilution. For HPLC conditions see 2.2.2.

### 2.2.7 Permeation experiments

In all cases, drug permeation was studied in Franz-type diffusion cells with a diffusion surface area of 1.7-1.8 $cm^2$ at 32℃ across excised full thickness pig ear skin. The ears of domestic pigs were obtained from a local abattoir directly post-mortem. The skin was separated from the cartilage tissue by a scalpel, stored in a freezer at –75℃ and used within 4 weeks. To avoid the effect of individual skin variability, every single permeation experiment was carried out with skin of the same pig ear and included all formulations that were compared. The receiver medium for the permeation experiments with a volume of 8.5 to 9 ml consisted of an aqueous phosphate buffer solution, pH 7.4, β=0.05, additionally containing 0.1% of sodium azide as a preservative. Skin integrity was tested by transepidermal water loss (TEWL) measurements (Tewameter TM 210,Courage Khazaka electronic GmbH, Germany) after 4 hours of equilibration. Then, a practically infinite dose of formulation of at least 1000 $mg/cm^2$ was applied onto the skin. The donor compartment was covered with a rubber stopper for occlusion. At predetermined time intervals, samples of the receiver medium were collected and replaced by fresh buffer. The entire duration of an experiment was 49 hours. The samples were analyzed directly for model drug concentration by HPLC (for conditions see section 2.2.2) without further treatment except centrifugation for 5 min. at 15800 g. Caffeine permeation across a silicon membrane (Perthese®, LP500-3, Bornel, France) was studied with the same procedure, but the duration of these experiments was 27.5 hours.

### 2.2.8 Drug distribution coefficients between stratum corneum and continuous phase of formulations

Skin sheets with a thickness of about 200 µm were prepared from pig ear skin using a pneumatic dermatome (Zimmer, Dover, OH, USA). These sheets were placed in a Petri dish, stratum corneum (SC) side up, on filter paper, soaked with 0.125 % trypsin/ 0.5mM EDTA solution and incubated at 37℃ for 16 hours (21). T hen, the SC was carefully peeled off from the underlying epidermal cells and extensively washed with isotonic sodium chloride solution to prevent further degradation. The isolated SC sheets were stored in a desiccator over silica gel for at least 24 hours, but not longer than two weeks, before use.

To determine distribution coefficients $K_{S/C}$ between SC and continuous phase of formulations, accurately weighted (about 5 mg) pieces of SC were placed into 1.5 ml eppendorf tubes and 1 g of formulation was added to achieve contact with the SC over its entire area. After an equilibration time of 28 hours, the SC pieces were slightly washed with isotonic sodium chloride solution for 10 sec. and carefully dabbed with filter paper to remove adhering formulation. Drug was extracted from the SC with buffer solution (pH 7.4, β=0.03) by

ultrasonication for 2 min (Branson Sonifier 250, output control level 4, duty cycle 40%, Branson Ultrasonics Corporation, Danbury, USA). After centrifugation, the supernatant was diluted and analyzed for drug concentration by HPLC (for conditions see 2.2.2). SC drug concentrations were calculated as mg model drug/dry weight SC in grams. The procedure was optimized for trypsin incubation time, formulation removal process after equilibration, range of linearity and drug extraction time.

### 2.2.9 Data analysis of permeation experiments

In order to interpret permeation data, it is postulated that continuous phased rug concentration of a multi-phase formulation governs permeation kinetics alone. This concentration is given by Eq. (2) (see 2.2.6). Assuming the conditions of a perfect sink (receiver concentration negligible), an infinite donor reservoir, assuring a constant continuous phase drug concentration $C_{cont}$, rate limiting membrane (skin) diffusion with the diffusion coefficient $D$ and drug distribution between the skin and the continuous phase of the formulation with the distribution coefficient $K_{S/C,}$ drug flux $J$ may be described by Fick`s first diffusion law. Drug flux $J$ is defined as the amount of drug permeated through the skin per unit time and unit area and is given by:

$$J = P \cdot C_{cont} \qquad (3)$$

with $P$ as the permeability coefficient (cm/s) with $h$ as thickness of the diffusion rate limiting membrane

$$P = \frac{D \cdot K_{S/C}}{h} \qquad (4)$$

Combining Eqs. (2) and (3) gives a term to calculate permeability coefficients considering continuous phase drug concentration:

$$P = J \cdot \frac{(1-\phi_{cont}) \cdot (K_{d/c} - 1) + 1}{C_{tot}} \qquad (5)$$

## 3 Results

### *3.1 Formulation characterization*

#### 3.1.1 Ultracentrifugation experiments

Ultracentrifugation was applied to fractionate the intact structures of the formulations as previously demonstrated as good methodology to investigate multi-phase dermatological formulations by separation of the comprising dispersed phase structures (18). Independently of the included model drugs, the study formulations yielded the following fractions: E a white, turbid fraction on top (fraction A) and a clear fraction in the bottom (fraction B). LD gave a clear fraction on top (fraction B) and a brown turbid fraction (fraction C) in the bottom. CF10 gave three fractions that appeared comparable, from top to bottom, to the fractions A, B and C, but the clear fraction B was little yellowish. CF50 gave only two factions, a fraction comparable to fraction A and a deep yellow, but clear fraction B in the bottom. These observations agree well with previous work where the study formulations which contained sodium nicotinate were characterized very detailed by complete chemical component analysis of all received fractions, freeze fracture scanning electron microscopy and particle size measurements (18). That investigation demonstrated that the fractions A and C contained emulsion droplets and liposomes, respectively. The deep yellow, clear fraction B of CF50 consisted of 13 weight-% phospholipids, 13 weight-% triglycerides, 10 weight-% polysorbate 20 and hydrophilic phase (13 weight-% ethanol and 51 weight-% buffer pH 7.4). This composition and further characteristics such as rheological behavior and spontaneous formation of the system strongly indicated a microemulsion structure. The clear fraction B of CF10 included an overall sum of 4 weight% of phospholpids, triglycerides and polysorbate 20 in a roughly comparable ratio to the microemulsion found within CF50. Hence, for CF10, a coexistence of liposomes, emulsion droplets and microemulsion aggregates was assumed.

In addition to the formulations that included the sodium nicotinate, all identical fractions received from the formulations that contained BTA-Cl and caffeine were analyzed for water and ethanol. Fig.1 compares all these results. A good agreement for the analyzed components is observed, as demonstrated by the comparable concentration bars, not depending on the incorporated drug. Furthermore, the ratio of water to ethanol is equal in each fraction and to the ratio of these components contained in the corresponding complete formulation, indicating that the sum of water and ethanol amounts to the continuous hydrophilic phase, independently of dispersed structure and incorporated model drug.

#### 3.1.2 Particle sizes of liopsomes and emulsion droplets

The diameters of liposomes and emulsion droplets of the formulations are shown in Fig.2. These structures are of comparable size, independently of the included model drug. A tendency of smaller emulsion droplets within the formulations with big amount of dispersed

phase (CF50 and E), compared to CF10, and of smaller liposomes within CF10, compared to the liposomes of LD, is obvious. This is in good agreement with the previous work and discussed there (18).

### 3.1.3 Microemulsion characterisation

NMR diffusion experiments and particle size measurements using PCS were carried out in order to verify the presence of the microemulsion structure within CF50 and to determine if the oil phase is continuous or droplet like. Direct PCS measurements of the fraction B of CF50, comprising the microemulsion, was not possible because of the big amount of dispersed phase, which required dilution for that purpose. Independently of different dilution steps and the included model drug, the measured diameters were in between 20 and 24 nm and the polydispersity index (PI) was almost always between 0.1 and 0.2, indicating a rather narrow size distribution of the analyzed structures (Table 2).

NMR diffusion measurements within this assumed microemulsion system gave self-diffusion coefficients for sodium nicotinate only twice less than within the gel (Table 3). The sodium nicotinate was used for that examination to obtain isolated $^{1}H$ NMR signal peaks and had, for this purpose, the function of a hydrophilic marker, because it distributed completely into the hydrophilic phase of formulations (see 3.1.4). However, the incorporation of the lipophilic marker benzene into this microemulsion that was isolated from a drug-free formulation CF50 gave a self-diffusion coefficient of 3.5E-11 $m^2/s$. That is about tenfold less than benzene self-diffusion within triglycerides (2.06E-10 $m^2/s$) which were assumed to be representative for a lipophilic bulk.

In case of fraction B of CF10, the relatively small amount of dispersed phase facilitated undiluted PCS inspection and gave diameters slightly larger as measured for the microemulsion structures within CF50, but with a broader variability, expressed as larger values for PI (Table 2).

### 3.1.4 Continuous phase drug concentrations and self-diffusion coefficients

According to the proposed concept in order to investigate drug delivery potential of multi-phase dermatological vehicles (see 2.2.9), an exact determination of continuous phase drug concentration is a crucial parameter. Independently of the existing microstructures and of the incorporated model drug, the continuous phase consisted of buffer and the total amount of ethanol in case of the study formulations (see 3.1.1). Drug distribution between the triglycerides and the simulated hydrophilic phase was determined by the shake-flask method. This method indicated no distribution of the charged substances (sodium nicotinate and BTA-Cl) into bulk triglycerides, while the caffeine gave a distribution coefficient of 0.2 between triglycerides and hydrophilic phase.

Hence, continuous phase drug concentrations were calculated considering the phase ratios from dispersed to continuous phases given by the formulation composition (Table 1) using Eq. (2). For that purpose, $K_{d/c}$ was approximated with zero, only for the caffeine a value of 0.2 was applied in case of triglycerides comprising formulations. Distribution into liposomes and other phospholipid based structures was neglected because of the relatively low amounts of phospholipids within the formulations, compared to triglycerides. These calculated concentrations are given in Table 4. Beside this theoretical calculation, ultrafiltration experiments were performed in order to measure continuous phase drug concentrations. The results are also given in Table 4 and agree well with the calculated values.

Furthermore, drug concentrations of the fractions B of LD and E following ultracentrifugation were used to estimate the distribution of the drugs between intact formulation structures. Previous work demonstrated that fraction B of E contained about 5 weight-% of polysorbate 20, but no triglycerides, and this fraction of LD was found to be free of phospholipids (18). Again, a slight distribution of caffeine into triglycerides was indicated by the caffeine concentration of fraction B of E, while sodium nicotinate and BTA-Cl concentrations in the fraction B of E and LD indicated negligible distribution into emulsion droplets and liposomes, supporting the above results (Table 4). Hence, the calculated continuous phase drug concentrations given in Table 4 were applied for further investigations.

The molecular mobility of a drug within a formulation is reportedly a further aspect that may contribute to drug delivery (3,4). Thus, we performed NMR diffusion experiments in order to determine self-diffusion coefficients for sodium nicotinate within all study formulations. The results are given in Table 3. The molecular mobility within the formulations was different and decreased in the order gel > CF10 > fraction B of E> E> LD = fraction B (microemulsion) of CF50. The sodium nicotinate gave high resulated $^{1}$H NMR spectra with narrow signal peaks. Only for E, broad signal peaks were obtained, for what the reason was not further investigated. For CF50, the diffusion coefficent within the isolated fraction B, comprising the microemulsion, was considered (see 3.1.3).

### *3.2 Permeation experiments*

#### 3.2.1 Permeation across a silicon membrane and pig ear skin

Fig.3 shows the permeation pattern of caffeine across a silicon membrane (Fig.3 a.) and across pig ear skin (Fig.3 b.). The permeation profile of caffeine for CF50 across the silicon membrane agrees well with the caffeine permeation profile for E. Likewise CF10, LD and the gel gave identical permeation profiles, compared among them, while the drug flux was about two times less for these three formulations, compared to CF50 and E. Permeation across pig ear skin, however, differed from permeation across the silicon membrane (Fig.3 b.).

Eq. (5) was applied to calculate permeability coefficients for BTA-Cl, sodium nicotinate and caffeine permeation for the study-formulations across pig ear skin and for caffeine across the

silicon membrane (Table 5). Caffeine permeability coefficients across the silicon membrane are equal for all formulations, indicating that continuous phase drug concentration governed this permeation alone. However, permeability coefficients across skin are different for the formulations, for caffeine, BTA-Cl and for sodium nicotinate. To interpret this finding, the permeability coefficients across skin for all multi-phase formulations were compared to the permeability coefficient for the gel. In addition, permeability coefficients obtained from CF50 and CF10 were compared to those obtained from the formulations that contained comparable continuous phase drug concentrations, E and LD, respectively. A significant enhancement (t-test, double sided, $p< 0.1$) compared to the gel was found for sodium nicotinate permeation from CF50 and CF10. However, formulations that were prepared without ethanol gave sodium nicotinate permeability coefficients in the same order of magnitude for all formulations and for a purely aqueous gel (Table 6). Compared to LD, all drugs showed significantly increased permeation from CF10 (t-test, double sided, $p< 0.1$). Likewise caffeine and sodium nicotinate permeation from CF50 was significantly increased (t-test, double sided, $p< 0.1$) compared to E. In addition to this permeation enhancement, a tendency of decreasing permeation for BTA-Cl from CF50, E and LD and for caffeine from LD and E was observed, compared to permeation from the gel (Table 5). This effect was significant for caffeine permeation from E (t-test, double sided, $p< 0.1$). Thus, further permeation experiments with purely emulsions which comprised variable amounts of dispersed phase of 2, 20 and 70 weight-% (E2, E20 and E70, respectively) were performed with all three model drugs (Table 5). Respective continuous phase drug concentration was tested using ultrafiltration and agreed with calculated concentrations (data not shown). Caffeine and BTA-Cl permeation decreased with increasing dispersed phase ratio of the emulsions, but not sodium nicotinate permeation.

### 3.2.2 Drug distribution into and diffusion within stratum corneum

In order to gain a deeper understanding of the dependence of differences in drug permeation on the physicochemical structure of the formulation, drug distribution coefficients between the stratum corneum (SC) and, according to the proposed concept, continuous phase of the formulations ($K_{S/C}$) were determined. Table 7 shows that the study formulations had an effect on the distribution of the model drugs into the SC. For all drugs, drug distribution into the SC was favored from the gel, compared to the study formulations. Closer examination suggested that drug distribution into the SC from the formulations with big amount of dispersed phase (CF50 and E) was smaller, compared to the formulations that contained lesser amount of dispersed phase (CF10 and LD). Distribution coefficients between the SC and the emulsion formulations with variable amounts of dispersed phase (E2, E20 and E70) were also determined for BTA-Cl and caffeine. A tendency of decreasing distribution into the skin with increasing amount of dispersed phase of these emulsions is obvious (Table 7). Equal results

were obtained for different liposomal dispersions, which contained variable amounts of dispersed phase of 2, 5 and 20 weight-% (LD2, LD5 and LD20, respectively) (data also given in Table 7).

Drug diffusion coefficients within the SC were calculated taking into account the permeability coefficients (Table 5) and the according $K_{S/C}$ values given in Table 7 using Eq. (4). For that purpose, the mean of $K_{S/C}$ for a specific drug and a specific formulation was applied to every single permeation experiment. The calculated diffusion coefficients are shown in Fig.4. The diffusion coefficients following permeation from CF10 and CF50 were significantly increased compared to the gel for all model drugs (t-test, double sided, $p< 0.1$). Comparable diffusion coefficients in the skin for the drugs following permeation from LD, E and the gel further indicated that the decrease in drug permeation (see 3.2.1) was a result of decreased distribution coefficients $K_{S/C}$ alone.

The same calculation was carried out with caffeine and BTA-Cl permeation data obtained from E2, E20 and E70 (Table 5) and the according $K_{S/C}$ values (Table 7). This inspection gave strongly equal diffusion coefficients within the stratum corneum and values in the same order of magnitude to those obtained from formulation E (Fig.5).

## 4 Discussion

Permeation across and distribution into the skin of hydrophilic model drugs from different multi-phasic dermatological o/w formulations was studied in order to understand the role of their microstructure on these processes. For that purpose, continuous phase drug concentrations of the formulations were considered, according to a proposed concept which postulates that this concentration is the only parameter governing permeation kinetics.

Independently of the included model drug, the used drug concentration did not cause major structural alterations of the study formulations, as attested by ultracentrifugation experiments and particle size measurements of liposomes and emulsion droplets. Comparable water and ethanol content of the received fractions following ultracentrifugation confirmed this finding and further indicated that the ratios form dispersed to continuous phases of the formulations were not influenced by the different model drugs. Hence, the used criteria were considered to be conclusive to apply the detailed structural investigation that was performed with the sodium nicotinate containing formulations previously to the formulations that contained caffeine and BTA-Cl (18).

Microemulsion structures were identified beside emulsion droplets within CF50 and in addition to coexisting emulsion droplets and liposomes within CF10. NMR diffusion experiments could demonstrate that the isolated microemulsion from CF50 comprised droplet-like lipophilic structures in a hydrophilic continuous environment. While conductivity measurements already

indicated hydrophilic continuous phase previously (18), it was not clear whether lipophilic phase is continuous or droplet like. A tenfold less benzene self-diffusion coefficient within this microemulsion, compared to benzene self-diffusion within triglycerides, however, strongly indicated restricted diffusion and, hence, a droplet-like lipophilic structure. In case of a bicontinuous structure, benzene self-diffusion within the microemulsion and the bulk lipophilic phase would be in the same order of magnitude (4). This, however, was true for sodium nicotinate self-diffusion within this system and the gel, supporting the previous finding of hydrophilic continuous phase (Table 3). The benzene and the sodium nicotinate were chosen for this examination because they gave high resulated $^{1}$H NMR spectra, not overlapping with the signals of other formulation compounds. The droplet-like character of the microemulsion aggregates was further supported by PCS measurements, which gave a droplet size of in between 20 and 24 nm, not depending on different dilution steps (Table 2). Additionally, the comparable particle size for the microemulsion structures of CF50 containing the different model drugs also supported the conclusions drawn above of the independence of the microstructure on the incorporated model drug (Table 2). The relatively small polydispersity index (PI) is a further evidence for a spontaneously arising microemulsion with defined, stable structure, because no efforts have been made to obtain such a narrow size distribution. The slightly larger particle sizes of the microemulsion aggregates measured for fraction B of CF10, compared to the microemulsion aggregates of CF50, were supposed to be due to some not completely separated coarse particles during ultracentrifugation, which simulate a larger z-average for the complete sample. This explanation is further supported by the values for the PI of the single experiments. The smaller the PI, the more agreed the particle size of these microemulsion aggregates for fraction B of CF10 with the data obtained from CF50 (Table 2). Hence, an equal structure for the microemulsion systems found within CF10 and CF50 is assumed and it is supposed that these structures may arise spontaneously beside other dispersed structures within multi-component formulations which consist of polysorbate 20, triglycerides, phospholipids and hydrophilic phase.

Independently of the microstructures, Eq. (2) was applied to calculate continuous phase drug concentrations of all model drugs for all study-formulations. These calculated concentrations were in good agreement with the continuous phase drug concentrations obtained from ultrafiltration experiments (Table 4). This is evidence for the validity of Eq. (2) and, importantly, further points out that no obvious association of the model drugs with the surface of the dispersed structures took place. The theoretical continuous phase drug concentrations derived from Eq. (2) consider distribution coefficients between dispersed and continuous phase structures obtained from the shake flask method, which represents the solubility properties of the drug in the system. Ultrafiltration, however, provides a methodology that considers the whole formulations, and, hence, may also reveal associations of the drugs with dispersed

formulation structures. Furthermore, the drug concentrations within fraction B of CF50, comprising the microemulsion, compared to the continuous phase drug concentrations obtained from ultrafiltration of CF50 (Table 4) indicated that this methodology can separate the microemulsion aggregates from the continuous phase, which is further supported by obtained colorless filtrates in all cases. This is an important result because the microemulsion aggregates were considered as dispersed structures in this work. Drug concentrations within fractions B of LD and E also confirmed the findings of the ultrafiltration experiments. In addition to all these results, a coulomb association of the sodium nicotinate with charged surfaces of dispersed phase structures, for example liposomes or microemulsion aggregates, would likely yield broad NMR signal peaks of the sodium nicotinate. Consequently, the continuous phase drug concentrations calculated with Eq. (2) were used for the interpretation of permeation and distribution data (Table 4).

Permeation experiments across a synthetic lipophilic barrier and across excised skin provide an easy methodology to discriminate between formulation effects related to physicochemical parameters and those correlated to biological factors on skin barrier function (5). Equal permeability coefficients for caffeine permeation across a silicon membrane, calculated with Eq. (5), demonstrated that the observed increased caffeine flux from CF50 and E (Fig.3 a.) compared to LD, CF10 and the gel, was governed by continuous phase drug concentrations alone (Table 5). This is evidence for the validity of the proposed concept. These experiments were performed with the caffeine because the silicon membrane was permeable for that substance.

Caffeine permeation profile across excised pig ear skin, however, was different compared to the permeation profile across the silicon membrane (Fig.3 a.,b.). Permeability coefficients for all formulations across skin, calculated with Eq. (5), were different, not only for caffeine, but also for BTA-Cl and sodium nicotinate (Table 5). This indicated further effects that had impact on skin permeation, in addition to continuous phase drug concentration. An enhanced permeation of the sodium nicotinate from CF10 and CF50, compared to LD, E and the gel was obvious. Sodium nicotinate permeation was further studied from comparable formulations to those given in Table 1, but designed without ethanol in order to investigate a possible synergism with the alcohol, taking into account the literature (6,7,9). Comparable permeability coefficients were obtained for all formulations, strongly indicating a synergism of ethanol and dispersed formulation structures of CF10 and CF50 to the observed permeation enhancement (Table 6). This also confirms the previous work where ethanol was removed from the formulations by evaporation and continuous phase drug concentration alone could explain the permeation kinetic (18). For caffeine and BTA-Cl, the interpretation of the different permeability coefficients was not that clear, because, somewhat unexpected, also smaller permeability

coefficients were calculated, compared to the gel, indicating also permeation retarding effects due to dispersed formulation structures (Table 5).

Taking into account Eqs. (3) and (4), steady state drug permeation may be affected by (I) altered drug diffusion coefficient in the skin, (II) altered drug distribution coefficient between the skin and the vehicle or differences in drug concentration (28,29). In order to explain the observed differences of the permeability coefficients, drug distribution coefficients between stratum corneum and the study formulations $K_{S/C}$ were determined, considering continuous phase drug concentrations (Table 7). These data and the according permeability coefficients (Table 5) were used to calculate diffusion coefficients in the stratum corneum using Eq. (4), a constant thickness for stratum corneum of 15 µm assumed. The stratum corneum was identified as site of action for the formulation effects by additional permeation experiments across stripped skin, which provided negligible diffusional resistance for all model drugs, compared to intact skin (data not shown). The calculated diffusion coefficients within the stratum corneum finally attested the complex formulations CF50 and CF10 properties to enhance drug diffusion coefficients within the stratum corneum for all model drugs (Fig.4). These two formulations were the only formulations including microemulsion structures beside emulsion droplets and liposomes, strongly indicating that the enhancing properties of CF10 and CF50 were due to an interaction between these microemulsion structures and the stratum corneum, because liposomes and emulsion droplets were also formed within LD and E, respectively. This assumption was supported by further sodium nicotinate permeation experiments that were performed with the isolated fractions B, comprising the microemulsion structures, referred to as MeCF50 and MeCF10 (Table 5), which gave comparable permeability coefficients to the intact formulations CF50 and CF10. Several publications report on improved transdermal or dermal drug delivery from microemulsion systems (11,12,13,14). Generally, two basic trends are observable from the reported studies that may contribute to the favorable drug delivery properties: high drug load capacity and penetration enhancer effects. The latter is true for the microemulsion structures identified in the study formulations, because the application of the described concept considers the available concentration, i.e. continuous phase drug concentration. The permeation enhancing effect is not only a result of the ethanol included in the formulation (28), as attested by taking into account ethanol containing references. The observed synergism with the ethanol may be due to a primary action of the alcohol with the stratum corneum, facilitating further interaction of the microemulsion structures with the stratum corneum lipids. Other authors proposed also such a synergism (6,7,9). In contrast to these publications, however, we could not confirm enhancing properties of conventional liposomal vesicles. Furthermore, usually extensive efforts are made for discovering pharmaceutical acceptable microemulsions, for example the construction of more dimensional phase diagrams (11,30). The microemulsions discussed in this work, however,

arise spontaneously beside other structures and, thus, provide a readily available tool to improve drug skin permeation.

The diffusion coefficients given in Figure 4 may also explain decreased permeation of the model drugs from some study formulations, compared to the gel. Such effects were most obvious for BTA-Cl and caffeine for E and LD (Table 5). Comparable diffusion coefficients of the model drugs within the skin, following permeation from LD, E and the gel, demonstrated that this decreased permeation was caused by decreased solubility of the model drug within the stratum corneum, expressed as smaller values for $K_{S/C}$ (Table 7, Fig.4). Caffeine and BTA-Cl permeation from different emulsions, which were designed in order to comprise widely varying amounts of dispersed phase, confirmed this finding and further indicated a dependency of the observed permeation retarding effect on the phase ratio of dispersed to continuous phase of the formulations (Table 7, Fig.5). Decrease in $K_{S/C}$ with rising amount of dispersed phase was also observed for different liposomal dispersions, comprising variable amounts of phospholipids (Table 7). The effects that lead to decreasing values for $K_{S/C}$ were most likely due to an interaction of the dispersed formulation structures with the stratum corneum, rather than a simple mechanical effect on the skin surface, as sometimes reported for such permeation retarding effects (31). Caffeine permeation experiments across the silicon membrane and the consideration of dry weight of stratum corneum for the calculation of $K_{S/C}$ may explain this. First, no retarded permeation was found for caffeine across the silicon membrane for E and LD, and secondly, $K_{S/C}$ was obtained from drug concentrations within the stratum corneum, equilibrated with the respective formulation. Thus, the situation of equilibrium and the consideration of dry weight of stratum corneum include a constant drug concentration within the stratum corneum if its solubility properties are not affected, independently of a possible protective film on its surface formed by dispersed formulation structures. It is worth mentioning that diffusion coefficients calculated with Eq. (4) gave lesser values, compared to corresponding true values in the hydrated state of stratum corneum because of the consideration of its dry weight. However, this yielded less variation of the results, compared to weighting of hydrated stratum corneum after equilibration.

In the situation of transdermal drug delivery from a multi-phase dermatological formulation, two diffusion-related processes take place: the discussed drug diffusion within the skin and drug diffusion within the formulation to the skin. Thus, self-diffusion of the sodium nicotinate within the study formulations was measured by NMR diffusion experiments (Table 3) and compared to the calculated diffusion coefficients within the stratum corneum (Fig.4). As mentioned above, the diffusion coefficients shown in Fig. 4 are smaller, compared to true values in the hydrated state of stratum corneum, taking into account Eq. (4). However, the values may be corrected by the factor 2.75, because fully hydrated stratum corneum binds the 2.75 fold amount of water of its dry weight (32). The corrected diffusion coefficients within the stratum corneum are at

least two orders of magnitude smaller (data not shown, but easy to estimate taking in account Fig. 4), compared to the sodium nicotinate diffusion coefficients in the formulations (Table 3). This finally indicates that diffusion in the skin dominates permeation kinetics, confirming a published work where diclofenac permeation from different phospholipid-based formulations was investigated (33). The sodium nicotinate was chosen for the NMR diffusion studies because its enhanced permeation from CF10 and CF50 was most obvious. The observed moderate difference of the self-diffusion coefficients (Table 3) for the study formulations was very likely due to unequal sterically hindered diffusion. According to the equation $\overline{\Delta r^2} = 6Dt$, the average diffusion way *r* of a molecule, three-dimensional diffusion assumed, may be calculated considering the effective diffusion time *t* and the respective diffusion coefficient *D*. For sodium nicotinate, this diffusion way exceeded the size of the dispersed structures by far (Fig.2). For example, in 250 ms, the calculated value for *r* within the gel was 29 µm, and within CF50, this average diffusion way was about 18 µm. Thus, the relatively long diffusion way during the measured effective diffusion time of 250 ms includes that the sodium nicotinate had to diffuse around dispersed structures, which become more important when they are small and, hence, closer packed (liposomes within LD and microemulsion aggregates within CF50). If micellar polysorbate 20 is also considered as diffusional barrier, this also explains the similar sodium nicotinate diffusion within E as within the isolated fraction B of E, because this fraction contained about 5 weight-% of micellar polysorbate 20 beside buffer and ethanol (see 3.1.4).

To conclude, the proposed continuous phase drug concentration concept allows delineating the regulation of skin permeation by the formulation as a result of physicochemical parameters, including drug distribution among distinct phases of formulation, and/or as a result of affecting skin permeability of the drug due to a vehicle-stratum corneum interaction. Thus, this concept valuably contributes to an effective development of dermatological formulations as well as to successfully drug delivery in clinical situations. Furthermore, the microemulsions that were identified within CF10 and CF50 provide a predictive tool to improve transdermal drug delivery, because they consist of non-irritant components and arise spontaneously within multi-component formulations.

**Acknowledgements**

NMR diffusion measurements were performed at the Institute of Organic Chemistry, University of Basel by Dr. Daniel Haeussinger. We are grateful to Dr. Daniel Haeussinger for his valuable contribution to this work.

## References

(1) C. Surber, E.W. Smith, The mystical effects of dermatological vehicles, Dermatology 210 (2005) 157-168.

(2) C. Schutz, Microemulsion: Distinctive combination of perfect invisibility and extreme performance, SÖFW-J. 129 (8) (2003) 16-19.

(3) M. Kreilgaard, E.J. Pedersen, J.W. Jaroszewski, NMR characterisation and transdermal drug delivery potential of microemulsion systems, J. Control. Release 69 (2000) 421-433.

(4) M. Kreilgard, Influence of microemulsions on cutaneous drug delivery, Adv. Drug Deliv. Rev. 54 (2002) 77-98

(5) M. Carafa, C.Marianecci, G.Lucania, E.Marchei, E.Satucci, New vesicular ampicillin-loaded delivery systems for topical application: characterisation, in vitro permeation experiments and antimicrobial activity, J. Control. Release 95 (2004) 67-74.

(6) D.D. Verma, A. Fahr, Synergistic penetration enhancement effect of ethanol and phospholipids on the topical delivery of cyclosporin A, J. Control. Release 97 (2004) 55-66.

(7) R. Valjakka-Koskela, M. Kirjavainen, J. Mönkkönen, A. Urtti, J. Kiesvaara, 1998. Enhancement of percutaneous absorption of naproxen by phospholipids, Int. J. Pharm. 175 (1998) 225-230.

(8) D.D. Verma, S. Verma, G. Blume, A. Fahr, 2003. Lipososmes increase skin penetration of entrapped and non.entrapped hydrophilic substances into human skin: a skin penetration and confocal laser scanning microscopy study. Eur. J. Pharm. Sci. 55 (2003) 271-277.

(9) E. Touitou, N. Dayan, L. Bergelson, B. Godin, M. Eliaz, Ethosomes-novel vesicular carriers for enhanced delivery: characterisation and skin penetration properties. J. Control. Release 65 (2000) 403-418.

(10) M. Kirjavainen, A. Urtti, R. Valjakka-Koskela, J.Kiesvaara, J.Mönkkönen, Liposome-skin interactions and their effects on the skin permeation of drugs, Eur.J. Pharm. Sci. 7 (1999) 279-286.

(11) Ph.J. Lee, R. Langer, P.V. Shastri, Novel microemulsion enhancer formulation for simultaneous transdermal delivery of hydrophilic and hydrophobic drugs, Pharm. Res. 20 (2) (2003) 264-269.

(12) M.B. Delgado-Charro, G. Iglesias-Vilas, J. Blanco-Méndez, M.A. Lopez-Quintela, J.P. Marty, R.H. Guy, 1997. Delivery of a hydrophilic solute through the skin from novel microemulsion systems, Eur. J. Pharm. Biopharm. 43 (1997) 37-42.

(13) U. Schmalfuss, R. Neubert, W. Wohlrab, Modification of drug penetration into human skin using microemulsions, J. Control. Release 46 (1997) 279-285.

(14) F. Dreher, P. Walde, P. Walther, E. Wehrli, Interaction of a lecithin microemulsion gel with human stratum corneum and its effect on transdermal transport, J. Control. Release 45 (1997) 131-140.

(15) B.W. Barry, Formulation of dermatological vehicles, In: B.W.Barry (Ed.) Dermatological Formulations Percutaneous absorption, Marcel Decker, New York 1983, pp. 297-350

(16) N. Leveque, S. Makki, J. Hadgraft, Ph. Humbert, Comparison of franz cells and microdialysis for assessing salicylic acid penetration through human skin, Int. J. Pharm. 269 (2004) 323-328

(17) F.P. Schwarb, G. Imanidis, E.W. Smith, J.M. Haigh, Ch. Surber, Effect of concentration and degree of saturation of topical fluocinolide formulations on in vitro membrane transport and in vivo availability on human skin. Pharm. Res., 16 (6) (1999) 909-915.

(18) H. Nalenz, G. Imanidis, How the alteration of multi-phasic dermatological formulations following application affects skin permeation of a hydrophilic model drug, Eur.J. Pharm. Biopharm., submitted

(19) D. Hummel, G. Imanidis, in: R. Marks, J.-L. Leveque, R. Voegeli, (Ed.), The Essential Stratum Corneum. Martin Dunitz, London (2002)119-124.

(20) N. Sekkat, Y.N. Kalia, R.H. Guy, 2002. Biophysical study of porcine ear skin in vitro and its comparison to human skin in vivo, J. Pharm. Sci. 91 (11) (2002) 2376-238.

(21) K. Yoneto, S.K. Li, W.I. Higuchi, S.Shimabayashi, Influence of the permeation enhancers 1-alkyl-2-pyrrolidones on permeant partitioning into the stratum corneum, J. Pharm. Sci., 87 (2) (1998) 209-214.

(22) H. Wagner, K.-H. Kostka, C.-M. Lehr, U.F. Schaefer, Correlation between stratum corneum/water-partition coefficient and amounts of flufenamic acid penetrated into the stratum corneum, J. Pharm. Sci., 91 (2002) 1915-1921.

(23) D. Van der Merwe, J.E. Riviere, Comparative studies on the effects of water, ethanol and water/ethanol mixtures on chemical partitioning into porcine stratum corneum and silastic membrane. Tox. In Vitro, 19 (2005) 69-77.

(24)Boehringer, Methoden der enzymatischen BioAnalytik und Lebensmittelanalytik, Boehringer Mannheim GmbH, Mannheim, 1997.

(25) D. Wu, A. Chen, C.S. Johnson Jr., An improved diffusion-ordered spectroscopy experiment incorporating bipolar-gradient pulses, J. Magn. Reson. Series A, 115 (1995) 260-264.

(26) M. Holz, H. Weingärtner, Calibration in accurate spin-echo self-diffusion measurements using proton and less-common nuclei, J. Magn. Reson. 92 (1991) 115-125.

(27) XWINNMR, Bruker Analytik GmbH, Sotware Dept., Rheinstetten, Germany.

(28) K. Moser, K. Kriwet, A. Naik, Y.N. Kalia, R. Guy, Passive skin penetration enhancement and its quantification in vitro, Eur. J. Pharm. Biopharm. 52 (2001) 103-112.

(29) J. Hadgraft, Skin, the final frontier, Int. J. Pharm. 224 (2001) 1-18.

(30) R. Aboofazeli, M.J. Lawrence, 1993. Investigations into the formation and characterisation of phospholipid microemulsions: I. Pseudo ternary phase diagrams of systems containing water-lecithin-alcohol-isopropyl myristate. Int. J. Pharm. 93 (1993) 161-175.

(31) A. zur Mühlen, A. Klotz, S. Weimans, M. Veeger, B. Thörner, B. Diener, M. Hermann, Using skin models to assess the effects of protection cream on skin barrier function, Skin Pharm. And Physiol., 17 (2004) 167-175.

(32) J.M. Nitsche, T.-F. Wang, G.B. Kasting, A two phase analysis of solute partitioning into the stratum corneum, J. Pharm. Sci. 95(3) (2006) 649-666.

(33) K.Kriwet, C.C. Mueller Goymann, Diclofenac release from phospholipid drug systems and permeation through excised human stratum corneum. Int. J. Pharm. 125 (1995) 231-242.

## Figures

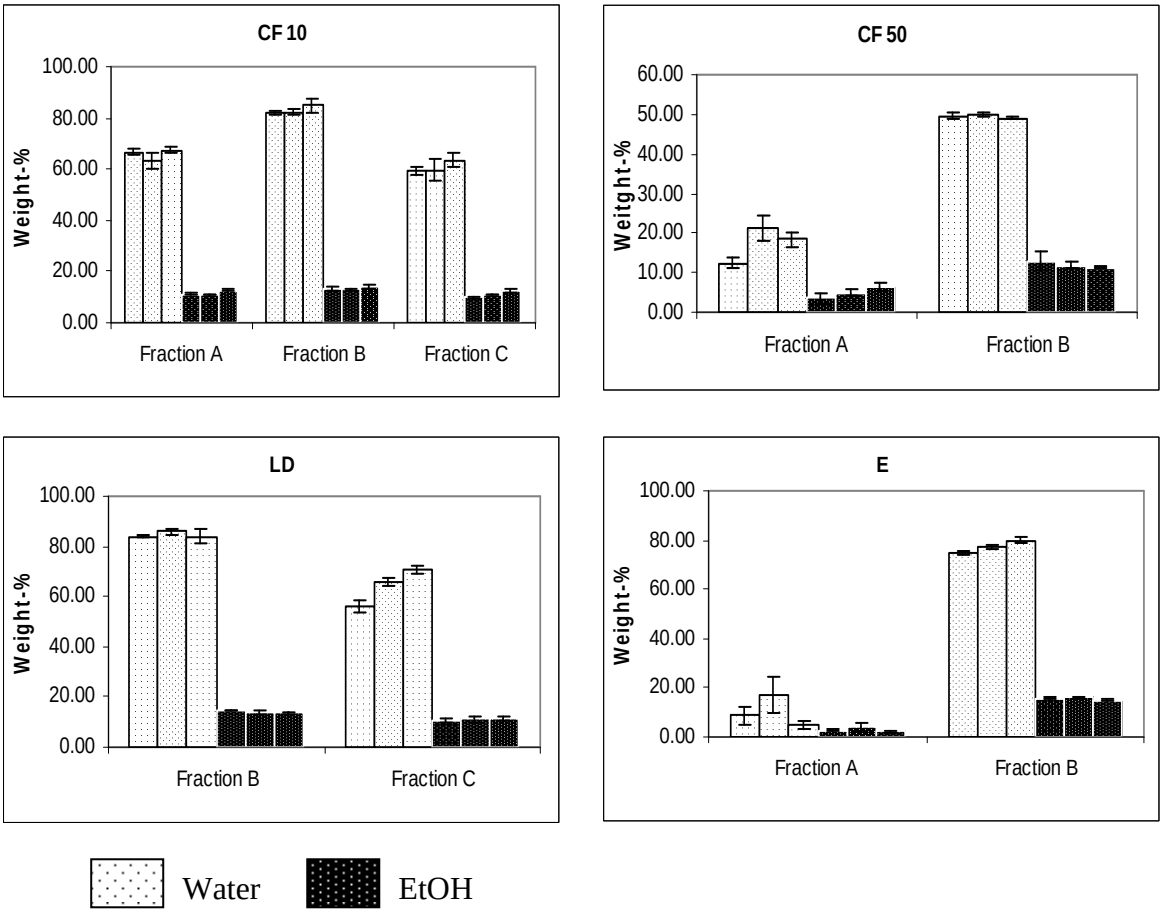


**Figure 1** Analyzed amounts of water and ethanol within fractions received from ultracentrifugation. One diagram represents one formulation. Equal bars for one fraction denote water or ethanol content within this fraction obtained from the formulation that contained, from left to right, sodium nicotinate, BTA-Cl or caffeine as model drug. Error bars denote SEM (n=3-4)

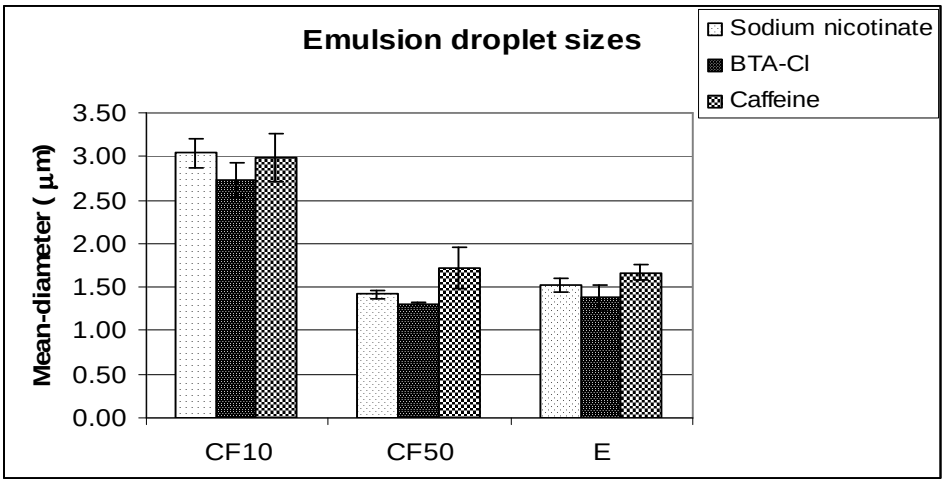


**a.**

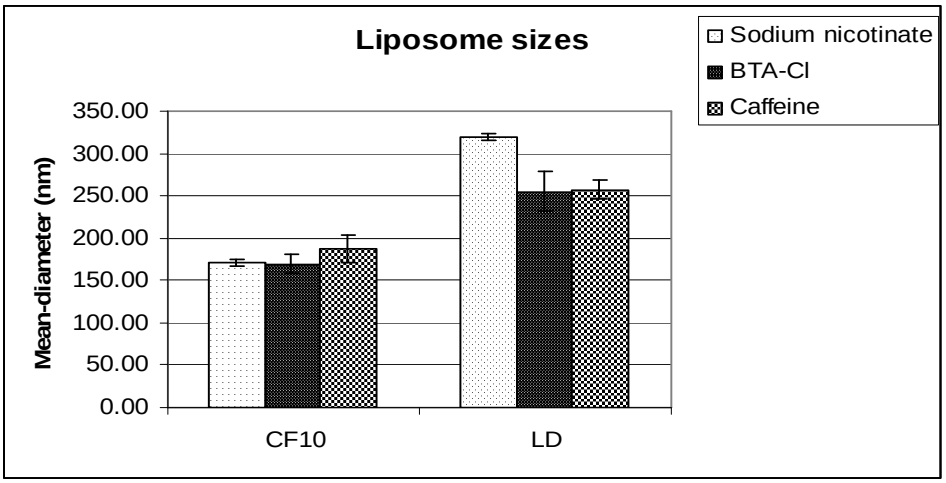


**b.**

**Figure 2** Diameters of emulsion droplets in µm (a.) and liposomes in nm (b.) of the formulations which contained the different model drugs. Error bars denote SEM, n=3-7

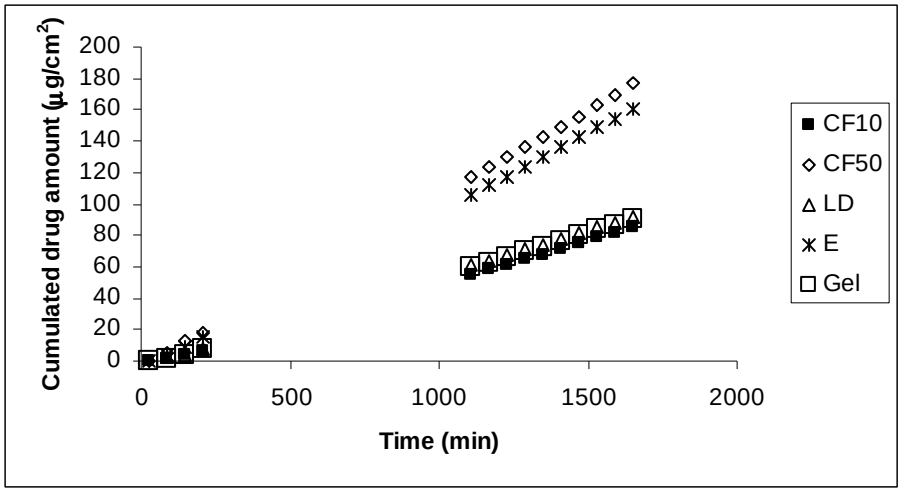


**a.**

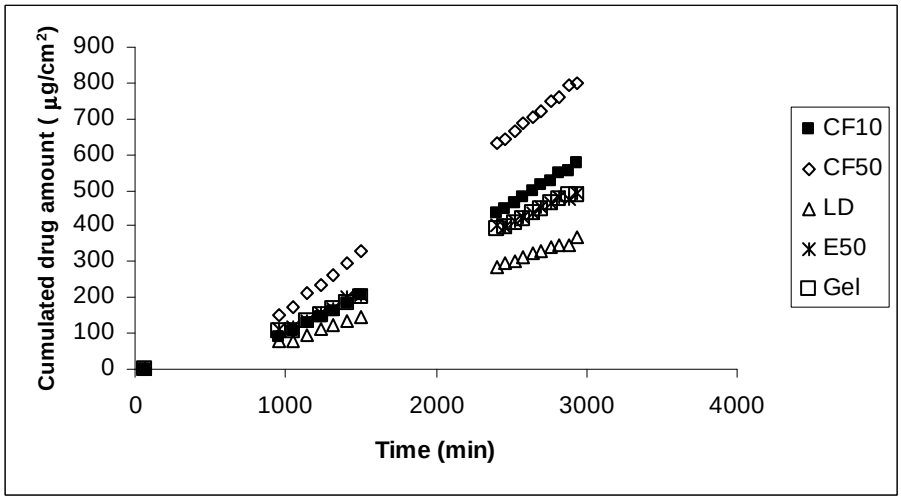


**b.**

**Figure 3** Permeation profile of caffeine following application of the study formulations across a silicone membrane (a.) and across excised pig ear skin (b.). For simplicity, error bars are not shown

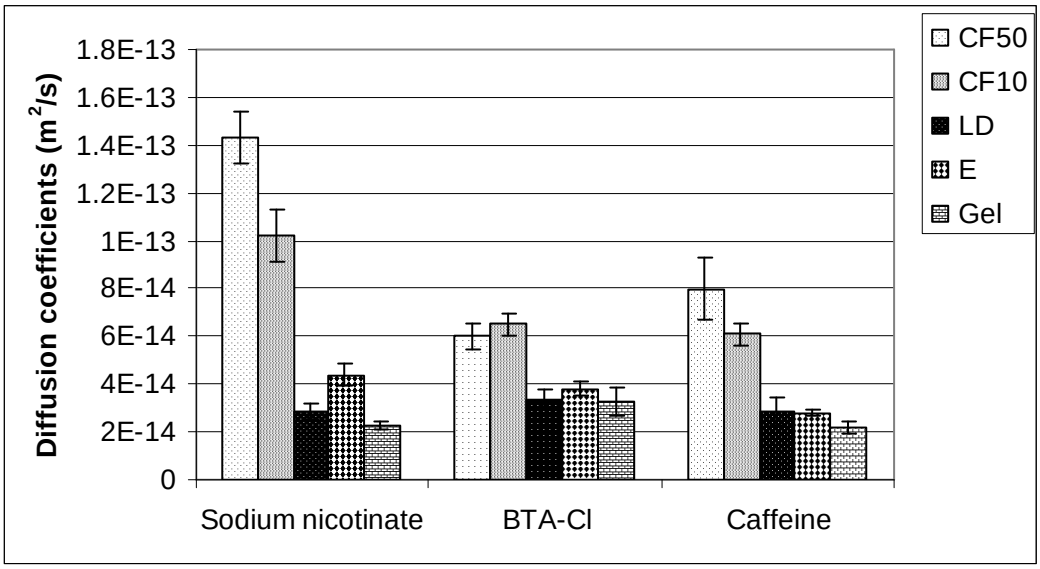


**Figure 4** Diffusion coefficients within the stratum corneum of the model drugs following permeation from the study formulations. Error bars denote SEM, n=4-7

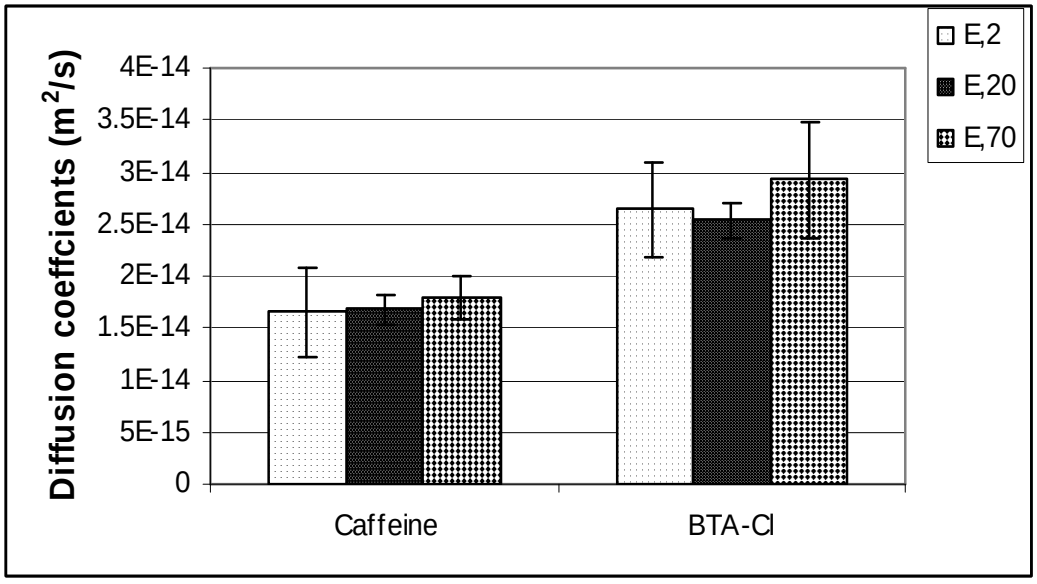


**Figure 5** Diffusion coefficients of caffeine and BTA-Cl within the stratum corneum following permeation from different emulsion formulations with variable amounts of dispersed phase of 2, 20 and 70 weight-% (E2, E20 and E70, respectively). Error bars denote SEM, n=3-6

## Tables

**Table 1**
Composition of the study formulations (in weight-%)

| | CF 10[a] | CF 50[b] | E[c] | LD[d] | Gel[e] |
|---|---|---|---|---|---|
| Model drug | 1.0 | 1.0 | 1.0 | 1.0 | 1.0 |
| Aqueous buffer pH 7.4 | 73.85 | 34.9 | 36.92 | 74.25 | 81 |
| Ethanol 96% | 14.1 | 6.6 | 9.98 | 11.82 | 17.5 |
| Mygliol 812N® | 6.75 | 36.0 | 47.9 | | |
| Polysorbate 20 | 1.35 | 8 | 4.0 | | |
| NAT 8539® | 2.4 | 13.38 | | 12.33 | |
| Tocopherol | 0.05 | 0.1 | | 0.1 | |
| Xanthan gum | 0.5 | 0.20 | 0.20 | 0.5 | 0.5 |

[a]Complex formulation with 10 weight-% dispersed phase, [b]Complex formulation with 50 weight-% dispersed phase, [c]Emulsion with 50 weight-% dispersed phase, [d]Liposomal dispersion with 10 weight-% dispersed phase, [e]Ethanolic gel. The model drug is sodium nicotinate, expressed as nicotinic acid, BTA-Cl or caffeine.

**Table 2** Diameters of microemulsion aggregates included in CF10 and CF50

| **Fraction B of CF50** | | | | | | |
|---|---|---|---|---|---|---|
| Included model drug | Sodium nicotinate | | BTA-Cl | | Caffeine | |
| Dilution | z-average | PI | z-average | PI | z-average | PI |
| 1/5 | 23.9 | 0.162 | 20.7 | 0.091 | 23.5 | 0.27 |
| 1/10 | 23.7 | 0.112 | 21.5 | 0.091 | 22.1 | 0.151 |
| 1/20 | 23.4 | 0.088 | 21.8 | 0.09 | 23.8 | 0.187 |
| 1/100 | 22.6 | 0.130 | 21.3 | 0.075 | 23.0 | 0.153 |
| **Fraction B of CF10** | | | | | | |
| Single experiments | | | | | | |
| 1 | 46.4 | 0.527 | 29.4 | 0.288 | 32.2 | 0.246 |
| 2 | 29.1 | 0.16 | 29.9 | 0.23 | 32.1 | 0.419 |
| 3 | 27.8 | 0.153 | 44.4 | 0.471 | 26.5 | 0.22 |

Values denote nm and PI stands for polydispersity index. Microemulsion aggregates comprised within fraction B separated from CF10 were inspected undiluted and the numbers1-3 denote single inspections of different samples

**Table 3** Sodium nicotinate self-diffusion coefficients within the formulations

| | CF10 | CF50 | LD | E | Gel |
|---|---|---|---|---|---|
| Diffusion Coefficients | 4.30E-10 | [a]2.18E-10 | 2.19E-10 | 2.49E-10<br>[b]3.30E-10 | 5.66E-10 |

Values obtained from NMR diffusion experiments, effective diffusion time 250 ms. [a]Denotes the self-diffusion coefficient in the isolated fraction B (microemulsion) of CF50, [b]denotes the self-diffusion coefficient within the isolated fraction B of E. All values in $m^2/s$

**Table 4** Ultrafiltration, ultracentrifugation and continuous phase drug concentrations

| Formulation | Model Drug | Calculated concentration[a] | Measured concentration UF[b] | Measured concentration fraction B, UZ[c] |
|---|---|---|---|---|
| CF50 | Sodium nicotinate | 22.22 | 26.96±3.32 | 14.54±0.073 |
| | BTA-Cl | 22.22 | 20.16±1.88 | 14.73±0.043 |
| | Caffeine | 18.52 | 17.55±4.76 | 13.04±0.048 |
| CF10 | Sodium nicotinate | 11.18 | 11.03±0.37 | 11.23±0.028 |
| | BTA-Cl | 11.18 | 10.40±0.41 | 11.03±0.084 |
| | Caffeine | 10.91 | 11.06±1.40 | 11.24±0.0071 |
| LD | Sodium nicotinate | 11.11 | 10.60±0.93 | 11.90±0.26 |
| | BTA-Cl | 11.11 | 10.28±1.51 | 10.43±0.76 |
| | Caffeine | 11.11 | 11.08±0.94 | 11.21±0.085 |
| E | Sodium nicotinate | 21.27 | 23.11±0.53 | 20.75±0.23 |
| | BTA-Cl | 21.27 | 21.15±1.14 | 20.41±0.38 |
| | Caffeine | 17.36 | 17.42±1.42 | 18.18±0.15 |

[a]Calculated concentrations with Eq. (2). [b]Concentrations resulting from ultrafiltration experiments. [c]Concentrations of received fractions B following ultracentrifugation of LD and E. Sodium nicotinate is expressed as nicotinic acid. All drug concentrations in mg/g ± SD, n=3-4

**Table 5** Permeability coefficients

| | Sodium nicotinate | BTA-Cl | Caffeine | Caffeine a.s.[a] |
|---|---|---|---|---|
| **CF50** | **3.03E-07±2.38E-08** | **2.42E-07±2.18E-08** | **3.10E-07±5.01E-08** | **9.88E-08±1.21E-08** |
| **CF10** | **3.56E-07±3.73E-08** | **4.57E-07±3.05E-08** | **4.25E-07±3.17E-08** | **8.36E-08±9.22E-09** |
| **LD** | **1.43E-07±1.24E-08** | **3.12E-07±3.61E-08** | **2.14E-07±4.46E-08** | **8.68E-08±8.68E-09** |
| **E** | **1.55E-07±1.20E-08** | **2.44E-07±2.08E-08** | **1.78E-07±8.20E-09** | **9.81E-08±1.06E-08** |
| **Gel** | **1.44E-07±8.56E-09** | **3.81E-07±1.70E-07** | **3.35E-07±4.15E-08** | **9.40E-08±8.58E-09** |
| MeCF50 | 2.60E-07±1.21E-08 | 2.04E-07±1.01E-08 | 2.63E-07±1.75E-08 | |
| MeCF10 | 3.87E-07±5.21E-08 | 4.36E-07±5.39E-08 | 3.00E-07±2.82E-08 | |
| E2 | 1.30E-07±3.25E-08 | 3.12E-07±5.44E-08 | 1.98E-07±5.13E-08 | |
| E20 | 9.11E-08±2.68E-08 | 2.44E-07±1.63E-08 | 1.72E-07±1.39E-08 | |
| E70 | 1.16E-07±3.93E-08 | 2.04E-07±3.90E-08 | 1.36E-07±1.54E-08 | |

Bold values correspond to the study formulations given in Table 1. MeCF50 and MeCF10 denote the microemulsion structures isolated from CF50 and CF10, respectively. Caffeine a.s. denotes permeability coefficients for caffeine across a silicon membrane. E2, E20 and E70 are different emulsion formulations with variable amounts of dispersed phase of 2, 20 and 70 weight-%, respectively. All values in cm/s ± SEM, n=4-6, [a]n=3

**Table 6** Sodium nicotinate permeability coefficients for ethanol free formulations

| | CF50[a] | CF10[a] | LD[a] | E[a] | Gel[a] |
|---|---|---|---|---|---|
| P | 1.01E-07± 1.54E-08 | 1.18E-07± 1.43E-08 | 1.04E-07± 2.43E-08 | 7.42E-08± 1.46E-08 | 8.32E-08± 5.41E-09 |

[a]Denotes the study formulations given in Table 1, but manufactured without ethanol. All values in cm/s ± SEM, n=3

**Table 7** Drug distribution coefficients $K_{S/C}$ between stratum corneum and continuous phase of formulations

| | Sodium nicotinate | BTA-Cl | Caffeine |
|---|---|---|---|
| **CF50** | **0.32 ± 0.076** | **0.61± 0.020** | **0.56± 0.089** |
| **CF10** | **0.52 ± 0.050** | **1.06± 0.076** | **0.99± 0.15** |
| **LD** | **0.76 ± 0.18** | **1.40± 0.081** | **1.12± 0.15** |
| **E** | **0.53 ± 0.10** | **0.96± 0.055** | **0.96± 0.14** |
| **Gel** | **0.96 ± 0.11** | **1.75± 0.12** | **2.31± 0.20** |
| E2 | | 1.77±0.10 | 1.79±0.12 |
| E20 | | 1.45±0.23 | 1.54±0.16 |
| E70 | | 1.04±0.096 | 1.13±0.082 |
| LD2 | | 1.78±0.044 | 1.99±0.18 |
| LD5 | | 1.51±0.073 | 1.23±0.16 |
| LD20 | | 0.92±0.063 | 1.03±0.095 |

Bold values correspond to the study formulations given in Table 1. E2, E20 and E70 denote different emulsion formulations with variable amounts of dispersed phase of 2, 20 and 70 weight-%, respectively. LD2, LD5 and LD20 denote different liposomal dispersions with variable amounts of dispersed phase of 2,5 and 20 weight-%, respectively. All values denote mean ± SEM. n=4-7

## D.2 How the alteration of multi-phase dermatological formulations following application affects skin permeation of a hydrophilic model drug


### Abstract

The goal of this work was to investigate the influence of multi-phase dermatological o/w formulations on in-vitro drug permeation across pig ear skin taking especially into consideration alterations these formulations undergo due to evaporation of volatile components following non-occlusive application. A concept is proposed that postulates changing continuous phase drug concentration during application as the only parameter governing permeation kinetics. Sodium nicotinate was used as model drug and the studied o/w formulations consisted of phospholipids, triglycerides, emulsifier, ethanol and water in proportions covering a wide range of values and phase ratios from dispersed to continuous phase. Depending on the individual composition, coexisting dispersed phase structures, such as liposomes, emulsion droplets and microemulsions were formed, as attested by ultracentrifugation experiments, chemical component analysis, scanning electron microscopy and particle size measurements. Evaporation of volatile componets during application yielded phase transitions, including vesicle to microemulsion, phase inversion from o/w to w/o and drug precipitation. Independently of structural changes, continuous phase drug concentration could quantitatively describe permeation kinetics without the need to consider formulation effects on skin barrier function. Hence, the proposed concept provides a predictive tool to describe quantitatively drug permeation from non-occlusively applied multi-phase dermatological formulations.


### 1 Introduction

In clinical practice, drugs are incorporated in a vehicle in order to be applied to the skin for topical or systemic therapy (1). Vehicles typically consist of several components that are often not mutually miscible, thus forming separate phases. The phases of such a formulation are intermixed, producing macroscopically homogeneous systems, while the structures on the microscopic level, however, may be completely different. It is meanwhile widely acknowledged that such formulations, which are conceived as drug delivery vehicles, regulate transdermal permeation. This regulation may take place based on physicochemical principles such as diffusion and partitioning of the active ingredient and/or by an interaction with the skin, affecting its permeability of the drug. For example, liposomal vesicles (2,3) or microemulsions (4,5,6) have been credited with enhancing skin permeation of active ingredient(s). Reviews from Kreilgard (7) and Bouwstra and Honeywell-Nguyen (8) give good overviews about the

range of publications that report on dermal and transdermal drug delivery from microemulsions and liposomes, respectively.

Another crucial aspect that is, however, not considered to any great extent in the literature is that the structural matrix and composition of the vehicle may undergo changes during application. Medications are typically applied to the skin as a thin layer under non-occlusive conditions and are intended to deliver the active ingredient for hours. After application, the composition of the formulation may change, commonly because of evaporation of volatile components (1). Such a change in the composition of a multi-component system likely elicits alterations of the phase structure of the system and of the concentration and distribution of the active ingredient in it. These alterations in turn can affect delivery performance. Consequently, the transformation of the formulation while on the skin surface may be a crucial factor determining drug delivery.

This influence of loss of volatile components on drug permeation was studied mostly with volatile solutions or was not always related to its effect on drug permeation. An early work highlights the importance of the rising drug concentration due to loss of volatile components as a possible mechanism to enhance percutaneous absorption of steroids, compared to occlusive application (9). Similar results were presented for minoxidil and water/ethanol/propylene glycol solutions as volatile vehicles (10). An interesting publication presents a drug delivery device where the evaporation of ethanol from an ethanol-water mixture increased the skin-vehicle partition coefficient, which compensates for the loss of drug due to skin permeation (11). The consequence is a near zero order flux over a long time-range and an absence of large excess of drug in the donor reservoir. Other investigations focus more detailed possible changes dermatological formulations undergo following application, but without correlating the observations with drug delivery (12,13). The common, but valuable conclusion of these studies is that the phase diagrams may reflect the arising structures during evaporation. The dependence of drug delivery on alterations multi-phase dermatological formulations undergo due to evaporation of volatile components, however, is restricted to a few systematic studies (14,15).

The goal of the present work was to investigate the dependence of drug skin permeation on the microstructure of multi-phase dermatological o/w formulations and, importantly, on alterations these formulations undergo due to evaporation of volatile components following application. The studied o/w formulations consisted of phospholipids, triglycerides, emulsifier, ethanol and water in proportions covering a wide range of values. These formulations were designed specifically for investigating the effect of mass fraction of formulations and its change following application on transdermal delivery. Sodium nicotinate was used as model hydrophilic drug. For interpretation of permeation data, a model is proposed that considers

drug distribution among distinct phases of such dispersed systems and postulates that continuous phase drug concentration alone governs drug permeation kinetics.

Coexisting structures of the different formulations were separated by ultracentrifugation and identified by freeze fracture scanning electron microscopy, chemical component analysis and particle size measurements. Methods were developed and optimized for determining the free drug concentration in the continuous phase of the formulations. Alterations the formulations undergo following application were examined with special emphasis on changing mass fractions of distinct phases in order to calculate the arising continuous phase drug concentration during application. Permeation experiments were carried out in-vitro using pig ear skin as a model for human skin (16). An optimized amount of formulation was applied in order to detect obvious alterations of the formulations and to theoretically determine steady state flux values that facilitate the data evaluation. This was deemed appropriate for reaching the specific goals of this study.

## 2 Materials and methods

### 2.1 Materials

Nicotinic acid was purchased from Sigma (St. Louis, MO, USA). Mygliol 812N®, medium chain triglycerides, was a gift from Hüls AG (Witten, Germany). NAT 8539®, consisting of 25 weight-% EtOH and 75 weight % Phospholipon 80, a soy bean lipid extract with 76 weight-% phosphatidylcholine, was a gift from Phospholipid GmbH (Cologne, Germany). Polysorbate 20, Sodium dihydrogenphosphate Dihydrate and Sodium azide were purchased from Fluka Chemie GmbH (Buchs, Switzerland). Alcohol dehydrogenase 100mg (3.4ml) suspension, Aldehyde dehydrogenase, lyophilized powder, 250U and NAD, free acid, grade II, approx.98%, were purchased from Roche Diagnostics AG (Rotkreuz, Swizterland). Tetra-n-butylammonium hydrogensulfate LiChropur, CombiTitrant5, a one-component reagent for the volumetric Karl Fischer titration, methanol and tetrahydrofurane, Lichrosolv, were obtained from Merck (Darmstadt, Germany). Acetonitril (HPLC, gradient grade) was obtained from Biosolv (Valheesward, Netherlands). 9-Anthryldiazomethane was purchased from Serva Electrophoresis, (Heidelberg, Germany). All other chemicals and reagents used in this study were of analytical grade. Bidistilled water was used in all cases.

### 2.2 Preparation of formulations

The representative formulations (Table 1) were prepared by mixing NAT 8539® and tocopherol with the ethanol (mixture 1), dissolving the nicotinic acid in phosphate buffer (β= 0.01) adjusted to pH of 7.4 (mixture 2) and suspending polysorbate 20 in Mygliol 812N® (mixture 3). For manufacturing CF10 and CF50, in a first step mixture 2 was added to mixture 3 and homogenised for 5 minutes at 20000 rpm using a Polytron Pt 3000 (Kinematica AG Littau, Switzerland). Subsequently, mixture 1 was added and the product was homogenised once

again for 5 minutes. E was produced by adding mixture 2, additionally containing the ethanol, to mixture 3, and LD was obtained by adding mixture 1 to mixture 2, followed by homogenisation as above. Xanthan gum was added at the end to the formulations followed by futher short homogenisation, except for the formulations that were used for ultracentrifugation. A purely aqueous gel with a drug load of 1 weight-% nicotinic acid was produced by adding 0.5 weight-% xanthan gum to mixture 2. In all cases, the formulations were allowed to equilibrate for at least 24 hours before use. The pH was measured with a pH-meter 691 and a sensor type Porotrode (Metrohm AG, Herisau, Switzerland). A pH value in the range of 7-7.5 was required to receive deprotonation of the nicotinic acid to nicotinate.

**2.3 Chemical component analysis of the formulations**

Chemical component analysis of the received fractions following ultracentrifugation (see 2.4) was performed as follows: Phospholipids were quantified by determination of anorganic phosphate after digestion of the phospholpids with a sulphuric/perchloric acid mixture. A spectroscopic method based on the formation of a coloured complex of phosphomolybdate with malachite green absorbing at 610 nm was applied (17).

Water was assayed by Karl-Fischer titration using a KF 701 Titrino (Metrohm AG, Herisau, Switzerland) and a one-component reagent CombiTitrant 5. The titer was exactly determined with double distilled water prior to every analytical run.

EtOH was quantified by an enzymatic method (18), based upon spectroscopic determination of accumulated NADH at 340 nm using a Perkin Elmer Spectrometer Lambda 20 (Perkin Elmer, Ueberlingen, Germany).

Sodium nicotinate, expressed as nicotinic acid, was assayed by HPLC (Hewlett Packard, series 1050, Hewlett Packard, Waldborn, Germany). A reversed phase RP-18 column (CC 125/2 Lichrospher 100-5 RP-18 ec) was used. The mobile phase consisted of phosphate buffer (pH 7.4, β=0.05), containing 5mM tetrabutylammonium hydrogenphosphate and 5% methanol. The flow rate was 0.25 ml/min. Detection was performed UV-spectrophotometrically at 214 nm. Sodium nicotinate extraction from the samples was done after suitable dilution with buffer pH 7.4 by sonification for 5 minutes. The samples were filtered through a siring filter (Titan 2, PTFE, 0.2 µm, Sun Sri, NC, USA) prior to injection.

Continuous phase nicotinate concentration was quantified following ultrafiltration using centrifugal filter devices (Microcon YM3) with a molecular weight cut-off of 3000 (Millipore, Bedford, MA, USA).

Triglycerides and polysorbate 20 were quantified by HPLC following saponification and derivatisation of the fatty acids with 9-anthryldiazomethane (ADAM) (19). Briefly, samples were weighted into eppendorf tubes and treated with 0.5 ml 1N NaOH solution (80% ethanol/ 20% water) during 7 hours at 60°C. After acidification with 0.2 ml 5N HCl, the free acids were extracted with 0.6 ml methylene chloride. 0.01 ml of this extract was added to 0.29 ml of

methanolic ADAM-solution (0.15%) and allowed to react for at least 1 hour at 25℃, protected from light using brown glass HPLC vials. The same chromatographic equipment as for the nicotinic acid assay was used. The injection volume was 10 µl and the composition of the mobile phase, flow rate 0.3 ml/min, was varied in a gradient mode as follows: mobile phase A consisted of 85 % acetonitrile and 15% water and mobile phase B contained 10 % THF and 90% acetonitrile. 0 -18 min: 100% A, 18- 30 min linear change to 100% B, 30-40 min 100% B, 40-50 min 100% A. The ADAM esters were detected at 255 nm.

**2.4 Physical methods to characterise the formulations**

Formulations were fractionated by ultracentrifugation using an ultracentrifuge type Centricon T-1075 and a rotor TFT 7013 (Kontron Instruments, Mailand, Italy), and Quick-Seal centrifuge tubes, 5/8X3 (Beckman Instruments, Palo Alto, USA). Formulations CF10 and LD were centrifuged for 2 hours, and CF50 and E for 1 hour at 222000-450000 g, xanthan gum omitted. The different operation times were optimised to fractionate intact structures.

Sample preparation for cryo-raster electron microscopy was done as follows: small droplets of the formulations were mounted on a specimen table and rapidly frozen in liquid propane at -196℃. Further processing and observation was perfo rmed in a Balzer SCU 020 cryo-preparation unit attached to a Joel JSM 6300 scanning electron microscope. The frozen samples were fractured in a high vacuum of less than $5*10^{-6}$ bar and a temperature of –100℃, followed by sputtering with gold (layer thickness 10nm) and observed with an acceleration voltage of 10 kV.

The z-average of liposomal vesicles was determined by photon correlation spectroscopy using a Malvern Zetasizer 1000HSa (Malvern Instruments Ltd., Malvern, UK). All measurements were carried out at 25℃. Samples were diluted with filtered buffer pH 7.4 until counting rates between 100 and 300 KCts/s were reached. The mean diameter of emulsion droplets was determined by laser diffraction using a Mastersizer S (Malvern Instruments Ltd., Malvern, UK) with a small sample unit and a beam lens with 300 mm focal distance. All samples were diluted till an obscuration of approx. 20% was reached.

**2.5 Permeation experiments**

Skin permeation was studied in Franz-type diffusion cells at 32℃ with a surface diffusion area of 1.7-1.8 $cm^2$ across excised full thickness pig ear skin. The ears of domestic pigs were obtained from a local abattoir no more than a few hours post-mortem. The skin was separated from the cartilage tissue by a scalpel, stored in a freezer at –75℃ and was used within 4 weeks. The receiver medium for the permeation experiments with a volume of 8.5 to 9 ml consisted of an aqueous phosphate buffer solution, pH 7.4, β=0.05, additionally containing 0.1% of sodium azide as a preservative. Skin integrity was tested by transepidermal water loss (TEWL) measurements (Tewameter TM 210, Courage Khazaka electronic GmbH, Germany) after 4 hours of equilibration prior to the application of the formulations. Then, a practically

infinite dose of formulation of 570 mg/cm$^2$ was applied non-occlusively to the donor compartment. At predetermined time intervals, samples of the receiver medium were collected and replaced by fresh buffer. The entire duration of an experiment was 54.5 hours. The samples were analysed directly for sodium nicotinate concentration by HPLC (for conditions see section 2.3.) without further treatment except centrifugation for 5 min. at 15800 g. Permeation from a purely aqueous gel was studied equally, but under occlusive conditions to keep the donor concentration constant.

**2.6. Evaporation studies**

Formulations were allowed to evaporate on the skin surface, conditions according to the permeation experiments (see 2.5). At representative time points, the formulations were removed from the skin surface, analysed for remaining water and ethanol (see 2.3) and microscopically inspected between crossed polarizers using a Zeiss light microscope (Zeiss, Oberkochen, Germany).

In addition, 150g-batches of the formulations were produced without xanthan gum and allowed to evaporate in a glass container situated in a water bath of 32° C without stirring. The amount of remaining ethanol and water was determined frequently (for conditions see 2.3). Corresponding electric conductivity was measured with a Conductometer 660 and a conductivity-measuring cell 60323110, cell constant 0.8 cm$^{-1}$, (Metrohm AG, Herisau, Switzerland) at 32 °C. CF10 was additionally evaluated by ultracentrifugation and chemical component analysis after evaporation to an amount of remaining water that corresponded to the situation at the end of the permeation experiments.

**2.7 Maximum solubility determination**

For solubility determination, sodium nicotinate was prepared first from nicotinic acid. For this purpose, the commercially available nicotinic acid was dissolved and adjusted to a pH of around 7.5, followed by evaporation of the water under vacuum using a Rotavapor (Büchi, Fluwil, Switzerland) at 40°C. The received sodium nicotinate was dried and stored over silica gel in a desiccator.

In order to estimate saturation concentrations in a solution or preparation, the dry sodium nicotinate was added until precipitation occurred. This mixture was stirred for 8 hours at 32°C, 14 hours at 4°C and again 8 hours at 32°C. Subsequently, the supernatant received after centrifugation for 30 min. (15800g) was analysed for sodium nicotinate (for conditions, see 2.3).

## 3 Results and discussion

### 3.1 Characterisation of the original formulations

The aim of the present work was to investigate the dependence of drug delivery on possible alterations representative dermatological formulations may undergo after application. For that

purpose, the microstructure of these formulations (Table 1) was of primary interest. First, scanning electron microscopy (SEM) was used to visualize the dispersed structures. Fig.1 a,b demonstrates the dissimilar appearance of micrographs obtained from emulsion droplets and liposomes, which are the typical structures of formulations E and LD, respectively, conditioned by their composition. Hence, these micrographs were used to relate the images of formulations CF10 and CF50, which are of more complex composition (Table 1), to one or both of these structures. In case of CF10, a discrimination between two different structures with similar appearance to the liposomes of LD and to the emulsion droplets of E is obvious, while the image of CF50 showed only one population of dispersed structures which appeared more similar to emulsion droplets than to liposomes (see Fig.2 a,b). The visible diameter of these structures, however, was clearly larger for CF10 than for CF50 and E, while the structures that appeared more similar to the liposomes of LD were smaller in size within CF10, almost near the resolution limit of the scanning electron microscope.

Laser diffraction was used to measure the mean diameter of the larger structures, related to emulsion droplets, for CF10, CF50 and E (Table 2). These measured droplet diameters agreed well with the estimated diameters considering the micrographs of CF50, CF10 and E. Laser diffraction, however, is not suitable to detect smaller dispersed structures, for example liposomes, beside larger dispersed structures, for example emulsion droplets.

For that reason and to further characterise the microstructure of formulations, comprising structures were separated using ultracentrifugation. LD and E yielded the following fractions (Fig.3): The emulsion E a turbid, white fraction on top (fraction A) and a clear colorless fraction (fraction B) in the bottom and the liposomal dispersion LD a clear colorless fraction on top (fraction B) and a turbid, yellow-brown, which is also the colour of the bulk-phospholpids NAT 8539®, fraction (fraction C) in the bottom. The outcome of this examination was that liposomes and emulsion droplets may be identified due to their behaviour following ultracentrifugation in case of the investigated formulations. CF10 gave three fractions with similar appearance to the described fractions A, B and C, strongly supporting the conclusions drawn from the SEM-images of coexisting emulsion droplets and liposomes (Fig.3). The clear fraction B of CF10, however, was little yellowish compared to this fraction of LD and E, indicating the presence of phospholipids, either due to incomplete fractionation of small liposomes or due to the presence of other structures that comprise phospholipids. Furthermore, the fractionation of the structures allowed analysing fraction C of CF10, which was supposed to contain liposomes, and this fraction of LD for particle sizes of comprising structures by photon correlation spectroscopy (PCS). These measurements could verify the observations based upon the electron micrographs above of smaller structures that appeared similar to liposomes within CF10, compared to the liposomes within LD (Table 3). All these observations were additionally confirmed considering the micrographs of the isolated fractions A and C of CF10 (Fig.4 a,b).

The image of fraction C showed only structures which appeared similar to the structures of LD, while fraction A revealed only the structures that were related to emulsion droplets, considering the SEM-image of E.

In case of the complex formulation with 50% dispersed phase (CF50), an isotropic clear, but strongly yellowish fraction in the bottom and a fraction in the top of similar appearance to the fractions A of CF10 and E appeared following ultracentrifugation, but no turbid brown fraction in the bottom (Fig.3). This supported the assumed presence of emulsion droplets and the lack of liposomes within this formulation, according to the interpretation of the electron microscopic inspection. Electron microscopy of the clear yellow fraction of CF50 gave an image without recognisable structure, likewise the clear fractions of the other formulations, while the micrograph obtained from the turbid white fraction A of CF50 showed closed packed, intact oil droplets (micrographs not shown). This is a good support for the validity of ultracentrifugation to separate intact structures of o/w dermatological formulations, which was also indicated by equal measured particle sizes for dispersed structures of the complete formulations as for the separated fractions containing these structures (Table 2, Table 3).

In a next step, we estimated the distribution of the formulation compounds between the separated structures of the formulations following ultracentrifugation by chemical component analysis of the received fractions (Table 4). Triglycerides were present in large amounts in fractions A of CF10, CF50 and E, and phospholipids in fractions C of CF10 and LD, supporting the conclusions drawn above that liposomes were sedimenting and emulsion droplets were creaming in case of the investigated formulations. For CF50, where no liposomal structures were formed, phospholipids were found mainly in the clear, yellow fraction, accompanied by remarkable amounts of polysorbate 20 and triglycerides (Table 4). Interestingly, the sum of these compounds within this fraction amounted about 35 weight-%. For comparison, the formulations CF10 and LD, which were both of turbid, milky appearance, included around three times less of triglycerides, polysorbate 20 and/or phospholipids. In addition, rheological inspections of the separated clear, yellow fraction of CF50 showed Newtonian flow behaviour (data not shown), strongly indicating the presence of a microemulsion within this formulation beside the emulsion droplets.

Per definition, a microemulsion consists of aqueous phase, organic phase and a surfactant/cosurfactant component, arises spontaneously, is thermodynamically stable and shows Newtonian flow behaviour (7,20). All these attributes are valid for the discussed structure. Interestingly, fraction B of CF10 also contained small amounts of triglycerides, phospholipids and polysorbate 20 in a roughly comparable ratio to the clear fraction of CF50, while the clear fractions of LD and E contained negligible amounts of phospholipids and triglycerides, respectively. This finding may explain the slightly yellowish colour for fraction B of CF10 mentioned above and indicated here again the formation of a spontaneously arising

system, rather than an incomplete fractionation of the liposomes and emulsion droplets following ultracentrifugation. As consequence, it is postulated that microemulsion structures consisting of phospholipids, triglycerides, polysorbate 20, aqueous buffer and ethanol may arise spontaneously if all these components are present. This implication is supported by the lack of liposomes within formulation CF50, where enough polysorbate 20 and triglycerides were present to incorporate all phospholipids in the microemulsion structure, while the relatively low polysorbate 20 content of CF10 very likely facilitated the formation of liposomal structures.

Furthermore, the chemical component analysis showed that the fraction C of CF10, identified as liposomes above, contained, in addition to predominantly phospholipids, considerable amounts of triglycerides and polysorbate 20 (Table 4). This is a possible explanation for the reduced vesicle size compared to the formulation LD (Table 3). The smaller z-average is considered due to a steric repulsion among the incorporated surfactant, which may increase the liposome particle curvature, and finally decreases the vesicle diameter (21).

Hence, all these results point out that the arising structures of multi-component dermatological formulations cannot be easily related to typical structures that are formed by single use of the compounds. Furthermore, the presence of phosholipids includes not automatically the formation of liposomes, an observation also reported by other working groups (22,23). To summarize, our representative dermatological formulations included a wide variety of possible structures, such as: conventional emulsion droplets, liposomes and microemulsion structures.

To test a possible dependency of transdermal drug permeation on these microstructures, we postulated that continuous phase drug concentration of a multi-phase formulation is the only parameter governing permeation kinetics (see 3.3). Determination of this concentration, in turn, includes the exact information about the composition of the continuous phase and about drug distribution between this phase and dispersed structures. A constant ratio of water to ethanol for every received fraction following ultracentrifugation and for the ratio of these components of the corresponding complete formulation in case of all formulations strongly indicated that the sum of water and ethanol amount to the continuous hydrophilic phase, independently of dispersed structures of the studied o/w formulations. This is demonstrated in Fig.5. To test the distribution of the sodium nicotinate among distinct phases, the same analysis was performed by plotting the total amount of hydrophilic phase of a specific fraction following ultracentrifugation against the corresponding amount of the model drug. This demonstrated in the same way as for the ethanol a complete distribution of the sodium nicotinate into the continuous hydrophilic phase for all formulations (Fig.6). Ultrafiltration experiments confirmed this finding and provide a faster and easier methodology to determine continuous phase drug concentrations of hydrophilic drugs for o/w formulations (Table 5).

### 3.2. Alterations of the formulations due to evaporation

Dermatological vehicles are typically applied non-occlusively and, thus, may undergo considerable compositional changes due to evaporation of volatile components. Therefore, alterations of the study formulations during and after evaporation of water and ethanol, which were the volatile components, were investigated. The cumulated amount of these compounds remaining in the formulations as a function of time, conditions according to the permeation experiments (see 3.3), is shown in Fig.7. CF10 and LD, both comprising an equal, relatively large volatile continuous phase before evaporation, showed comparable evaporation pattern. In case of CF50 and E, which initially contained a comparatively small amount of volatile phase, CF50 retained more water than E. It is worth mentioning that ethanol evaporated faster than water and was undetectable 30 hours after application, independently of the formulation structure.

To investigate alterations due to loss of volatile components of the formulations more detailed, practically big amounts were allowed to evaporate to final water contents that corresponded to the end of the permeation experiments. First, CF10 was allowed to evaporate to remaining water content of about 50%, precisely determined by Karl-Fischer titration. This formulation gave by ultracentrifugation three fractions, as observed before evaporation, but with a turbid brown fraction of equal appearance to the liposomal fraction (fraction C) of the original CF10 in the middle of the centrifugal tube, and a clear, yellow fraction (fraction B) in the bottom. This observation indicated a switch in the order of fractions C and B as well as potential compositional changes of fraction B because of the deepened yellow colour.

On basis of the remaining water of this complete formulation after evaporation, the amount of non-volatile components was calculated with the objective to prepare a formulation with similar composition. This simulated formulation gave also three fractions following ultracentrifugation that appeared comparable to the fractions received from CF10 after evaporation. Hence, all the received fractions of both formulations were analysed for their chemical composition as established for the initial formulations (Table 6). Interestingly, the fractions of the simulated formulation had a comparable chemical composition to the fractions received after evaporation of CF10. As consequence, the conclusion may be drawn that the arising phase structures during evaporation are predictable on the basis of composition alone, supporting the work of other groups (12,13).

Interpretation of the chemical composition of the individual fractions given in Table 6 more detailed supported the assumption of the switch in the order of the initial fractions B and C above. After evaporation, the brown fraction, although still comprising quantities of phospholipids, included also remarkable triglycerides and polysorbate 20, and triglycerides are of lower density, compared to phospholipids. The clear fraction, in turn, was enriched with phospholipids, triglycerides and polysorbate 20, compared to fraction B of the original CF10,

which also comprised a small quantity of microemulsion aggregates (Table 4). Furthermore, comparing the ratios of these components of the fractions B and C before and after evaporation (Table 4; Table 6) demonstrates that the ratio from phospholipids to triglycerides and polysorbate 20 increased for fraction B, while the ratio of phospholipids to these compounds decreased for fraction C after evaporation. Hence, a solubilisation of the vesicles is postulated as a preliminary state before a transition of the phospholipids from vesicle to microemulsion took place. The fact that the investigated formulation CF10 after evaporation, which is analogues to the original CF50 when buffer changes the ethanol, comprised liposomes, but not CF50, was supposed to be due to the presence of the ethanol in case of the latter.

The difference in chemical composition of fraction A of the formulation after evaporation, compared to this fraction of the prepared formulation with equal composition, was very likely due to an observed coalescence of the emulsion droplets during evaporation. It should be mentioned that the data given in Table 6 are no averages of several experiments because it was impossible to fix the exactly same remaining amount of water of a formulation after evaporation, but the examination was repeated with a formulation that was allowed to evaporate to comparable amount of remaining water, which gave the same results (data not shown).

In case of CF50, ultracentrifugation was impossible after evaporation of volatile components because of the big amount of dispersed phase. However, for this formulation, a phase inversion from o/w to w/o was detected by conductivity measurements during evaporation when the remaining water content fell below a value of about 20 weight-%, while the same inspection of formulation E, initially containing an equal phase ratio of dispersed to continuous phase, gave no phase inversion (Table 7). This may also explain the larger amount of retained water for CF50 after evaporation, compared to E (see above). Hence, multi-phase formulations that contain polysorbate 20, triglycerides and phospholipids seem to be able to form w/o systems during evaporation of volatile components, but not the more simple emulsion. Possibly the amphiphilic nature of the phospholipids is responsible for the formation of w/o systems (22). In order to verify this assumption, a big amount of CF10 was also allowed to evaporate to a remaining water content in the same order of magnitude to CF50 after evaporation, which also yielded a w/o formulation (Table 7).

In case of formulation E, ultracentrifugation was also not possible after evaporation for the same reason as described above for CF50. However, microscopic inspection using crossed polarizers revealed the formation of acicular crystals during evaporation of this formulation when the remaining water content fell below a value of about 18 weigh-% (Fig.8). A buffer solution that contained sodium nicotinate generated the same crystals after evaporation, but not a drug-free formulation. The sodium nicotinate precipitation within E was found to be due to

a decrease of its maximum solubility in the remaining buffer after evaporation. After coalescence of the emulsion droplets, that was the macroscopically and microscopically observed situation after evaporation, the polysorbate 20 was supposed to distribute into the remaining aqueous buffer due to its hydrophilicity (HLB 17). This polysorbate 20/buffer mixture was simulated to determine the maximum sodium nicotinate solubility in it. This maximum solubility was 41.27 mg/g, while the maximum solubility in a purely aqueous buffer was about one order of magnitude larger and gave a value of 445.69 mg/g. This result will be crucial for the interpretation for the permeation experiments (see 3.3), but the reason for this effect and why no drug precipitation took place during evaporation of the other formulations was not further investigated.

**3.3 Permeation studies**

The dependence of the discussed microstrutures and alterations due to evaporation of volatile components following non-occlusive application on sodium nicotinate skin permeation was studied. Permeation from an occlusively applied purely aqueous gel was determined as reference. Fig.9 shows that the cumulative drug permeation differed between the four formulations and was for all of them higher, compared to the gel. This effect was observed previously for volatile solutions and explained by the increasing concentrations of drug during evaporation (9,10). However, closer examination of the experiments obviously demonstrated that CF10 and LD exhibited continuously increasing drug fluxes during the investigated time, while the formulations E and CF50 showed linear and decreasing permeation profiles, respectively. This could not be easily related to overall rising drug concentrations, and was also not due to deterioration of skin barrier function, as attested by the reference gel formulation that gave linear sodium nicotinate permeation with time. Hence, a model was developed to interpret the permeation data that considers the situation within the formulations, i.e. the partition of the drug and the phase ratio of dispersed to continuous phase of multi-phase formulations. In order to quantify the results, it is postulated that only the drug concentration in the continuous phase governs permeation kinetics. The drug concentration within distinct phases of a multi-phase formulation is given by:

$$C_{tot} = \phi_{cont} \cdot C_{cont} + \phi_{disp} \cdot C_{disp} \qquad (1)$$

where, $C_{tot}$ is the overall drug concentration in the formulation, $C_{cont}$ and $C_{disp}$ the concentration of the continuous and dispersed phase, respectively, and $\phi_{cont}$ and $\phi_{disp}$ the mass-fraction of the continuous and dispersed phase, respectively. These mass fractions are given by:

$$\phi_{cont} = \frac{M_{cont}}{M_{tot}}; \phi_{disp} = (1 - \phi_{cont}) = \frac{M_{disp}}{M_{tot}} \qquad (2)$$

where, $M_{tot}$, $M_{cont}$ and $M_{disp}$, denote the mass of the total formulation, of the continuous phase and of the dispersed phase, respectively. The distribution of a drug between the dispersed and the continuous phase can be expressed as the partition coefficent $K_{d/c}$:

$$K_{d/c} = \frac{C_{disp}}{C_{cont}} \tag{3}$$

A combination of Eqs. (1), (2) and (3) offers the term to calculate continuous phase drug concentration:

$$C_{cont} = \frac{C_{tot}}{(1-\phi_{cont}) \cdot (K_{d/c} - 1) + 1} \tag{4}$$

Eqs. (1), (2) and (4) are of general validity. Thus, some additional considerations are necessary to apply them to the situation of non-occlusive application. The fractions $\phi_{cont}$ and $\phi_{disp}$ may change, which, in turn, affects the concentrations $C_{tot}$, $C_{cont}$ and $C_{disp}$. Furthermore, a change of the composition of the fractions may also influence the partition coefficent $K_{d/c}$. Hence, the superscript $^{t}$ is introduced to denote the arising conditions during evaporation, and the superscript $^{0}$ will symbolize the situation in the according original formulation for further discussion.

For o/w formulations, it is assumed: (I) evaporation of the continuous phase with time, (II) no evaporation and negligible skin permeation of the dispersed phase and (III) no drug precipitation and negligible drug permeation. Then, during evaporation, the following correlations may be set up:

$$\frac{M_{tot}^{t}}{M_{tot}^{0}} = \frac{C_{tot}^{0}}{C_{tot}^{t}} \tag{5}$$

$$\frac{M_{tot}^{t}}{M_{tot}^{0}} = \frac{(1-\phi_{cont}^{0})}{(1-\phi_{cont}^{t})} \tag{6}$$

Finally, the combination of Eqs. (4), (5) and (6) offers a general term that allows calculating continuous phase drug concentration at a specific state during evaporation of a multi-phase formulation:

$$C_{cont}^{t} = \frac{C_{tot}^{t}((1-\phi_{cont}^{0})\cdot(K_{d/c}-1)+1)}{C_{tot}^{0}((1-\phi_{cont}^{t})\cdot(K_{d/c}^{t}-1)+1)}\cdot C_{cont}^{0} \quad (7)$$

Because of the observed drug precipitation within formulation E and the phase inversion that took place in case of CF50 during evaporation, the model was applied to the permeation data of formulations CF10 and LD. For this purpose, the partition coefficient $K_{d/c}$ for sodium nicotinate was assumed as zero. Thus, the overall drug concentration at a specific state during evaporation may be calculated as:

$$C_{tot}^{t} = \phi_{cont}^{t}\cdot C_{cont}^{t} \quad (8)$$

Furthermore, Eq. (7) may be simplified and gives the term:

$$C_{cont}^{t} = \frac{C_{tot}^{t}\cdot\phi_{cont}^{0}}{C_{tot}^{0}\cdot\phi_{cont}^{t}}\cdot C_{cont}^{0} \quad (9)$$

However, more than 10 weight-% of the applied sodium nicotinate was removed from the formulations due to skin permeation during the experiments. Thus, it was deemed appropriate to correct the overall concentrations. These concentrations are given by:

$$C_{tot}^{0} = \frac{m_{NA,0}}{M_{tot}^{0}} \quad (10)$$

and

$$C_{tot}^{t} = \frac{m_{NA,0}-m_{NA,Rt}}{M_{tot}^{t}} \quad (11)$$

where, $m_{NA,0}$ and $m_{NA,Rt}$ denote the applied mass of sodium nicotinate, expressed as nicotinic acid, in the complete formulation at time zero and the mass transported to the receiver at time t, respectively. Finally, the combination of Eqs. (6), (9), (10) and (11) offers a term to calculate continuous phase drug concentration for CF10 and LD for the situation during evaporation of volatile formulation compounds considering the conditions of the permeation experiments of this work:

$$C_{cont}^{t} = \frac{m_{NA,0}-m_{NA,Rt}}{m_{NA,0}}\cdot\frac{(1-\phi_{cont}^{t})}{(1-\phi_{cont}^{0})}\cdot\frac{\phi_{cont}^{0}}{\phi_{cont}^{t}}\cdot C_{cont}^{0} \quad (12)$$

The validity of this term was demonstrated by measuring continuous phase sodium nicotinate concentrations of LD and CF10 using ultrafiltration. The chosen remaining water contents for that examination corresponded to the end of the permeation experiments and were the basis for the value of the specific $\phi^t_{cont}$ in the calculation. These concentrations were in very good agreement with the calculated values with Eq. (12) (Table 8).

In order to calculate continuous phase drug concentrations for the analysis of permeation data, the term $\phi^t_{cont}$ is approachable from the evaporation profile if permeation and evaporation were investigated under the same experimental conditions. Finally, on basis of the overall drug concentrations and continuous phase drug concentrations, two different permeability coefficients may be calculated to interpret the permeation data:

$$P_{app} = \frac{J_{t+D}}{C^t_{tot}} \qquad (13)$$

and

$$P_{\text{int}} = \frac{J_{t+D}}{C^t_{cont}} \qquad (14)$$

where, $P_{app}$ is the apparent permeability coefficient, calculated with the overall drug concentration at a specific state during evaporation, and $P_{int}$ is the intrinsic permeability coefficient at that time, calculated with continuous phase drug concentration. $J_{t+D}$ denotes the sodium nicotinate flux that was related to these concentrations, respectively. This flux, however, may be the result of a donor concentration some time before the current time that was used to determine $J_{t+D}$. Thus, this assumed time delay, symbolised with the subscript $_{+D}$, was estimated. For that purpose, several experiments were performed by changing an aqueous gel containing 1.1 weight-% of sodium nicotinate, expressed as nicotinic acid, after a fixed time point with a quadruple more concentrated gel. Fig. 10 shows that this time is just about 2 hours, while the conventional lag time till steady state flux was reached, calculated from the same permeation profile, was much longer. As consequence, a delay of two hours between the calculated concentrations of the formulations and the resulting drug fluxes $J_{t+D}$ was considered for the calculation of the permeability coefficients according to Eqs. (13) and (14). Because of the steadily increasing drug fluxes in case of CF10 and LD during the permeation experiments (see above), different drug fluxes were calculated, each with the slope of two consecutive data points obtained from the permeation pattern in-between 2670 and 3270 minutes (Fig.9). This entire time was also used to estimate the corresponding $\phi^t_{cont}$ from the evaporation profile, assuming linear kinetics for the evaporation during this time slice

(Fig.7). Finally, all possible $P_{app}$ and $P_{int}$ values for CF10 and LD were calculated using Eqs. (8), (12), (13) and (14).

To test the hypothesis that continuous phase drug concentration governs transport kinetics, these $P_{app}$ and $P_{int}$ values were plotted against the corresponding small time intervals that were used to calculate the fluxes $J_{t+D}$ (Fig.11, Fig.12). The diagrams demonstrate that the $P_{app}$ values tend to increase with time, which may be attributed to weaker rising overall drug concentrations of the formulations during evaporation, compared to continuous phase drug concentrations. If this assumption exclusively explains the observation of rising $P_{app}$ values with time, the permeability coefficient calculated with continuous phase drug concentrations, referred to as $P_{int}$, should be constant with time. This tendency was observed (Fig.11, Fig.12) and demonstrated that continuous phase drug concentration explains the transport kinetics more precisely than the overall drug concentration and supports strongly our hypothesis above that this concentration is responsible for the arising drug flux during evaporation. Hence, all the intrinsic permeability coefficients of CF10 and LD, which were calculated as described, were averaged in order to obtain one permeability coefficient for further discussion for these formulations.

For formulation E, the precipitation of sodium nicotinate was assumed to be the reason for the obtained constant drug flux during the analysed time between 2670 and 3270 min. Consequently, intrinsic permeability coefficients were obtained by Eq. (14) from the slope of the permeation pattern within this entire time and the saturation concentration of the drug in the aqueous polysorbate 20/buffer solution that resulted after evaporation of volatile components (see 3.2). Permeation data obtained form the purely aqueous gel were analysed equally using the theorectical concentration as $C^{t}_{cont}$ for the calculation with Eq. (14).

Table 9 finally gives the averaged intrinsic permeability coefficients from several repeated experiments for all formulations, calculated with continuous phase drug concentration. The data of CF10 and LD are the mean of averaged intrinsic permeability coefficients over the entire analysed time as discussed above. It is obvious that all these formulations gave strongly similar intrinsic permeability coefficients, while the cumulative permeated drug amount varied about tenfold for CF10 and LD, compared to the gel, and about twofold compared to E (Fig.9). This clearly demonstrates that the obviously varying permeability from the employed formulations may be explained by continuous phase drug concentration alone, without the need to consider formulation effects on skin barrier function. The data obtained from CF50 were not included in the quantitative evaluation because of the phase inversion that took place under the experimental conditions. Nevertheless, that result also points out a possible event due to evaporation of volatile components after application of a dermatological formulation and, hence, how this effect may affect drug permeation.

Dermatological medications are typically applied as a thin layer and will remain on the skin only for a few hours, which are not exactly the conditions for the studies described in this work. Hence, the discussed alterations of formulations due to evaporation of volatile components likely take place much faster in clinical situations. Furthermore, the residue of formulation may be removed before steady state drug flux is reached, commonly due to mechanical agitation. The applied experimental conditions, however, were deemed appropriate for reaching the specific goals of this study and allowed observing alterations following formulation application in `slow-motion`. Although enhancer properties for microemulsions (4) and liposomes (24) or a drug-carrier function for the latter (25,26) were not confirmed, the proposed concept provides a tool for studying and predicting skin permeation in the situation of non-occlusive application. It further demonstrated that continuous phase drug concentration, if not considered, may superimpose a dissolution dependency in the delivery rate. Furthermore, the concept also provides a methodology to identify possible enhancer properties of appropriate formulations, which is the aim of a current project in this lab and will be reported in the future.

**4.Conclusion**

In conclusion, the microstructure of representative multi-phase dermatological formulations, different phase transitions these formulations may undergo due to evaporation of volatile components and how these parameters affect drug delivery was pointed out. Dermatological o/w formulations consisting of triglycerides, phospholipids, emulsifier and hydrophilic phase have the potential to form emulsion droplets, vesicles and microemulsions, conditioned by their individual composition. Depending on compositional changes during evaporation of volatile components, phase transitions including conversion of vesicle to microemulsion, drug crystallisation and o/w to w/o inversion took place in the employed formulations. These results are based upon a combination of different characterisation methods for multi-phase dermatological formulations, comprising a new methodology that includes chemical component analysis of separated microstructures following ultracentrifugation.

Dependence of drug skin permeation on the kind of non-occlusively applied vehicles and on the alteration vehicles undergo due to evaporation can be quantitatively described by a proposed model taking into consideration continuous phase drug concentration, independently of the existing dispersed structures. This model offers a predictive tool to correlate the arising continuous phase drug concentration of a formulation during evaporation of volatile components with drug permeation from this formulation and, possibly, to delineate the regulation of skin permeation by the formulation as a result of controlling continuous phase drug concentration or as a result of affecting skin barrier function.

**Acknowledgements**

Scanning electron microscopy was performed at the Interdepartmental Electron Microscopy (IEM) Unit of the Biocenter, University of Basel by Marcel Düggelin and Dr. Markus Dürrenberger. We are grateful to Marcel Düggelin and Dr. Markus Dürrenberger for the valuable contribution to this work.

## References

(1) C. Surber, E.W. Smith, The mystical effects of dermatological vehicles, Dermatology 210 (2005) 157-168.

(2) R. Valjakka-Koskela, M. Kirjavainen, J. Mönkkönen, A. Urtti, J. Kiesvaara, 1998. Enhancement of percutaneous absorption of naproxen by phospholipids, Int. J. Pharm. 175 (1998) 225-230.

(3) G. Betz, R. Imboden, G. Imanidis, Interaction of liposome formulations with human skin in vitro, Int. J. Pharm. 229 (2001) 117-129.

(4) Ph.J. Lee, R. Langer, P.V. Shastri, Novel microemulsion enhancer formulation for simultaneous transdermal delivery of hydrophilic and hydrophobic drugs, Pharm. Res. 20 (2) (2003) 264-269.

(5) M.B. Delgado-Charro, G. Iglesias-Vilas, J. Blanco-Méndez, M.A. Lopez-Quintela, J.P. Marty, R.H. Guy, Delivery of a hydrophilic solute through the skin from novel microemulsion systems, Eur. J. Pharm. Biopharm. 43 (1997) 37-42.

(6) U. Schmalfuss, R. Neubert, W. Wohlrab, Modification of drug penetration into human skin using microemulsions, J. Control. Release 46 (1997) 279-285.

(7) M. Kreilgard, Influence of microemulsions on cutaneous drug delivery, Adv. Drug Deliv. Rev. 54 (2002) 77-98.

(8) J.A. Bouwstra, P.L. Honeywell-Nguyen, 2002. Skin structure and mode of action of vesicles, Adv. Drug Deliv. Rev. 54 (2002) 41-55.

(9) M.F. Coldman, B.J. Poulsen, T. Higuchi, Enhancement of percutaneous absorption by the use of volatile : nonvolatile systems as vehicles, J. Pharm. Sci. 58 (1969) 1098-1102.

(10) C.M. Chiang, G.L. Flynn, N.D. Weiner, G.J. Szpunar, Bioavailability assessment of topical delivery systems: Effect of vehicle evaporation upon in vitro delivery of minoxidil from solution formulations, Int. J. Pharm. 55 (1989) 229-236.

(11) S.X. Chen, R.T Lostritto, 1997. Maintaining a near zero-order drug delivery from minidose reservoirs: simultaneous drug diffusion and binary vehicle evaporation, J. Pharm. Sci. 86 (6) (1997) 739-746.

(12) S.E. Friberg, H. Tian, P.A. Aikens, Phase changes during evaporation from a vegetable oil emulsion stabilized by a polyoxyethylene (20) sorbitanoleate, tween 80. Colloids And Surf. A 121 (1996) 1-7.

(13) A. Al-Bawab, S.E. Friberg, Phase behavior of the α-hydroxyoctanoic acid /laureth 4/white oil/water system and preliminary evaluation of the phase changes during evaporation of its emulsion, J.Cosmet.Sci. 53 (2002) 151-164.

(14) L.A.M. Ferreira, J. Doucet, M. Seiller, J.L. Grossiord, J.P. Marty, J. Wepierre, J., In vitro percutaneous absorption of metronidazole and glucose: comparison of o/w, w/o/w and w/o systems, Int. J. Pharm. 121 (1995) 169-179.

(15) C.C. Müller-Goymann, U. Alberg, Modified water containing hydrophilic ointment with suspended hydrocortisone-21-acetate – the influence of the microstructure of the cream on the in vitro drug release and in vitro percutaneous penetration, Eur. J. Pharm. Biopharm. 47 (1999) 139-143.

(16) N. Sekkat, Y.N. Kalia, R.H. Guy, Biophysical study of porcine ear skin in vitro and its comparison to human skin in vivo, J. Pharm. Sci. 91 (11) (2002) 2376-238.

(17) P.P. Van Veldhoven, G.P. Mannaerts, Inorganic and organic phosphate measurements in the nanomolar range, Anal. Biochem. 161 (1987) 45-48.

(18)Boehringer, Methoden der enzymatischen BioAnalytik und Lebensmittelanalytik, Boehringer Mannheim GmbH, Mannheim, 1997.

(19) M. Khossravi, Y.H. Kao, R.J. Mrsny, T.D. Sweeney, Analysis methods of polysorbate 20: A new method to asses the stability of polysorbate 20 and established methods that may overlook degraded polysorbate 20, Pharm. Res. 19 (5) (2002) 634-639.

(20) C. Schutz, Microemulsion: Distinctive combination of perfect invisibility and extreme performance, SÖFW-J. 129(8) (2003) 16-19.

(21) L.M. Tasi, D.Z. Liu, W.Y. Chen, Microcalorimetric investigation of the interaction of polysorbate surfactants with unilammellar phosphatidylcholines lipososmes, Coll. And Surf. 213 (2003) 7-14.

(22) I. Stoye, K. Schröder, C.C. Müller-Goymann, Transformation of a liposomal dispersion containing ibuprofen lysinate and phospholipids into mixed micelles-physico-chemical characterisation and influence on drug permeation through excised human stratum corneum. Eur. J. Pharm. Biopharm. 46 (1998) 191-200.

(23) R. Aboofazeli, M.J. Lawrence, Investigations into the formation and characterisation of phospholipid microemulsions: I. Pseudo ternary phase diagrams of systems containing water-lecithin-alcohol-isopropyl myristate, Int. J. Pharm. 93 (1993) 161-175.

(24) D.D. Verma, S. Verma, G. Blume, A. Fahr, Lipososmes increase skin penetration of entrapped and non.entrapped hydrophilic substances into human skin: a skin penetration and confocal laser scanning microscopy study, Eur. J. Pharm. Sci. 55 (2003) 271-277.

(25) E. Touitou, N. Dayan, L. Bergelson, B. Godin, M. Eliaz, Ethosomes-novel vesicular carriers for enhanced delivery: characterisation and skin penetration properties. J. Control. Release 65 (2000) 403-418.

(26) G. Cevc, Lipid vesicles and other colloids as drug carriers on skin, Adv. Drug Deliv. Rev. 56 (2004) 675-711.

## Figures

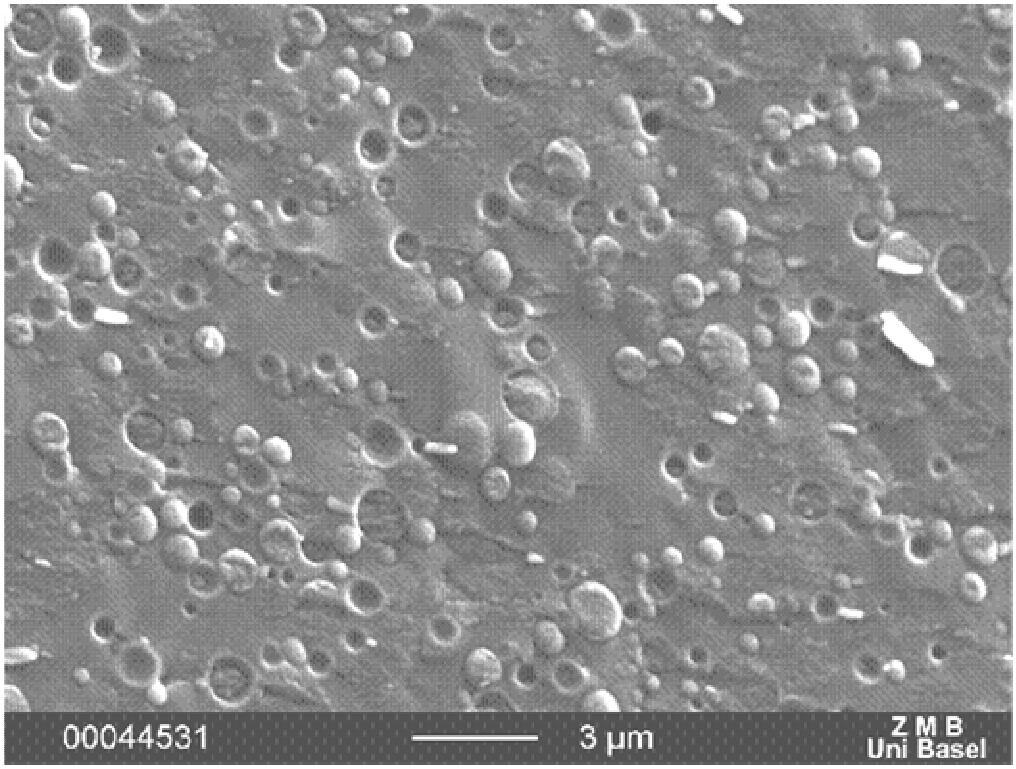


**a.**

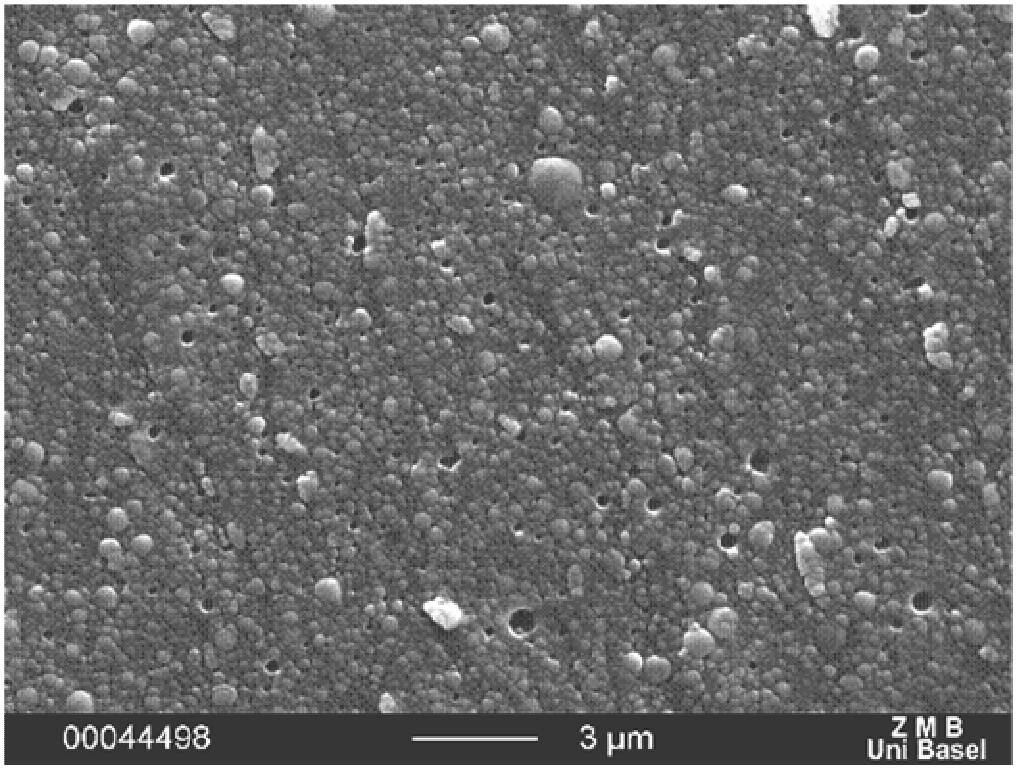


**b.**

**Figure 1** SEM-Images; formulation E (a.), formulation LD (b.)

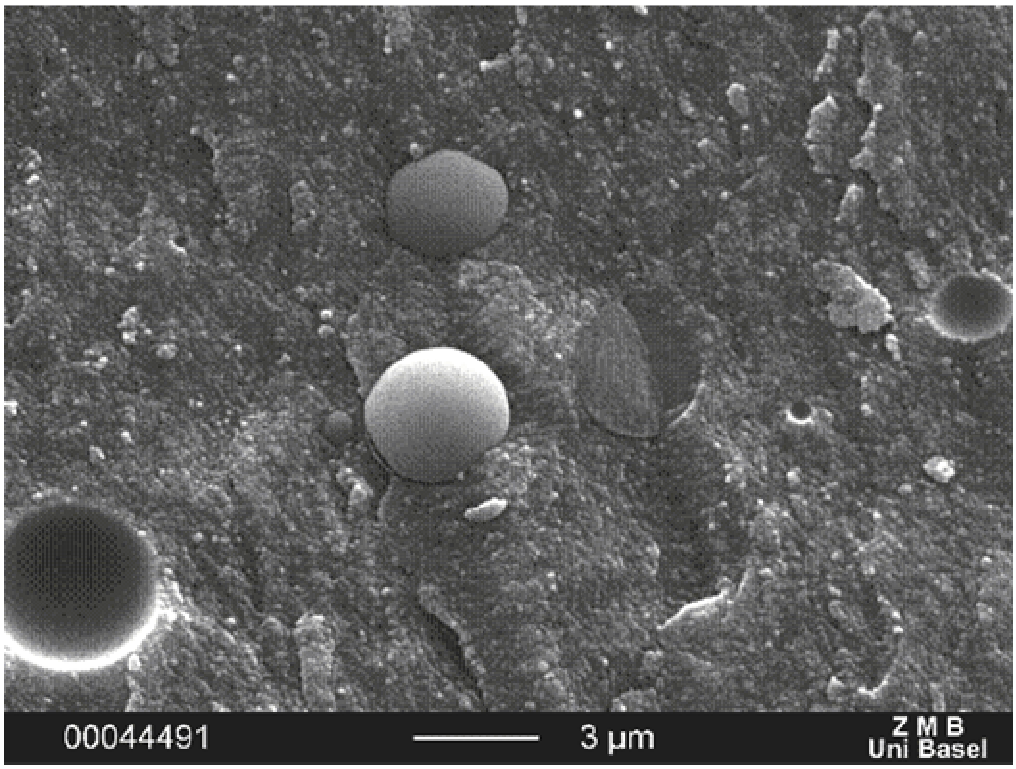


**a.**

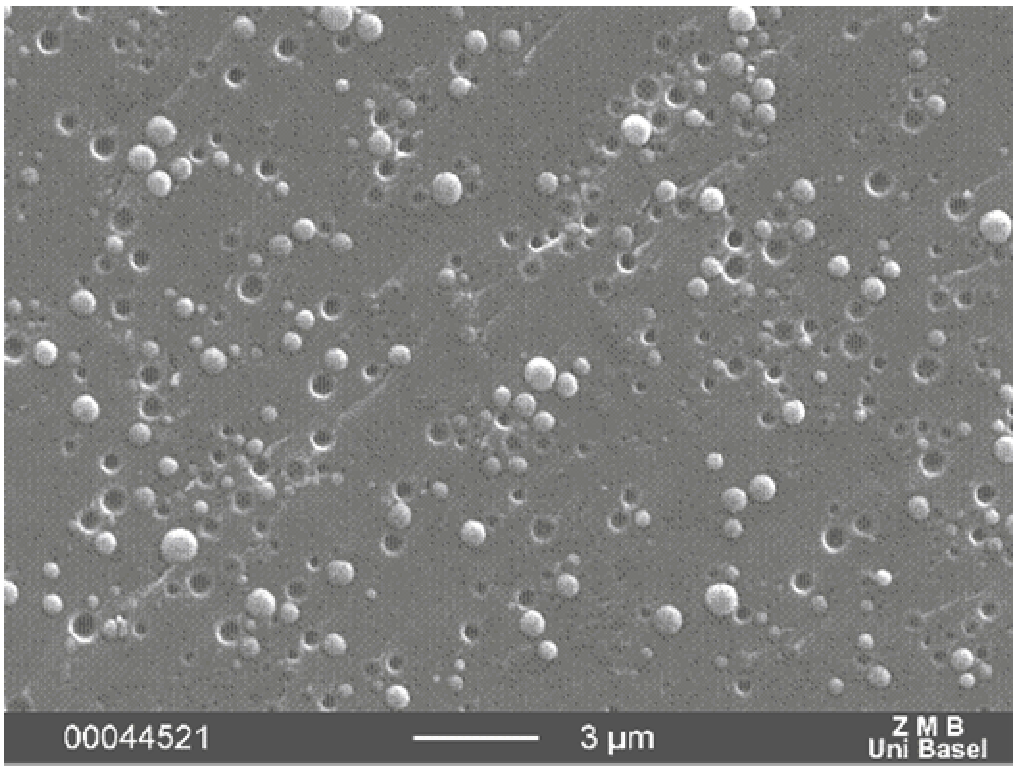


**b.**

**Figure 2**. SEM-Images; formulation CF10 (a.), formulation CF50 (b.)

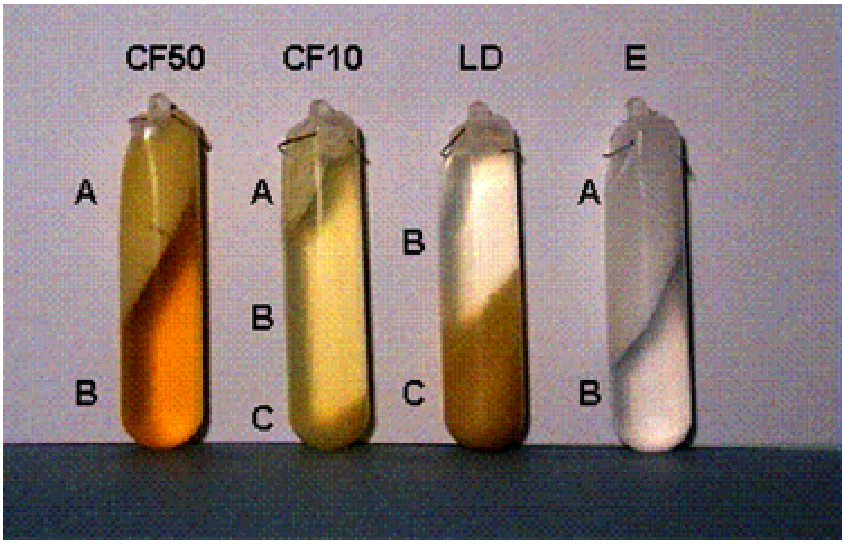


**Figure 3** Tubes with received fractions following ultracentrifugation of the individual formulations. A, B and C denote distinct fractions

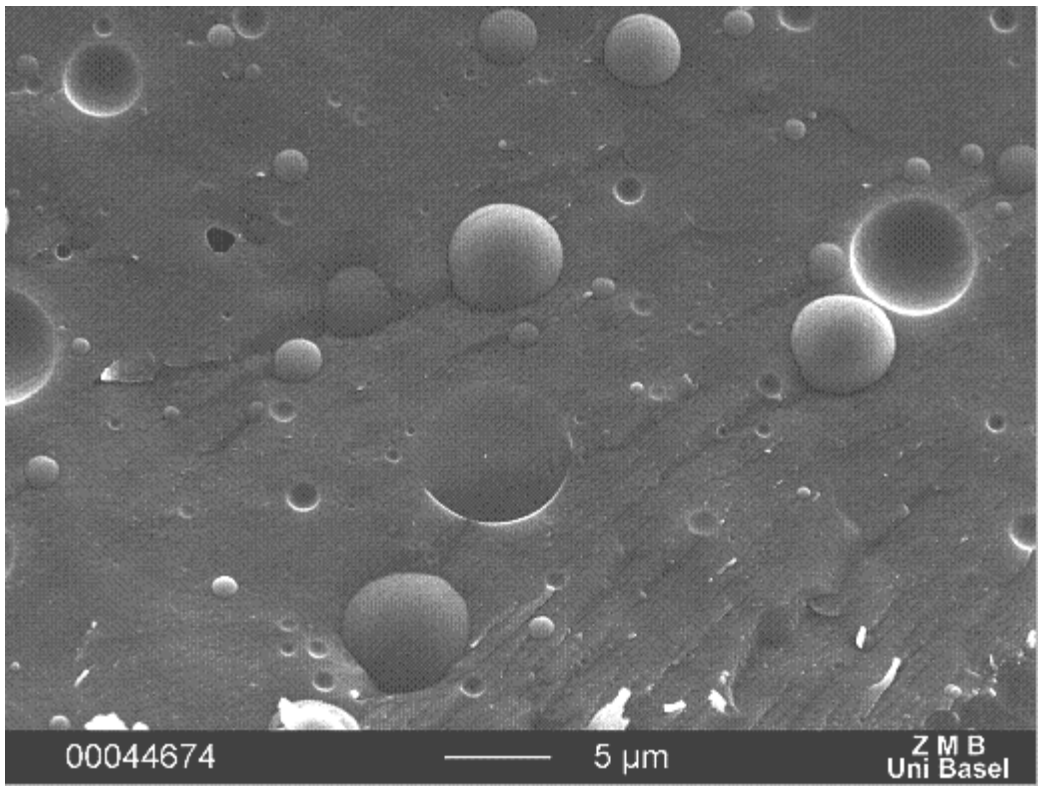


**a.**

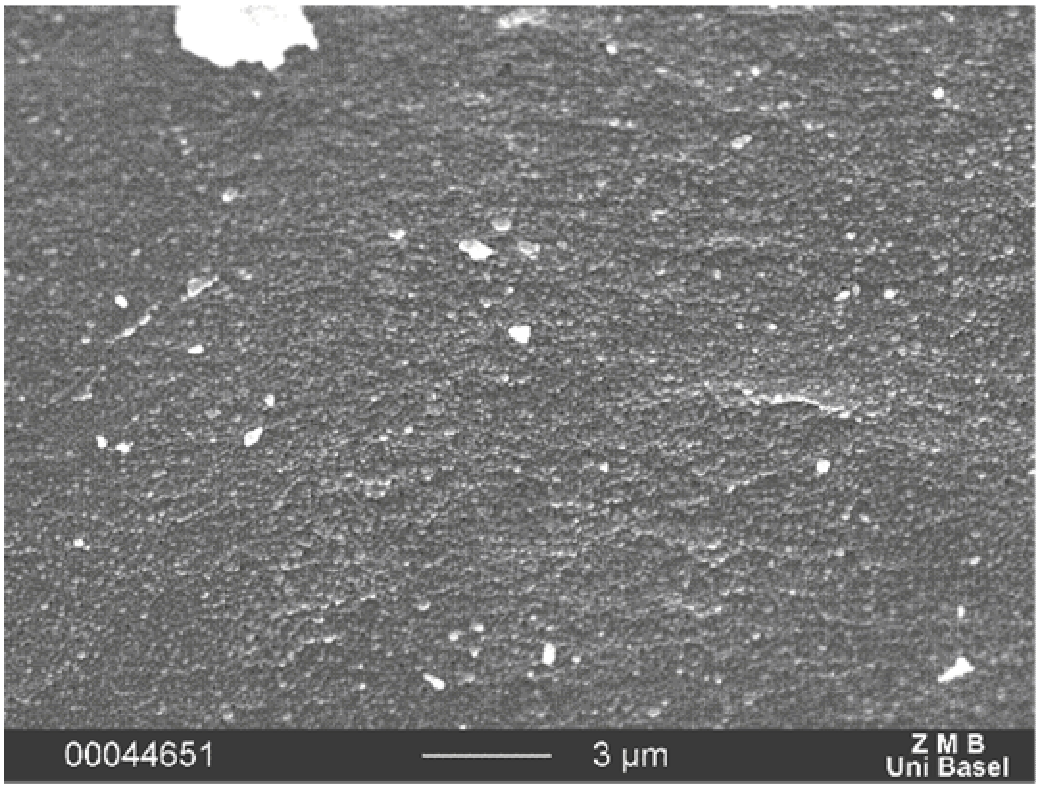


**b.**

**Figure 4** SEM-images of fraction A (a.) and C (b.) of CF10 received from ultracentrifugation of formulation CF10

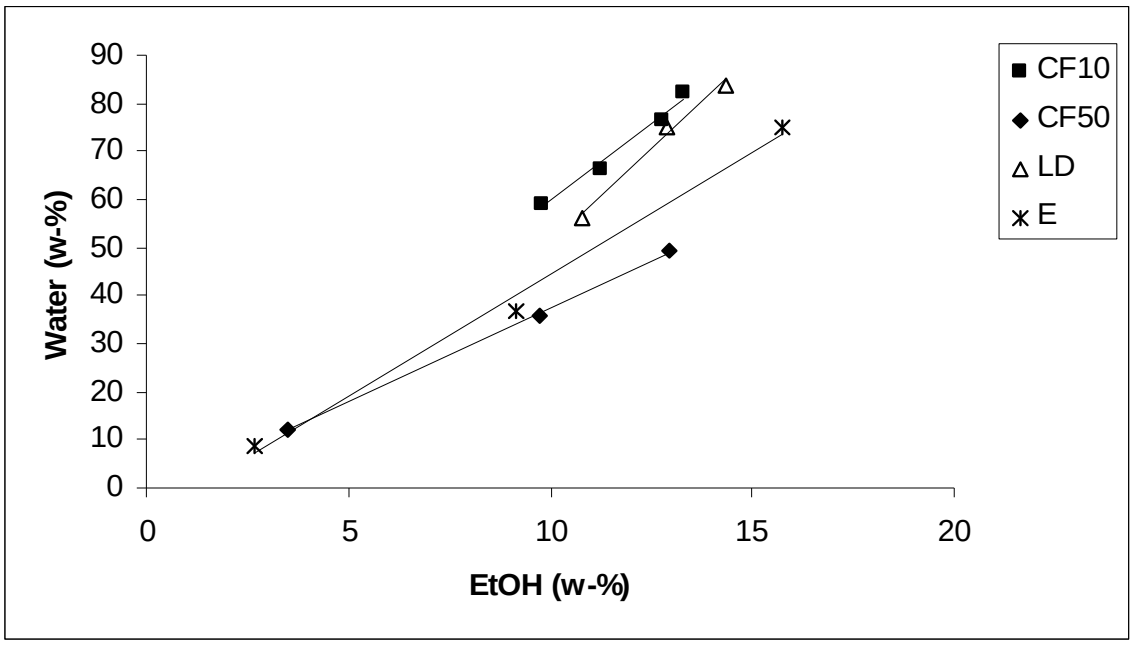


**Figure 5** Correlation between ethanol and water content of the fractions received from ultracentrifugation of the individual formulations. The plot also includes data of unfractionated formulations

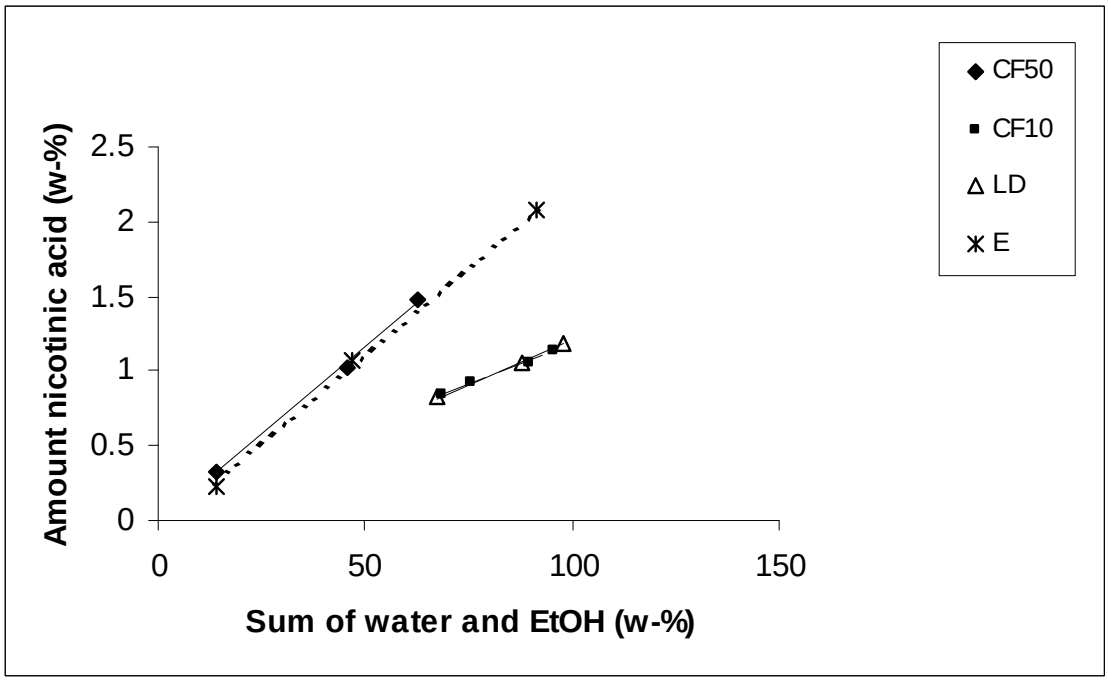


**Figure 6** Correlation between complete continuous phase (sum of water and ethanol) and sodium nicotinate content, expressed as nicotinic acid, of the fractions received from ultracentrifugation of the individual formulations. The plot also includes data of the unfractionated formulations

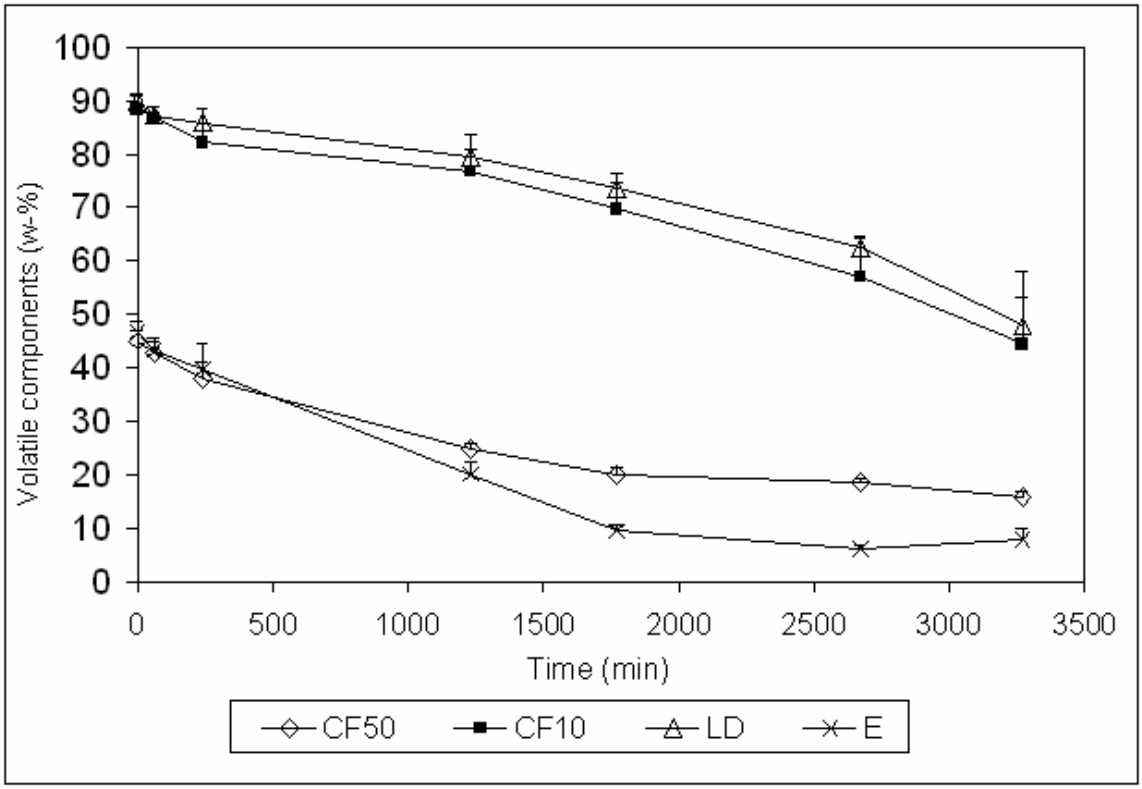


**Figure 7** Evaporation pattern of the formulations, error bars denote standard deviations (time 60/240/1230/1770 min. n=3; 3270 min. n=8; 2670 min. n=7 in case of the liposomal dispersion and formulation 1, the others n=3)

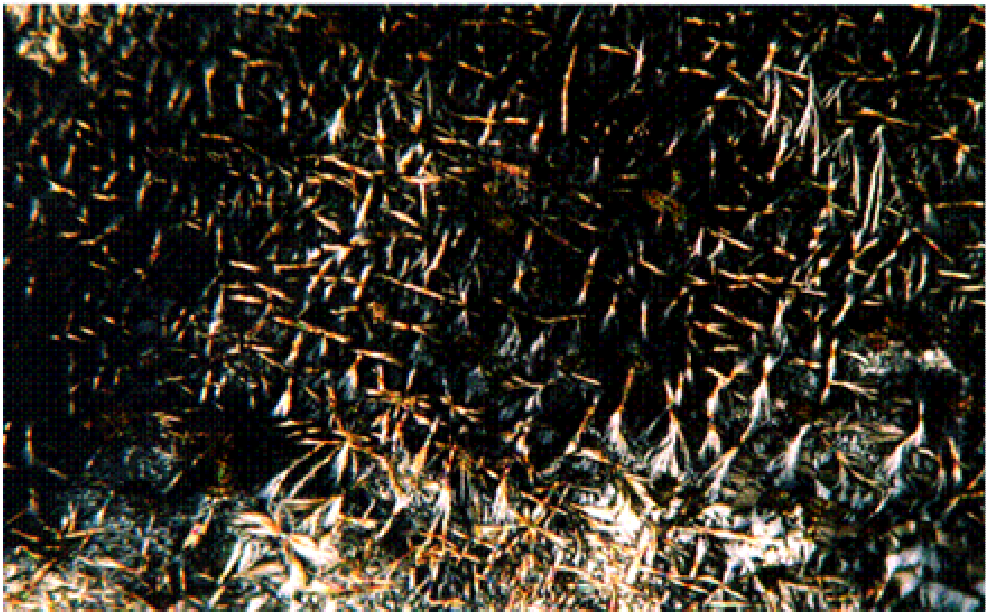

**Figure 8** Polarising microscopy of precipitated sodium nicotinate after evaporation of formulation E

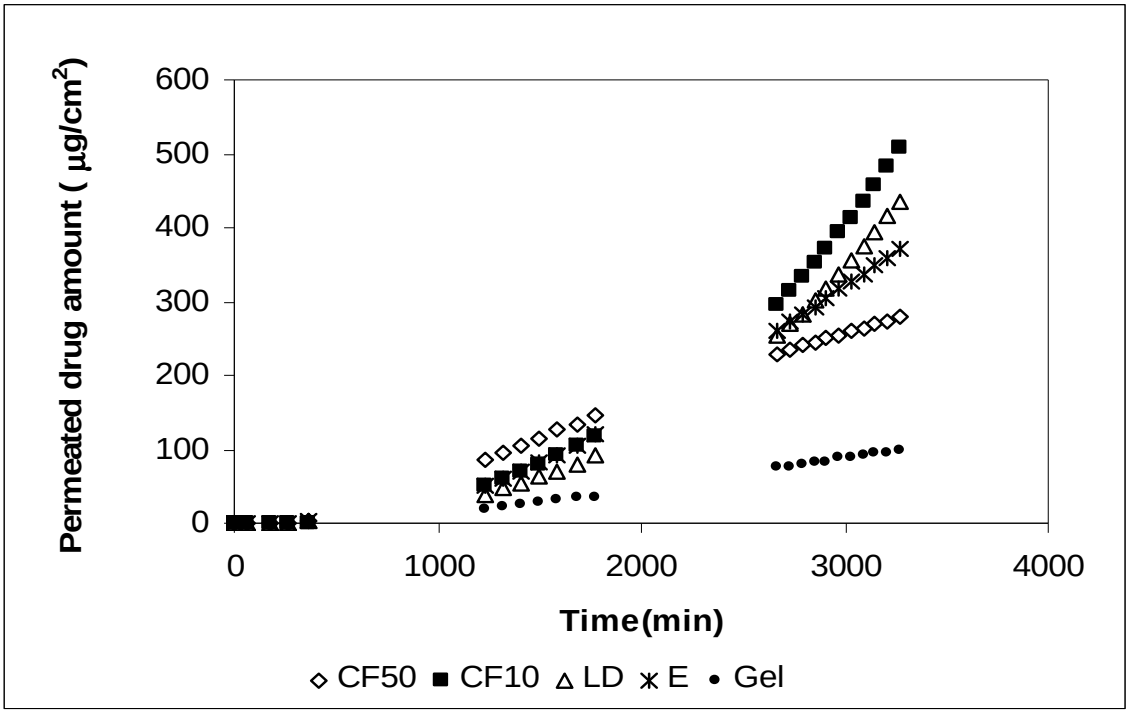


**Figure 9** Cumulative sodium nicotinate permeation, expressed as nicotinic acid, as a function of time, n=8. For simplicity, error bars are not shown

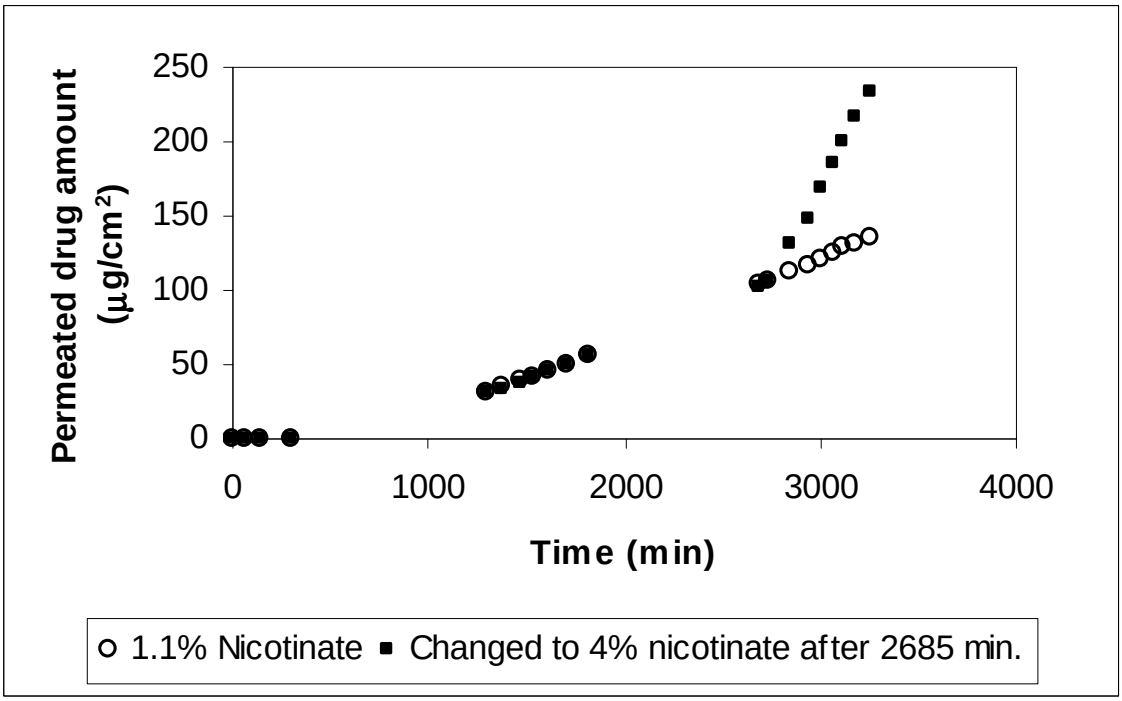


**Figure 10** Effect of donor concentration and delay till the effect is detectable in the receiver compartement. After 2685 min., a donor solution containing 1.1% sodium nicotinate was replaced by solution that contained 4% of sodium nicotinate, expressed as nicotinic acid, respectively.

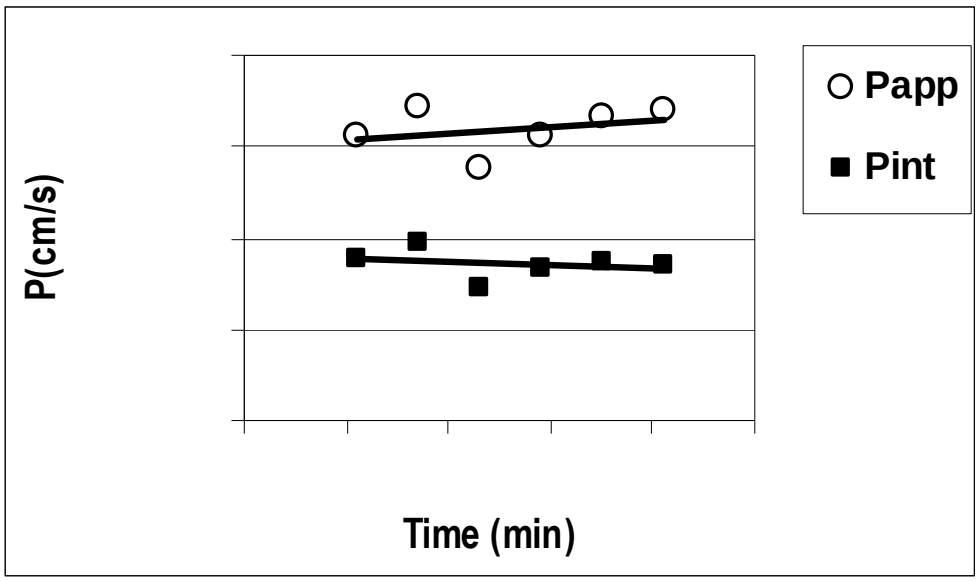


**Figure 11** Plot of apparent and intrinsic permeability coefficients $P_{app}$ and $P_{int,}$ respectively, of formulation CF10 against the time points that were used to calulate the according fluxes

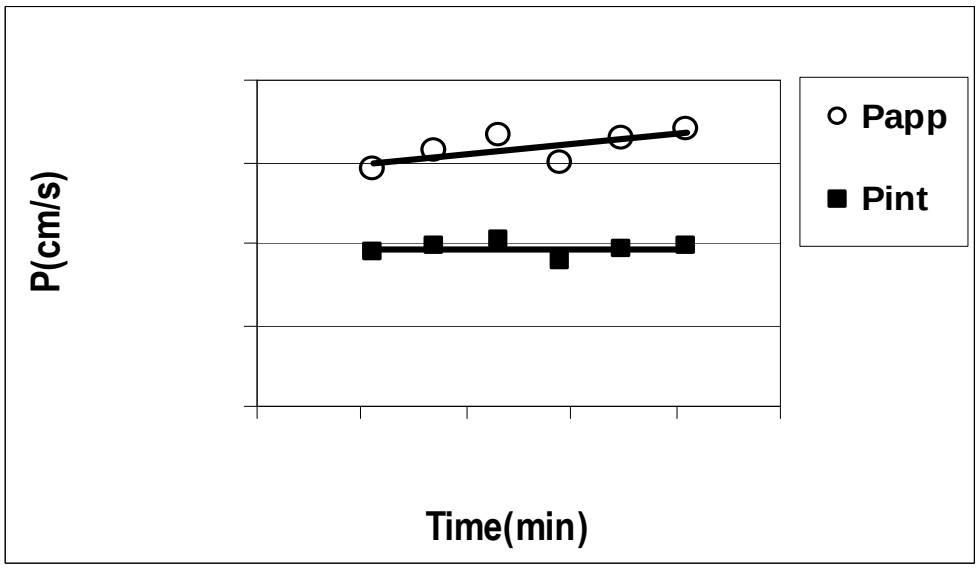


**Figure 12** Plot of apparent and intrinsic permeability coefficients $P_{app}$ and $P_{int,}$ respectively, of formulation LD against the time points that were used to calulate the according fluxes

## Tables

**Table 1** Composition of the formulations (in weight-%)

| | CF 10 [a] | CF 50[b] | E[c] | LD[d] |
|---|---|---|---|---|
| Nicotinic acid | 1.0 | 1.0 | 1.0 | 1.0 |
| Aqueous Buffer pH 7.4 | 73.85 | 34.9 | 36.92 | 74.25 |
| Ethanol 96% | 14.1 | 6.6 | 9.98 | 11.82 |
| Mygliol 812N | 6.75 | 36.0 | 47.9 | |
| Polysorbate 20 | 1.35 | 8 | 4.0 | |
| NAT 8539® | 2.4 | 13.38 | | 12.33 |
| Tocopherol | 0.05 | 0.1 | | 0.1 |
| Xanthan gum | 0.5 | 0.20 | 0.20 | 0.5 |

[a]Complex formulation with 10 weight-% dispersed phase, [b]Complex formulation with 50 weight-% dispersed phase, [c]Emulsion with 50 weight-% dispersed phase, [d]Liposomal dispersion with 10 weight-% dispersed phase

**Table 2** Mean diameter of emulsion droplets

| | CF10 | CF50 | E |
|---|---|---|---|
| Complete formulation | 2.87±0.25 | 1.48±0.125 | 1.44±0.078 |
| Fraction A | 3.05±0.63 | 1.45±0.12 | 1.43±0.10 |

The complete formulations and fractions A obtained from ultracentrifugation were analysed. Values result from laser diffraction measurements and denote µm ± SD, n=3

Table 3 **Z-average of liposomal vesicles**

| | CF10[a] | LD |
|---|---|---|
| Complete Formulation | | 326±11 |
| Fraction C | 169±11 | 325± 2.40 |

The complete formulation and the fractions C obtained from ultracentrifugation were analysed. Values result from PCS measurements and denote nm ± SD, n=3. [a] The presence of emulsion droplets prohibited an determination of liposomes within the complete formulation

**Table 4** Composition of received fractions following ultracentrifugation of all formulations

| | Nicotinic acid[a] | Water[a] | EtOH[a] | Phospholipis[b] | Mygliol 812N[c] | Polysorbate 20[c] | Summation |
|---|---|---|---|---|---|---|---|
| CF10 | | | | | | | |
| A | 0.95±0.04 | 66.50±2.17 | 11.23±0.87 | 0.74±0.13 | 12.54±6 .02 | 1.49±0.64 | 93.43 |
| B | 1.12±0.03 | 82.06±0.89 | 13.32±0.98 | 1.00±0.17 | 1.43±0. 72 | 1.50±0.77 | 100.43 |
| C | 0.83±0.06 | 59.24±3.17 | 9.77±0.51 | 15.64±5.04 | 2.98±1. 88 | 5.03±0.84 | 93.49 |
| CF50 | | | | | | | |
| A | 0.83±0.06 | 12.17±1.90 | 3.53±1.18 | 5.61±1.85 | 74.11±3. 62 | 3.89±1.70 | 99.66 |
| B | 1.45±0.07 | 49.39±1.21 | 12.92±2.53 | 12.71±0.87 | 13.40± 0.87 | 9.37±1.70 | 99.22 |
| LD | | | | | | | |
| A | 1.19±0.03 | 83.90±0.60 | 14.37±0.14 | 0.14±0.17 | | | 99.60 |
| C | 0.81±0.17 | 56.13±5.53 | 10.76±1.61 | 27.25±11.87 | | | 94. 95 |
| E | | | | | | | |
| A | 0.19±0.11 | 8.76±7.59 | 2.68±0.90 | | 77.26±21.47 | 2.65±0 .68 | 91.54 |
| B | 2.08±0.03 | 74.96±1.97 | 15.75±0.71 | | 0.22±0.14 | 5.33±0 .37 | 98.34 |

Values denote weight-% of each analysed component within a fraction A, B or C ± SD. [a]n=4,[b] n=6-8, [c] n=3, Tocopherol was not determined. Summation is the sum of all determined means of all components for each fraction

**Table 5** Calculated and measured continuous phase sodium nicotinate concentration of the formulations

| | CF10 | Cf50 | E | LD |
|---|---|---|---|---|
| Calculated continuous phase concentration[a] | 11.18 | 22.22 | 21.27 | 11.11 |
| Measured continuous phase concentration[b] | 11.03±0.37 | 26.96±3.31 | 23.11±0.53 | 10.6±0.93 |

[a]Calculated concentrations are based upon negligible partition of sodium nicotinate, expressed as nicotinic acid, into the dispersed phase structures of the formulations. [b]Measured concentrations result from ultra-filtration experiments, n=3. Values denote mg/g ± SD

**Table 6** Chemical composition of received fractions following ultracentrifugation of formulation CF10 after evaporation and of a prepared formulation of equal composition

| | Nicotinic acid | Water | Phospholipids | Mygliol 812N | Polysorbate 20 | Summation |
|---|---|---|---|---|---|---|
| Complete, ev. | 5.28 | 48.95 | 9.82 | 34.89 | 7.76 | 106.70 |
| Complete, sim. | 4.75 | 48.00 | 9.64 | 34.09 | 7.27 | 103.77 |
| A, ev. | 0.41 | 3.00 | 1.74 | 80.23 | 1.94 | 87.32 |
| A, sim. | 1.26 | 9.23 | 3.60 | 83.76 | 3.98 | 101.83 |
| B, ev. | 7.47 | 75.14 | 6.73 | 4.57 | 5.27 | 99.17 |
| B, sim. | 6.57 | 75.23 | 6.37 | 3.03 | 6.98 | 98.17 |
| C, ev. | 7.43 | 64.75 | 11.66 | 4.60 | 9.94 | 98.37 |
| C, sim. | 6.86 | 63.98 | 12.15 | 6.97 | 10.98 | 100.94 |

Values denote weight-% of each analysed component of a fraction. The abbreviations ev. and sim. indicate the formulation after evaporation and the identical prepared formulation that simulates the one after evaporation. The composition of the formulation rests upon the remaining water content after evaporation. No ethanol remained in the formulation after evaporation.

**Table 7** Change of electric conductivity of formulation CF10, CF50 and E during evaporation of volatile components

| CF10 | | CF50 | | E | |
|---|---|---|---|---|---|
| Rem. water[a] | El.Cond.[b] | Rem. water[a] | El.Cond.[b] | Rem. water[a] | El.Cond.[b] |
| 76.41 | 1549 | 37.9 | 1830 | 39.53 | 2360 |
| 25.46 | 480 | 25.94 | 1200 | 21.82 | 1800 |
| 19.6 | 32 | 14.2 | 40 | 14.51 | 1200 |
| 12.78 | 8.3 | 12.09 | 10 | 7.78 | 600 |

[a]Remaining water (weight-%), [b]electric conductivity (µS/cm)

**Table 8** Calculated and measured continuous phase sodium nicotinate concentrations of formulation LD and CF10 after evaporation to a specific remaining water content

| Formulations | Remaining water (weight-%) | Calculated continuous phase concentration[a] (mg/g) | Measured continuous phase concentration[b] (mg/g) |
|---|---|---|---|
| LD | 63.44 | 57.63 | 60.93 |
| CF10 | 48.95 | 102.41 | 103.05 |

[a]The concentrations were calculated using Eq. (12). [b]Measured concentrations result from ultrafiltration experiments

**Table 9** Intrinsic permeability coefficients calculated with continuous phase drug concentration

| Formulation | CF10 | LD | E | Aqueous gel[a] |
|---|---|---|---|---|
| $P_{int}$ | 8.56E-08 ±2.18E-08 | 9.62E-08 ±2.72E-08 | 7.43E-08 ±2.34E-08 | 7.87E-08 ±8.53E-09 |

Values denote cm/s ± SEM, n=8, [a]n=19

# E. Appendices

This chapter contains additional validation procedures, data and analyses to the publications that are not jet described.

## E.1 Model Drugs

The criteria for the selection of the model drugs were similar molecular weight, strongly hydrophilic solubility properties and aromatic structure because HPLC-quantification was performed UV-spectrophotometrically.

***Nicotinic acid***

Nicotinic acid had the function of a hydrophilic, negatively charged model drug and has the following structure:

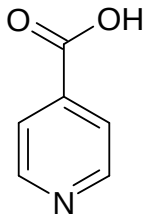


MW=123.11 g/mol, pka=4.85
Sigma (St. Louis, MO, USA)

Within the study formulations, the hydrophilic continuous phase of formulations was adjusted to a pH of 7.4 with sodium hydroxide. Hence, this situation yielded complete deprotonation of nicotinic acid to sodium nicotinate.

***Benzyltrimethylammonium chloride (BTA-Cl)***

BTA-Cl had the function of a hydrophilic, positively charged model drug and has the following structure:

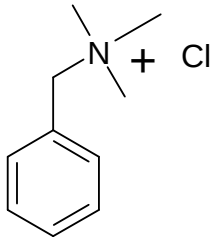


MW=185.70 g/mol
Fluka Chemie Gmbh (Buchs, Switzerland)

***Caffeine***

Caffeine had the function of a hydrophilic, uncharged model drug and has the following structure:

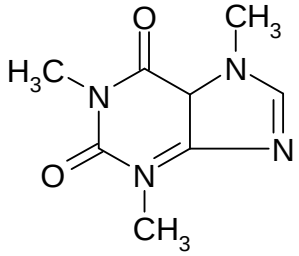

MW=197.19 g/mol
Sandoz (Basel, Sitzerland)

## E.2 Characterisation of the Formulations

The characterisation of the study formulations CF10, CF50, E and LD included, among other methodologies, chemical component analysis of the received fractions following ultracentrifugation and NMR-measurements (For composition of the formulations and detailed methodology, see chapters D.1 and D.2).

### E.2.1 Phospholipid Content

Phospholipids were quantified by determination of anorganic phosphate after digestion of the phospholpids with a sulphuric / perchloric acid mixture. A spectroscopic method based on the formation of a coloured complex of phosphomolybdate with malachite green absorbing at 610 nm was applied (1).

**Table E.2.1** Phospholipid content derived from NAT 8539® calibration curves

| Concentration NAT 8539® (µg/ml) | Absorption | Concentration phospholipids (weight-%) | Accuracy |
|---|---|---|---|
| Calibration curve 1 | | | |
| 3.72 | 0.110 | 65.39 | -3.77 |
| 6.197 | 0.161 | 63.63 | -5.60 |
| 9.3 | 0.230 | 64.87 | -4.30 |
| 12.39 | 0.303 | 66.25 | -2.87 |
| 24.8 | 0.575 | 66.00 | -3.12 |
| Calibration curve 2 | | | |
| 2.46 | 0.055 | 45.33 | -24.66 |
| 4.92 | 0.105 | 50.33 | -19.45 |
| 9.85 | 0.218 | 56.13 | -13.41 |
| 12.3 | 0.241 | 49.94 | -19.85 |
| 18.46 | 0.384 | 54.71 | -14.88 |
| Calibration curve 3 | | | |
| 2.486 | 0.064 | 29.00 | -41.67 |
| 4.972 | 0.124 | 50.65 | -19.11 |
| 9.944 | 0.253 | 63.94 | -5.27 |
| 12.43 | 0.322 | 67.75 | -1.30 |
| 24.86 | 0.621 | 69.91 | 0.95 |

Because of the heterogeneity of the bulk phospholipids NAT 8539®, a $NaH_2PO_4$ standard solution was used for calibration curves. The valuable absorption range for the method was

estimated by calculating phospholipid content of NAT 8539® from several NAT 8539® calibration curves. The absorption values given in Table E.2.1 are averages of two separately performed chemical digestions of every analytical run. The accuracy rests on the theoretical content of phospholipids (totally 69%, including Phosphatidyl choline, Lysophosphatidylcholine, Cephalin and Phosphatic acid) that are contained in NAT 8539® according to the manufacturer (for definition of the accuracy see E.2.3). On basis of the accuracy values given in Table E.2.1, all samples were diluted to obtain an absorption value of at least 0.100 in order to quantify phospholipids.

### E.2.2 Quantification of Polysorbate 20 and Triglycerides

Polysorbate 20 and triglycerides (Mygliol 812N®) were quantified by HPLC following saponification and derivatisation with 9-anthryldiazomethane (ADAM) of the lauric acid and capric acid, respectively (see chapter D.2) (2). Fig.E.2.1 shows representative chromatograms obtdained from (a) blank ADAM, (b) formulation LD, (c) Mygliol 812N® (triglycerides) and (d) polysorbate 20. The marked acid peaks 2 and 3 of Fig.E.2.1 were assigned to the specific ADAM-esters according to chromatograms received from capric acid and lauric acid, respectively (chromatograms not shown). Peak 1 is supposed to result from the caprylic acid ADAM-ester. The chromatogram received from formulation LD (Fig.E.2.1 (b)) shows that the phospholipids used contained no lauric,- capric,- and caprylic acid or other compounds that could interfere with the peaks of the ADAM-esters of these fatty acids. Thus, triglycerides or polysorbate 20 may be quantified beside phospholipids. Furthermore, the chromatogram received from bulk triglycerides (Fig.E.2.1 (c)) shows no lauric acid peak, although medium chain triglycerides may contain up to three percent of lauric acid (3). The capric acid gave better results for quantification of triglycerides than the caprylic acid. Hence, triglycerides were quantified on basis of capric acid ADAM-esters. However, the chromatogram received from polysorbate 20 shows small peaks of caprylic- and capric acid ADAM-esters, in accordance with the substance description (4). Thus, the capric acid peaks that were used to quantify the triglycerides were corrected by subtraction of the area caused by polysorbate 20 in the sample in some cases (this correction was necessary in case of the fractions B of CF10, CF50 and E, see chapter D.2 for details).

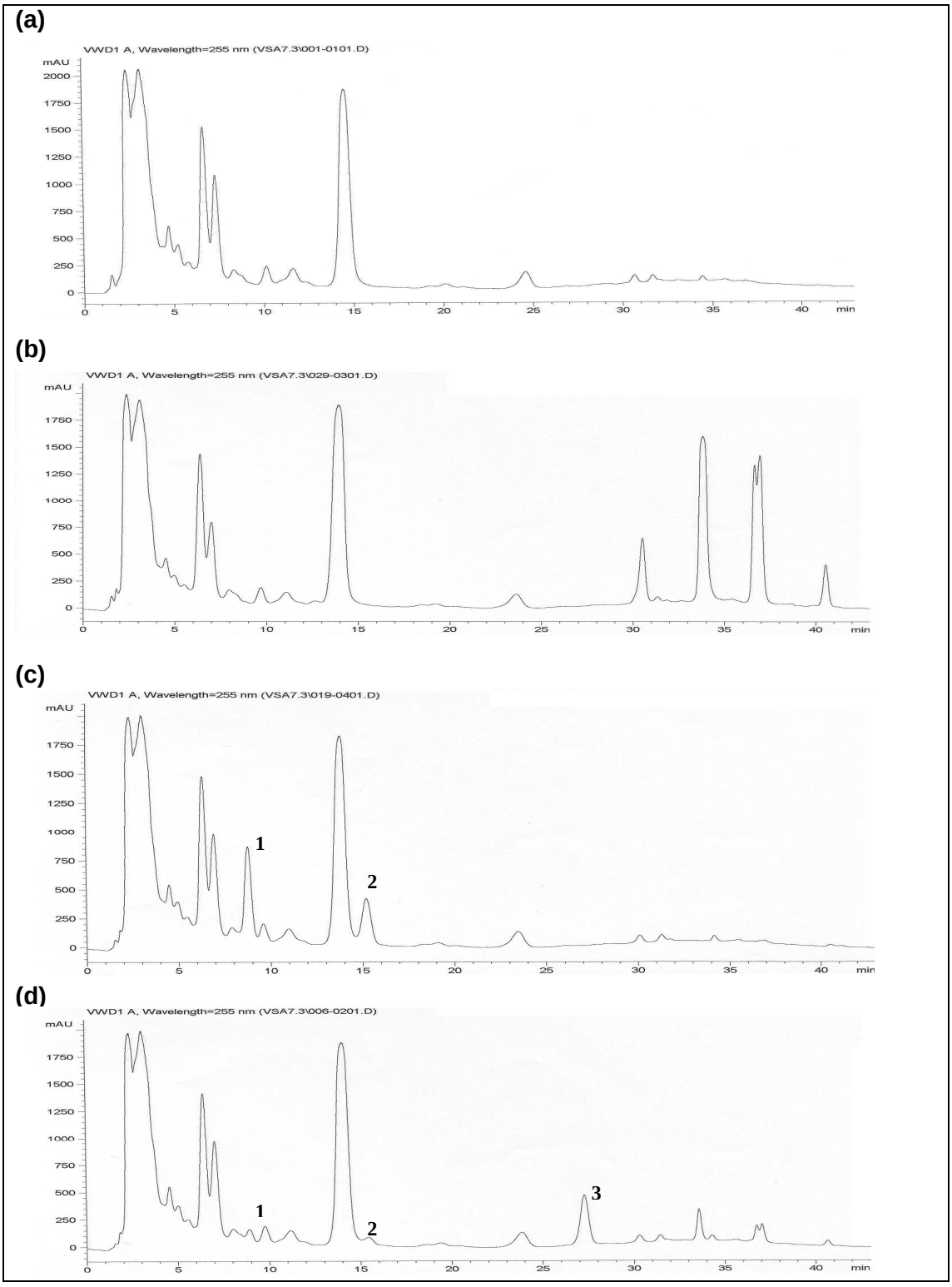


**Figure E.2.1** Chromatograms of (a) blank ADAM, (b) formulation LD, (c) Mygliol 812N® and (d) Polysorbate 20. (1) Caprylic acid (C8:0), (2) Capric acid (C10:0), (3) Lauric acid (C12:0)

Furthermore, the time to yield complete saponification of the respective compounds was from interest. This time was estimated by measuring the obtained peak areas of a mixture of triglycerides and polysorbate 20 (36.3 and 58.8 µg/ml in the final sample for injection, respectively) of the ADAM-esters of the fatty acids at different time points after incubation with

sodium hydroxide solution (see chapter D.2). The constant peak area after 5 hours of saponification (Fig.E.2.2) indicated complete saponification after that time.

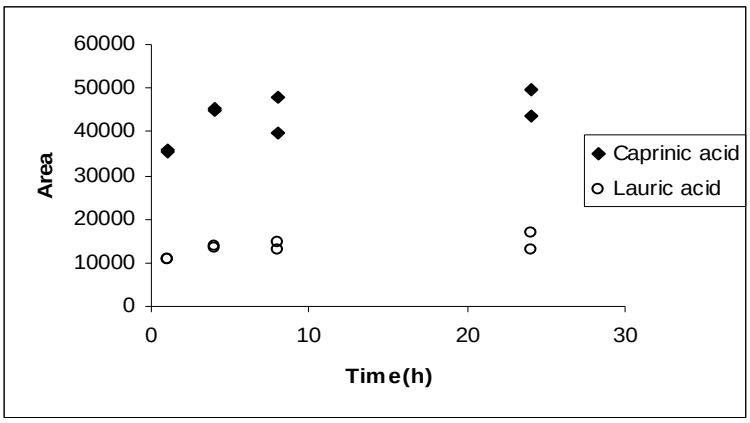


**Figure E.2.2** Saponification time of the analysed fatty acids

### E.2.3 Validation Parameters Derived from Chemical Component Analysis

In addition to chemical component analysis of received fractions following ultracentrifugation (see D.1, D.2), the complete formulations were analysed for the respective compound equally to test the validity of the applied assays.

**Table E.2.2** Measured and true concentrations (C(meas) and C(true), respectively) of respective components of the formulations

| Formulation | CF50 | | CF10 | | LD | | E | |
|---|---|---|---|---|---|---|---|---|
| | C(true) | C(meas) | C(true) | C(meas) | C(true) | C(meas) | C(true) | C(meas) |
| Drugs | | | | | | | | |
| NA | 1 | 1.03±0.02 | 1.00 | 1.03±0.04 | 1.00 | 1.04±0.02 | 1.00 | 1.07±0.08 |
| BTA-Cl | 1 | 1.03±0.02 | 1.00 | 1.02±0.03 | 1.00 | 1.01±0.03 | 1.00 | 1.04±0.03 |
| Caffeine | 1 | 0.94±0.06 | 1.00 | 0.99±0.07 | 1.00 | 1.00±0.08 | 1.00 | 0.96±0.08 |
| Bases | | | | | | | | |
| Water(I) | 34.91 | 35.77±0.38 | 74.22 | 76.45±1.99 | 74.63 | 75.16±1.76 | 36.99 | 36.83±0.79 |
| Water(II) | 34.91 | 35.30±1.70 | 74.22 | 75.63±1.84 | 74.63 | 76.05±0.02 | 36.99 | 37.91±0.81 |
| Water(III) | 34.91 | 35.58±0.75 | 74.22 | 77.12±1.12 | 74.63 | 74.94±1.68 | 36.99 | 39.16±3.24 |
| EtOH(I) | 9.95 | 9.73±2.23 | 14.77 | 12.80±0.48 | 14.98 | 12.88±0.74 | 10.00 | 9.14±0.72 |
| EtOH(II) | 9.95 | 8.01±0.47 | 14.77 | 13.69±2.08 | 14.98 | 12.96±1.04 | 10.00 | 9.01±1.14 |
| EtOH(III) | 9.95 | 8.45±0.81 | 14.77 | 13.04±0.89 | 14.98 | 12.88±0.76 | 10.00 | 8.43±0.24 |
| PL(I) | 10.04 | 9.38±0.98 | 1.81 | 1.76±0.13 | 9.29 | 8.70±0.81 | | |
| Mygliol(I) | 36.01 | 38.54±0.98 | 6.78 | 7.13±0.46 | | | 48.00 | 48.62±1.19 |
| PS 20(I) | 8.00 | 7.20±0.50 | 1.36 | 1.56±0.25 | | | 4.01 | 3.76±0.51 |

NA denotes sodium nicotinate, expressed as nicotinic acid, BTA-Cl denotes benzyltrimethylammonium chloride, PL are phsopholipids, Mygliol triglycerides and PS 20 denotes polysorbate 20. The index (I), (II) and (III) behind the respective components distinguishes between analyzed data obtained from the same formulation containing NA, BTA-Cl or caffeine as model drug, respectively. Data denote weight-%±SD, n=3-6

Table E.2.2 compares the analysed amounts of assayed components with the true values given by the respective formulation composition. On basis of these data, the accuracy (*AC*), the precision (*P*) and the recovery (*R*) of the respective analytical method was calculated as:

$$AC = \frac{M - TV}{TV} \cdot 100 \qquad \text{(E1)}$$

$$P = \frac{SD}{M} \cdot 100 \qquad \text{(E2)}$$

$$R = \frac{M}{TV} \cdot 100 \qquad \text{(E3)}$$

where, *M* is the mean of the analysed individual component, *TV* is the true value and SD is the standard deviation (5).

**Table E.2.3** Validation parameters derived from chemical component analysis of the complete formulations

| Formulation | CF50 | | | CF10 | | | LD | | | E | | |
|---|---|---|---|---|---|---|---|---|---|---|---|---|
| | *AC* | *P* | *R* | *AC* | *P* | *R* | *AC* | *P* | *R* | *AC* | *P* | *R* |
| Drugs | | | | | | | | | | | | |
| NA | 3.22 | 2.10 | 103.33 | 3.06 | 3.98 | 103.15 | 3.92 | 1.61 | 104.08 | 6.29 | 7.34 | 106.71 |
| BTA-Cl | 3.17 | 1.54 | 103.27 | 2.16 | 3.08 | 102.21 | 0.95 | 2.94 | 100.95 | 4.25 | 2.85 | 104.43 |
| Coffein | -5.89 | 6.15 | 94.44 | -1.20 | 7.45 | 98.81 | -0.06 | 7.63 | 99.94 | -4.15 | 8.11 | 96.02 |
| Bases | | | | | | | | | | | | |
| Water(I) | 2.41 | 1.06 | 102.46 | 2.91 | 2.60 | 103.00 | 0.71 | 2.35 | 100.71 | -0.45 | 2.14 | 99.55 |
| Water(II) | 1.11 | 4.83 | 101.13 | 1.86 | 2.44 | 101.89 | 1.87 | 0.03 | 101.91 | 2.41 | 2.14 | 102.47 |
| Water(III) | 1.88 | 2.09 | 101.92 | 3.76 | 1.46 | 103.90 | 0.42 | 2.24 | 100.42 | 5.53 | 8.27 | 105.85 |
| EtOH(I) | -2.31 | 22.97 | 97.74 | -15.41 | 3.74 | 86.65 | -16.35 | 5.76 | 85.95 | -9.38 | 7.83 | 91.42 |
| EtOH(II) | -24.27 | 5.87 | 80.47 | -7.92 | 15.23 | 92.67 | -15.59 | 8.04 | 86.52 | -10.99 | 12.62 | 90.10 |
| EtOH(III) | -17.71 | 9.59 | 84.96 | -13.27 | 6.80 | 88.29 | -16.33 | 5.91 | 85.96 | -18.58 | 2.79 | 84.33 |
| PL(I) | -7.05 | 10.40 | 93.41 | -3.04 | 7.26 | 97.05 | -6.78 | 9.27 | 93.65 | | | |
| Mygliol(I) | 6.56 | 2.53 | 107.02 | 4.80 | 6.42 | 105.05 | | | | 1.29 | 2.45 | 101.30 |
| PS 20(I) | -11.07 | 7.00 | 90.03 | 12.92 | 15.91 | 114.84 | | | | -6.57 | 13.44 | 93.83 |

NA denotes sodium nicotinate, expressed as nicotinic acid, BTA-Cl denotes benzyltrimethylammonium chloride, PL are phsopholipids, Mygliol triglycerides and PS 20 denotes polysorbate 20. The index (I), (II) and (III) behind the respective components distinguishes between analysed data obtained from the same formulation containing NA, BTA-Cl or caffeine as model drug

A recovery ± 20 % and deviation of less than ±20 for the accuracy and the precision, respectively, was tolerated. Hence, all methods were valuable to analyze the respective

component within the formulation matrix (Table E.2.3). The detected higher deviations for the ethanol were attributed to its volatility.

### E.2.4 NMR Diffusion Experiments

In order to determine self-diffusion coefficients of sodium nicotinate and benzene, NMR diffusion experiments were performed (see chapter D.1) (6). Fig.E.2.3 shows two NMR spectra obtained from the aromatic protons of sodium nicotinate. Fig.E.2.3 (a) gives a typical spectrum, with signal peaks of high resolution, as obtained from sodium nicotinate within all study formulations, except the emulsion E, where broad signal peaks were observed. This spectrum is given in Fig.E.2.3 (b).

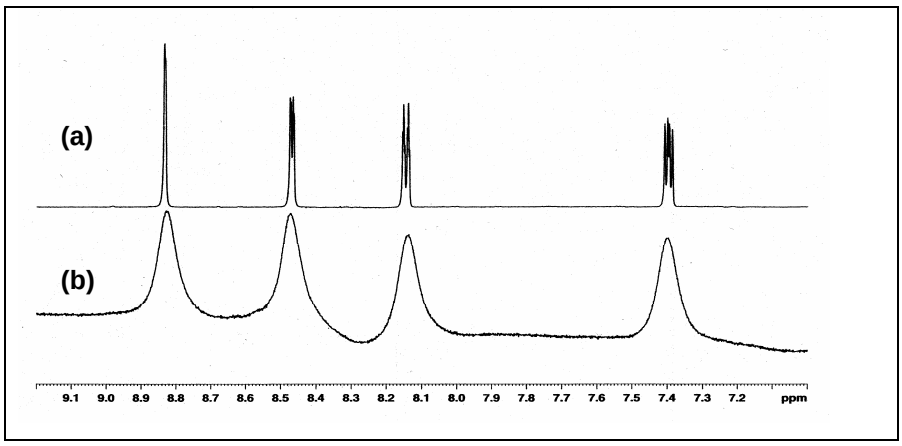


**Figure E.2.3** NMR spectra of sodium nicotinate obtained from (a) the drug within the isolated microemulsion of CF50 and (b) from formulation E

The reason for these broad signal peaks was not further invesitigated. Ultrafiltration experiments, however, excluded an association of sodium nicotinate with dispersed structures, which could be a possible explanation for this observation (see chapter D.1).

Diffusion experiments were performed by varying the gradient strength while keeping the diffusion times and gradient lengths constant. Self-diffusion coefficients were fitted from the intensity decrease of a NMR signal of interest using Eq. (E4) (7):

$$I_g = I_0 \cdot e^{-D\cdot(\delta\cdot H\cdot G\cdot 2\cdot\pi)^2\cdot(\Delta-\frac{\delta}{3})\cdot 10000} \qquad \text{(E4)}$$

where, $I_g$ and $I_0$ are the signal intensities in the presence and absence of magnetic field gradient pulses with the amplitude G and the duration δ. $\Delta$ Denotes the experimental diffusion time, $D$ the diffusion coefficient and H is given with 4258 Hz/G and depends on the gyromagnetic constant for $^1$H. Fig. E.2.4 shows a typical fit.

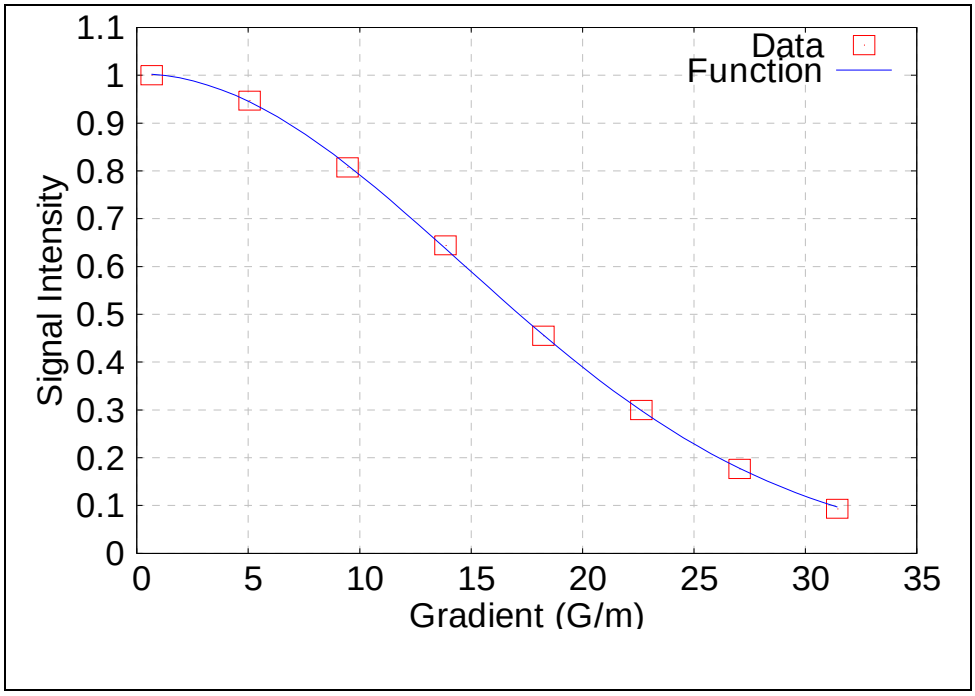


**Figure E.2.4** Example of a fit to determine self-diffusion coefficients using Eq. (E4)

## E.3 Permeation Experiments

This chapter contains validation procedures and additional experiments to the permeation experiments (see chapters D.1 and D.2) that are not jet described.

### E.3.1 Determination of the Effective Transport Area

The custom-made Franz-type diffusion cells used in this work consist of an upper and a lower glass-compartment (Fig.E.3.1). For all permeation experiments, the skin was placed between these two compartments, stratum corneum side up, followed by application of the donor formulation. For interpretation of drug flux according to Fick`s first diffusion law, information about the effective transport area is essential (see chapter C.4). The area of the upper and lower compartment of the applied diffusion cells (Au and Al in Fig.E.3.1, respectively) was not identical (see Table E.3.1).

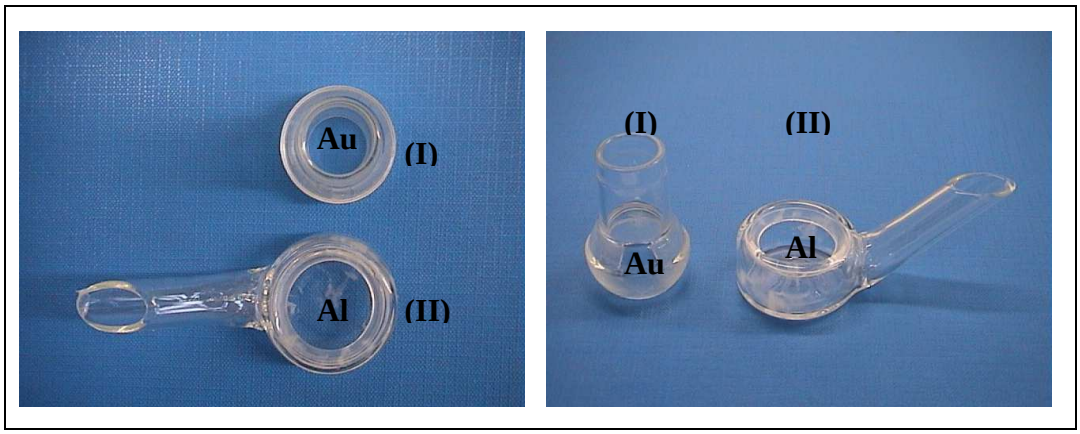


**Figure E.3.1** Diffusion cells, upper (I) and lower (II) compartment and upper and lower skin-contact area, Au and Al, respectively

Thus, several permeation experiments with identical purely aqueous sodium nicotinate solutions as donor vehicle were carried out occlusively to estimate the relevant diffusion area.

**Table E.3.1** Permeability coefficients calculated with the upper (Pu) and lower (Pl) areas of the diffusion cell compartments

| | Cell1 | Cell2 | Cell3 | Cell4 | | |
|---|---|---|---|---|---|---|
| Upper Area | 2.125 | 1.767 | 1.86 | 1.72 | | |
| Lower Area | 2.99 | 3.05 | 3.24 | 4.05 | | |
| Experiment1 | | | | | Average | RelSD |
| Pu | 2.3E-07 | 3.69E-07 | 3.2E-07 | 3.92E-07 | 3.27E-07 | 21.8 |
| Pl | 1.64E-07 | 2.14E-07 | 1.84E-07 | 1.66E-07 | 1.82E-07 | 12.7 |
| Experiment2 | | | | | | |
| Pu | 2.69E-07 | 3.28E-07 | 3.58E-07 | 4.25E-07 | 3.45E-07 | 18.8 |
| Pl | 1.91E-07 | 1.9E-07 | 2.06E-07 | 1.8E-07 | 1.92E-07 | 5.47 |

Pu and Pl denote permeability coefficients (cm/s) calculated with the skin contact area of the upper and lower cell compartment, respectively. RelSD is the relative standard deviation (%). Areas are given in $cm^2$. Two experiments were performed.

Table E.3.1 shows that the permeability coefficients calculated with the area of the lower cell compartment gave a smaller variation, indicating that this area represents the effective diffusion area more precisely. Hence, the areas of the lower cell compartments were used for the interpretation of all permeation experiments in this work.

### E.3.2 Validity Testing of TEWL Measurements

Skin integrity was tested prior to every permeation experiment by measuring the transepidermal water loss (TEWL) across the skin. The validity of this method was evaluated by comparing TEWL-values obtained from intact skin with TEWL data measured across stripped skin after an equilibration time of about 4 hours, experimental conditions according to the permeation experiments (see chapters D.1, D.2). Stripped skin reportedly looses its barrier properties and, hence, TEWL values will increase (8).

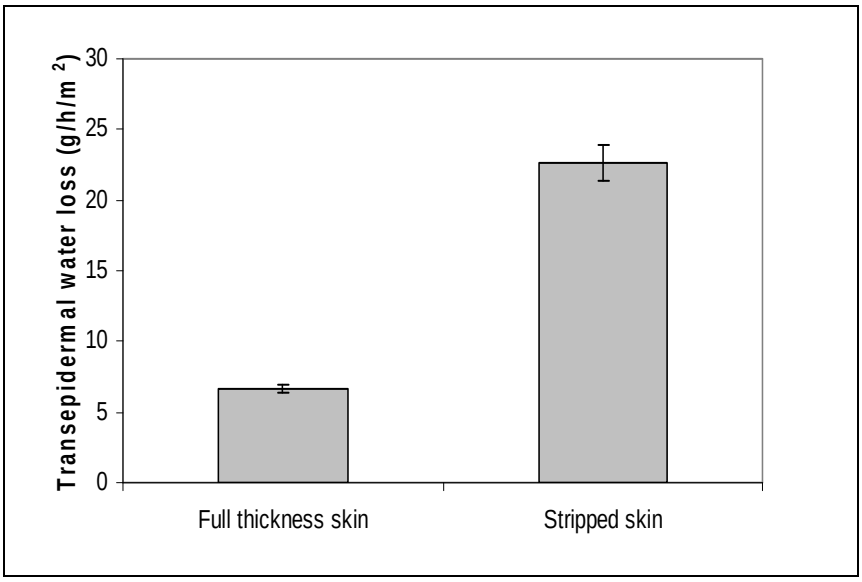


**Figure E.3.2** Transepidermal water loss across excised full thickness pig ear skin (n=112) and across excised stripped pig ear skin (n=33) Error bars denote standard error of means (SEM)

Fig.E 3.2 clearly demonstrates that the experimental in-vitro conditions used in this work allow distinguishing between intact and damaged skin using the technique of transepidermal water loss measurements.

### E.3.3 Formulation Dosage Facilitating Alterations due to Evaporation

To investigate sodium nicotinate permeation from non-occlusively applied formulations (see chapter D.2), evaluation of an appropriate dosage of formulations was required. On the one hand, the applied amount had to be small enough to enable alterations due to loss of volatile components during the investigated time, but on the other hand, the remaining amount of formulation had to be sufficient enough facilitating physicochemical characterisations at the end of experiments. For that reason, different amounts of formulation CF10 were applied on pig ear skin, equal conditions to the permeation experiments (see chapter D.2). After 54 hours,

the formulations were removed from the skin surface and analysed for remaining water and ethanol.

**Table E.3.2** Remaining volatile components after 54 hours of application

| Formulation applied[a] | Remainig water (%) | Remaining ethanol (%) |
|---|---|---|
| 100 mg/cm$^2$ | Not removable | -- |
| 300 mg/cm$^2$ | 34.58 | 0 |
| 350 mg/cm$^2$ | 53.66 | 0 |
| 400 mg/cm$^2$ | 45.51 | 0 |
| 500 mg/cm$^2$ | 72.8 | 0 |

[a]Formulation CF10, initially containing 90 weight-% of volatile phase

Table E.3.2 shows that 100 mg/cm$^2$ applied formulation is less to make a collection possible after the duration of an experiment, while a dosage of 500 mg/cm$^2$ is too large to cause major alterations of the formulation composition due to loss of volatile components. Thus, 300 mg/cm$^2$ was identified as valuable formulation dosage for the project published in chapter D.2.

### E.3.4 Distribution Experiments between Stratum Corneum and Formulations

The method for the determination of drug distribution coefficients between the stratum corneum (SC) and continuous phase of formulations was developed (see chapter D.1). The following validation procedures were performed. (I) The time of sonification to obtain complete drug extraction from the SC was investigated, (II) the recovery of the respective drug from SC tissue was from interest and (III) the concentration dependency of formulation concentration on drug concentration within the stratum corneum was studied.

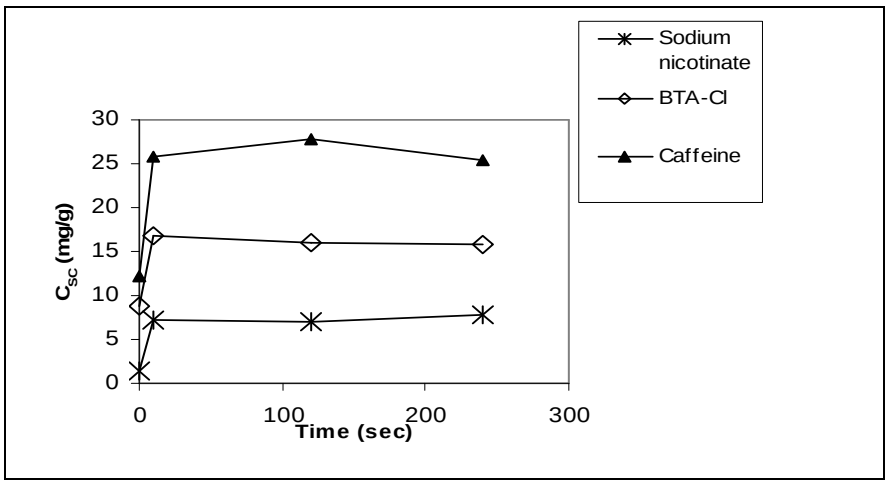


**Figure E.3.3** Theoretical drug concentrations of SC ($C_{SC}$(mg/g)) as a function of sonification time (s). Results were obtained from equilibrated SC tissue with donor solutions containing 1 weight-% of drug in aqueous/ethanolic buffer solution pH 7.4

Fig.E.3.3 demonstrates that after 10 seconds of sonification, all drug was extracted from the SC tissue, independently of the used drug. However, without sonification, considerable amount

of drug would remain in the SC, as attested by the extracted amount without sonification. For experimental details and HPLC assays see chapter D.1.

**Table E.3.3** Drug retention within the SC

| | Sodium nicotinate | BTA-Cl | Caffeine |
|---|---|---|---|
| Retention (%)/ mg SC± SD | 1.82±0.57 | 2.79±0.73 | 2.54±1.60 |

Because the SC constitutes a complex, heterogeneous matrix (see chapter C.1.2), binding and absorption of the drugs to this tissue may not be automatically excluded. Hence, the recovery of the drugs from SC was investigated. For that purpose, 10 µl of aqueous drug solution (1 weight-%) was added to the surface of accurately weighted pieces of SC. Then the drug solution was allowed to evaporate over night, followed by drug extraction as described in chapter D.1. The results are expressed as drug retention (in % of complete amount of drug) / mg SC (Table E.3.3). However, blank runs, where SC was replaced by filter paper, gave similar results, indicating that drug binding to the SC may be neglected for the tested hydrophilic model drugs.

To make sure that the SC is not saturated with the drugs and to confirm the dependency of formulation concentration on drug concentration within SC, distribution coefficients between SC and solutions (17 % ethanol in aqueous buffer pH 7.4) of different drug concentrations were determined. The range of these concentrations was chosen in order to include continuous phase drug concentrations of the study-formulations E, CF50, LD and E.

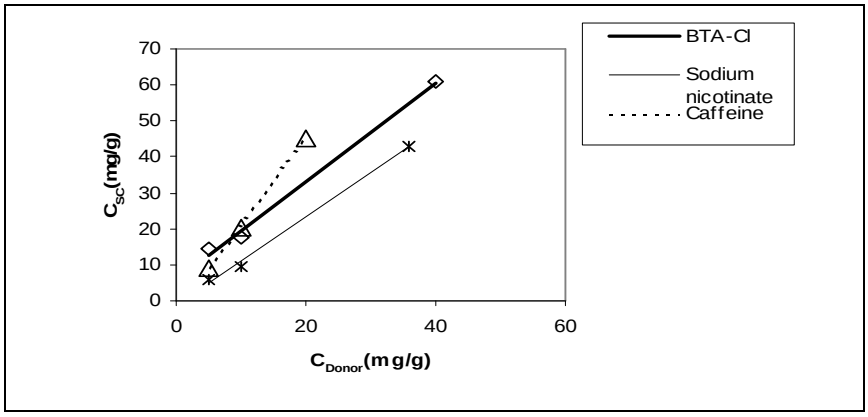


**Figure E.3.4** Dependence of drug concentration of stratum corneum ($C_{SC}$(mg/g)) on donor drug concentration ($C_{Donor}$(mg/g))

Fig.E.3.4 clearly demonstrates linearity between SC drug concentration and donor drug concentration, according to theory. The unequal values for the different drugs further indicate that the measured concentrations were not due to remaining formulation on the SC. This was evidenced with additional experiments that were performed by covering hydrated SC with drug

containing formulation CF50. This formulation was removed and the SC pieces were tested for drug concentration. No drug was found.

### E.3.5. Sodium Nicotinate Liberation Experiments

Sodium nicotinate liberation experiments from the study formulations across a porous matrix were carried out in order to test the validity of the continuous phase drug concentration concept additionally to the caffeine permeation experiments across a silicon membrane (see chapter D.1). A setup of two layers of HDS Aqueous Polymer Hydrogel (Hydrogel Design System, Langhorn, USA), sandwiched between two shields of cellulose filter paper, was found to be an appropriate matrix for that purpose (Fig.E.3.5).

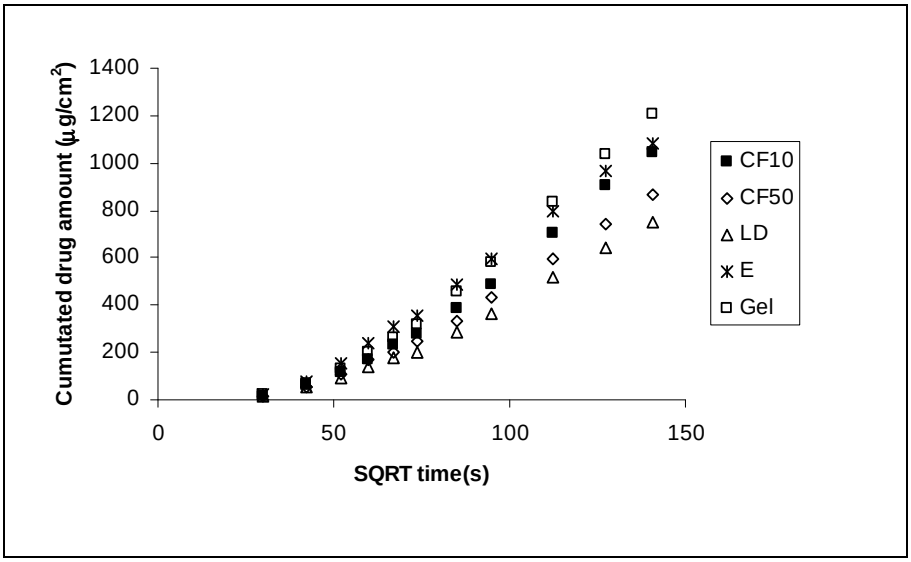


**Figure E.3.5** Cumulated liberated sodium nicotinate amount from the study-formulations

The sodium nicotinate gave a linear liberation profile with the square root of time at later time points of the experiment. This liberation pattern may be described by:

$$Q = 2 \cdot C_{tot} \cdot \sqrt{\frac{D \cdot t}{\pi}} \qquad \text{(E5)}$$

where, $Q$ is the amount of drug released to the sink per unit area, $C_{tot}$ is the overall dissolved drug concentration of the formulation, $t$ the time and $D$ the diffusion coefficient of drug within the formulation (9). Liberation constants $L$ were derived from Eq. (E5) from the slope of the linear portion of the liberation curve (Fig.E.3.5). According to the continuous phase drug concentration concept (see chapters D.1, D.2), these constants were corrected by the continuous phase drug concentration and gave $L^{k1}$. However, Eq. (E5) indicates that a further correction is necessary, because diffusion of drug within the formulations may not be neglected in the situation of negligible diffusional resistance of the membrane. Hence, the

liberation constants were additionally corrected by dividing through the square root of sodium nicotinate self diffusion coefficients derived from NMR diffusion experiments (see chapter D.1). These different liberation constants are given in Table E.3.4.

**Table E.3.4** Liberation constants of sodium nicotinate

| | $L$ (µg/cm$^2$/SQRT(s)) | $L^{k1}$ (cm/SQRT(s)) | $L^{k2}$ |
|---|---|---|---|
| CF10 | 11.72 | 0.0011 | 5053 |
| LD | 8.25 | 0.00074 | 5018 |
| Gel | 13.45 | 0.0013 | 5652 |
| E | 10.93 | 0.00051 | 3256 |
| CF50 | 9.36 | 0.00042 | 2853 |

$L$ denotes the liberation constants, where the superscript $^{k1}$ denotes a correction by dividing through continuous phase drug concentrations (µg/cm$^{3)}$, and $^{k2}$ a further correction by dividing through the square root of the diffusion coefficient (cm/Sqrt(s))of drug within the formulation.

This correction yielded comparable liberation constants $L^{k2}$ for LD, CF10 and the gel, indicating the validity of the continuous phase drug concentration concept. $L^{k2}$ values for E and CF50 were also comparable, but different to the values obtained from CF10, LD and E. This may be due to diffusion of water from the receptor to the donator compartment of the diffusion cells, decreasing the concentration directly above the membrane.

## References

(1) Van Veldhoven, P.P., Mannaerts GP, Inorganic and organic phosphate measurements in the nanomolar range, Anal. Biochem. 161 (1987) 45-48.

(2) M. Khossravi, Y.H. Kao, R.J. Mrsny, T.D. Sweeney, Analysis methods of polysorbate 20: A new method to asses the stability of polysorbate 20 and established methods that may overlook degraded polysorbate 20, Pharm. Res. 19 (5) (2002) 634-639.

(3) Triglycerida saturata media, Pharmacopoe Eur.(1997) 1775-1776

(4) Polysorbate 20, Pharmacopoe Eur.(1997) 1519

(5) http://www.ich.org/LOB/media/MEDIA417.pdf

(6) D. Wu, A. Chen, C.S. Johnson Jr., An improved diffusion-ordered spectroscopy experiment incorporating bipolar-gradient pulses, J. Magn. Reson. Series A, 115 (1995) 260-264

(7) XWINNMR, Bruker Analytik GmbH, Sotware Dept., Rheinstetten, Germany

(8) Sekkat, N., Kalia, Y.N., Guy, R.H., 2002. Biophysical study of porcine ear skin in vitro and its comparison to human skin in vivo, J. Pharm. Sci., 91 (11), 2376-2381

(9) Higuchi, W.I., 1967. Diffusion models useful in biopharmaceutics, J. Pharm. Sci., 56 (3) 315-324

## List of Instruments

Balance, Mettler AT 261 DeltaRange®, No. P27846, Mettler Toledo AG, Greifensee ZH, Switzerland

Balance, Mettler PM 400, No. G22900, Mettler Toledo AG, Greifensee ZH, Switzerland

Centrifuge, Centrifuge Sigme 302K, No. 22644, Sigme, Osterode/Harz, Germany

Spectrometer, Perkin Elmer Spectrometer Lambda 20, No. 20029, Perkin Elmer, Ueberlingen, Germany

Ultrasonic bath, Retsch Type URG, No. 306059007, Retsch GmbH&Co., Haan, Germany

Glas diffusion cells, custom made, Glastechnik Rahm, 4132 Muttenz, Switzerland

HPLC equipment, Hewlett Packard, Seires 1050, Hewlett Packard, Switzerland
Quaternary Pump Type 79852AX, No. 3117G01875
Autosampler Type 79855A, No. 3141G01637
UV-Detector Type 79853A, No. 3140J02551
Degasser Type 79856AX, No. 3019G01795

PH-meter, Metrohm 744 pH meter, Type 1.744.0010, No. 12190, Metrohm, Herisau, Switzerland

Karl-Fischer equipment, KF 701 Titrino, Type 8.701.1001, No. OF8/244 Metrohm AG, Herisau, Switzerland

Polytron Pt 3000, No. 9261 Kinematica AG Littau, Switzerland

Ultracentrifuge Centricon T-1075, No. 06921356 Kontron Instruments, Mailand, Italy
Rotor TFT 7013

Zetasizer HsA1000, No. 34283/59 Malvern Instruments Ltd., Malvern, UK

Mastersizer S, No. 6142 Malvern Instruments Ltd., Malvern, UK

Conductometer 660, Type 1.660.0016, No. 0H7/143, Metrohm, Herisau, Switzerland

Tewameter TM 210, No. 9428 0023, Courage Khazaka electronic GmbH, Germany

Versamax Tunable Multiplate Reader, No. SIN/B 02553, Molecular Devices Corporation, Sunnyville, USA

Branson Sonifier 250, Branson Ultrasonics Corporation, Danbury, USA

Bruker Avance DRX NMR spectrometer 600.13 MHz, Bruker BioSpin AG, Fällanden, Switzerland

Pneumatic Dermatome, No. 101687, Zimmer Inc., Dover, OH, USA